STUDY OF MOLECULAR LASERS

Annual Report - November 1, 1971

Cornell University

Ithaca, New York 14850

Sponsored by:

Advanced Research Projects Agency

ARPA Order No. 660

UNCLASSIFIED

Security Classification

DOCUMENT CONTROL DATA - R&D

(Security classification of title, body of abstract and indexing annotation must be entered when the overall report is classified)

1. ORIGINATING ACTIVITY (Corporate author) Cornell University Ithaca, New York 14850	2a. REPORT SECURITY CLASSIFICATION Unclassified 2b GROUP NA

3. REPORT TITLE

STUDY OF MOLECULAR LASERS

4. DESCRIPTIVE NOTES (Type of report and inclusive dates)

Annual Report (2nd Semi Annual) - 1971

5. AUTHOR(S) (Last name, first name, initial)

Peter L. Auer
George J. Wolga

6. REPORT DATE	7a. TOTAL NO. OF PAGES	7b. NO. OF REFS
November 1, 1971	86	47

8a. CONTRACT OR GRANT NO. N00014-67-A-0077-0006 b. PROJECT NO. c. d.	9a. ORIGINATOR'S REPORT NUMBER(S) NA 9b. OTHER REPORT NO(S) (Any other numbers that may be assigned this report) NA

10. AVAILABILITY/LIMITATION NOTICES

11. SUPPLEMENTARY NOTES	12. SPONSORING MILITARY ACTIVITY
	Office of Naval Research

13. ABSTRACT

Research concerning molecular and chemical lasers was conducted in the following areas:

1. Vibrational Deexcitation and Energy Transfer in the HF, DF, HF-CO_2 and DF-CO_2 Chemical Lasers.
2. Shock Tube Studies of Vibrational Relaxation in CO_2 induced by collisions with H_2O, D_2O, CH_4, CD_4, CH_3F.
3. Efficient atom production by molecular dissociation in a high power S-band microwave discharge.
4. Chemical laser studies in the following systems: $C_2H_2 + O$; $CS_2 + O$.
5. Chemical reaction rate determination for the following reactions: $H + Cl_2 \rightarrow HCl + Cl$; $H + F_2 \rightarrow HF + F$; $NO + F_2 \rightarrow NOF + F$
6. Study of rapid gas mixing in a subsonic gas flow enhanced by the controlled introduction of turbulence.
7. High pressure vibrational relaxation studies in CO_2.

DD FORM 1 JAN 64 1473

Unclassified

Security Classification

14. KEY WORDS	LINK A		LINK B		LINK C	
	ROLE	WT	ROLE	WT	ROLE	WT
Molecular Lasers Chemical Lasers Vibrational Relaxation Energy Transfer Rapid Gas Mixing Chemical Reaction Rates						

INSTRUCTIONS

1. ORIGINATING ACTIVITY: Enter the name and address of the contractor, subcontractor, grantee, Department of Defense activity or other organization *(corporate author)* issuing the report.

2a. REPORT SECURITY CLASSIFICATION: Enter the overall security classification of the report. Indicate whether "Restricted Data" is included. Marking is to be in accordance with appropriate security regulations.

2b. GROUP: Automatic downgrading is specified in DoD Directive 5200.10 and Armed Forces Industrial Manual. Enter the group number. Also, when applicable, show that optional markings have been used for Group 3 and Group 4 as authorized.

3. REPORT TITLE: Enter the complete report title in all capital letters. Titles in all cases should be unclassified. If a meaningful title cannot be selected without classification, show title classification in all capitals in parenthesis immediately following the title.

4. DESCRIPTIVE NOTES: If appropriate, enter the type of report, e.g., interim, progress, summary, annual, or final. Give the inclusive dates when a specific reporting period is covered.

5. AUTHOR(S): Enter the name(s) of author(s) as shown on or in the report. Enter last name, first name, middle initial. If military, show rank and branch of service. The name of the principal author is an absolute minimum requirement.

6. REPORT DATE: Enter the date of the report as day, month, year; or month, year. If more than one date appears on the report, use date of publication.

7a. TOTAL NUMBER OF PAGES: The total page count should follow normal pagination procedures, i.e., enter the number of pages containing information.

7b. NUMBER OF REFERENCES: Enter the total number of references cited in the report.

8a. CONTRACT OR GRANT NUMBER: If appropriate, enter the applicable number of the contract or grant under which the report was written.

8b, 8c, & 8d. PROJECT NUMBER: Enter the appropriate military department identification, such as project number, subproject number, system numbers, task number, etc.

9a. ORIGINATOR'S REPORT NUMBER(S): Enter the official report number by which the document will be identified and controlled by the originating activity. This number must be unique to this report.

9b. OTHER REPORT NUMBER(S): If the report has been assigned any other report numbers *(either by the originator or by the sponsor)*, also enter this number(s).

10. AVAILABILITY/LIMITATION NOTICES: Enter any limitations on further dissemination of the report, other than those imposed by security classification, using standard statements such as:

(1) "Qualified requesters may obtain copies of this report from DDC."

(2) "Foreign announcement and dissemination of this report by DDC is not authorized."

(3) "U. S. Government agencies may obtain copies of this report directly from DDC. Other qualified DDC users shall request through _____."

(4) "U. S. military agencies may obtain copies of this report directly from DDC. Other qualified users shall request through _____."

(5) "All distribution of this report is controlled. Qualified DDC users shall request through _____."

If the report has been furnished to the Office of Technical Services, Department of Commerce, for sale to the public, indicate this fact and enter the price, if known.

11. SUPPLEMENTARY NOTES: Use for additional explanatory notes.

12. SPONSORING MILITARY ACTIVITY: Enter the name of the departmental project office or laboratory sponsoring *(paying for)* the research and development. Include address.

13. ABSTRACT: Enter an abstract giving a brief and factual summary of the document indicative of the report, even though it may also appear elsewhere in the body of the technical report. If additional space is required, a continuation sheet shall be attached.

It is highly desirable that the abstract of classified reports be unclassified. Each paragraph of the abstract shall end with an indication of the military security classification of the information in the paragraph, represented as *(TS)*, *(S)*, *(C)*, or *(U)*.

There is no limitation on the length of the abstract. However, the suggested length is from 150 to 225 words.

14. KEY WORDS: Key words are technically meaningful terms or short phrases that characterize a report and may be used as index entries for cataloging the report. Key words must be selected so that no security classification is required. Identifiers, such as equipment model designation, trade name, military project code name, geographic location, may be used as key words but will be followed by an indication of technical context. The assignment of links, rules, and weights is optional.

ARPA Order Number 660

Program Code Number N00014

Cornell University

Effective Date of Contract
January 1, 1967

Contract Expiration Date
September 30, 1971

Amount of Contract $812,380.00

Contract Number N00014-67-A-0077-0006

Principal Investigator - P. L. Auer
607-256-4127

Scientific Officer - Dr. Walter Sooy

Study of Molecular Lasers

INDEX

SUMMARY

This report contains a statement of work accomplished during the past year in the area of chemical and molecular lasers. In formulating this program five distinct problems were identified as being basic to progress in the further development of existing molecular and chemical lasers and to the discovery of new laser systems. The problems identified, and the methods employed in each area will now be summarized:

1. Vibrational Deexcitation and Energy Transfer

In every molecular and chemical laser the lasing molecules are subjected to collisions with each molecular constituent of the gas thereby providing a source of loss of vibrational energy. In addition, in certain lasers, e.g., DF-CO_2 collisions between molecules and the transfer thereby of vibrational energy from one molecule to another is an efficient mechanism for achieving specific molecular excitation. In most known and important molecular lasers many important rates of deexcitation and energy transfer were unknown. As a result of our effort we have experimentally determined many of these rates.

a. The method of laser induced fluorescence was applied to study these rates in the HF, DF, HF-CO_2 and DF-CO_2 chemical lasers. As a result of this work the rate of vibrational deexcitation of DF; the rates of energy transfer from HF and DF to CO_2, and the rates of deexcitation of CO_2 in the upper laser level by HF and DF have been measured.

b. Shock tube studies in CO_2 were devoted to the measurement of vibrational relaxation in CO_2 induced by a selected sequence of molecular collision partners. These partners were selected to elucidate the effects of mass, moment of inertia, dipole moment, and energy mismatch between nearly resonant energy levels upon the deexcitation efficiency. Collision partners with CO_2 were H_2O, D_2O, CH_4, CD_4 and CH_3F. The rates were measured from 300°K to 1200°K and were correllated with prior

work where available and with theory.

c. Work was initiated to determine the collisional deactivation of CO_2 in the upper laser level by itself and other molecules over a pressure range 1 - 100 atmospheres and a temperature range 300° - 600°K. This work is motivated by the recent advent of CO_2 lasers operating at as high a pressure as 1 atmosphere and by the desirability of developing lasers that operate at even higher pressures to maximize volumentric energy storage. Relevent rates at and above one atmosphere are simply not known. The method employed is again laser induced fluorescence for which we have developed a chemical HBr laser with relatively high power output (100 - 1000 watts) which matches several strong absorptions in CO_2 and N_2O. This work is continuing.

2. Atom Production for Chemical Laser Initiation

Most known chemical lasers require the presence of specific free atoms to act as initiators of and participants in the chemical reactions from which laser excitation is derived. It is therefore desirable to establish methods of copious and efficient atom production. Atoms are frequently produced by electrical discharges of various types in a molecular gas whereby molecular dissociation upon electron impact provides one or more atoms. A few cases are known in which purely chemical means may be employed for atom production.

a. We have studied atom production by various gas discharge means and have found that a microwave discharge can be operated with good results. Using a 1500 watt cw magnetron operating at 2.45 GHz we have obtained up to 50% dissociation of O_2 at pressures of 5-6 Torr with the addition of an optimum amount of N_2. At 4 liters per sec pumping speed and 2.3 Torr the O atom production rate was 1.4×10^{20} atoms/sec. Thus production rate was basically limited by pumping capacity and could easily be increased by more than an order of magnitude. At these flow rates of atomic oxygen it becomes possible to design

chemical lasers such as the CS_2 + O system that produces lasing in CO at the Kilowatt level, cw. We are considering the parametric study of such a laser which could be readily undertaken with the atom generation means we have developed.

b. One of the better known purely chemical means of atom production involves the NO + F_2 → NOF + F reaction by which atomic fluorine is produced. This reaction has been applied to the purely chemical DF - CO_2 vibrational transfer chemical laser. The rate at which the reaction proceeds is not known accurately and we have begun a study of it utilizing the method of paramagnetic resonance absorption to directly measure density of F and NO as the reaction proceeds. This work is continuing.

3. Detailed Study of Chemical Laser Systems

Two chemical laser systems have been studied in detail utilizing parametric variation of reactants and diluents as well as spectroscopic study of emission wavelengths, populations and time sequence of particular emissions.

a. The highly energetic reaction between aceteline (C_2H_2) and atomic oxygen to yield vibrationally excited CO in a laser configuration. The results obtained indicate that a high vibrational temperature characterizes the CO produced and that under normal operating conditions a relatively high rotational temperature in excess of 600°K also occurs. Addition of diluent decreases the rotational temperature and it would appear that effective gas cooling should result in laser action. Computer fitting of the spectral intensity data obtained is in progress and will result in knowledge of vibrational populations in the chemically produced CO.

b. A study of the CS_2 + O reaction which also leads to lasing in CO is in progress. The object in this study is to elucidate the mechanisms that operate in this reaction. A chemical CO laser utilizing this reaction was operated and relative laser emission intensity as a function of vibrational

transition was studied as were the time delays after initiation of the reaction for the different vibrational transitions. At present non lasing chemiluminescent spectral information is being studied. In combination these data will permit an unambiguous formulation of a mechanism and the rate constants to be determined.

4. Reaction Rates for Chemical Lasers

Many chemical reactions that are employed in chemical lasers have unknown or poorly known rates. These rates must be determined in order to permit a computer model for the laser to be developed and thereby to obtain reliable prediction and analysis of laser performance. We have undertaken to measure these unknown and important rates by using the method of microwave electron paramagnetic resonance (EPR) to monitor the presence, appearance and disappearance of the paramagnetic free atoms and molecules. A fast flow vacuum system coupled to a high sensitivity EPR spectrometer was assembled and means for gas injection suitable for chemical rate determination was designed. Rate information on the reactions $H + F_2 \rightarrow HF + F$ and $H + Cl_2 \rightarrow HCl + Cl$ has been obtained and the reaction $NO + F_2 \rightarrow NOF + F$ is being studied. These rates are basic to an understanding of the operation of HF, HCl, and DF - CO_2 purely chemical lasers.

5. Turbulent Induced Rapid Gas Mixing

Many important molecular and chemical lasers require rapid and efficient gas mixing into flowing gas streams. Introduction of controlled turbulence into the stream of mixing gases promises to permit faster gas mixing than simple diffusive mixing. Reliable experimental and theoretical design information is lacking at the subatmospheric pressures characteristic of many laser systems. We have undertaken an experimental and theoretical study of turbulent mixing with the goal of determining reliable design information at the pressures of interest. A mixing wind tunnel was built and turbulent mixing studied by the introduction of posts, grids, and injectors. The enhancing effect of turbulence on the mixing was observed. Further tests including more extensive variation of operating parameters will supply the required design characteristics for effective turbulent mixing.

VIBRATIONAL DEEXCITATION AND ENERGY TRANSFER IN THE HF, DF, HF-CO_2, and DF-CO_2 CHEMICAL LASERS

T. A. Cool

Much progress has been achieved recently in the development on continuous-wave (cw) chemical lasers despite a serious lack of understanding of the mechanisms of those vibrational energy transfer processes which play major roles in chemical laser operation.

Prior to the completion of the measurements described here, reliable data were available for the self deactivation of HF as reported by Airey and Fried[1], and more recently by Solomon, et al[2], and Bott and Cohen[3]. No data were available, however, concerning the rate of vibrational deactivation of DF or the rates for the important processes by which vibrational energy is transferred from HF and DF to the $CO_2(001)$ upper laser level. In addition the rates for the vibrational deactivation of $CO_2(00°1)$ molecules by collisions with HF and DF molecules were unknown.

We have used the laser excited fluorescence method[4-6] to determine the rate constants for these key processes at 350°K, a typical temperature for chemical laser operation. These rates are given below:

(a) $DF\ (v=1) + CO_2(000) \rightarrow DF\ (v=0) + CO_2(001)$; $k = 17.5 \pm 2.5 \times 10^4\ sec^{-1}\ torr^{-1}$

(b) $DF + CO_2(001) \rightarrow DF + CO_2(000)$; $k = 1.9 \pm 0.4 \times 10^4\ sec^{-1}\ torr^{-1}$

(c) $DF\ (v=1) + DF\ (v=0) \rightarrow 2DF\ (v=0)$; $k = 2.0 \pm 0.2 \times 10^4\ sec^{-1}\ torr^{-1}$

(d) $HF\ (v-1) + CO_2(000) \rightarrow HF\ (v=0) + CO_2(001)$; $k = 3.7 \pm 0.3 \times 10^4\ sec^{-1}\ torr^{-1}$

(e) $HF + CO_2(001) \rightarrow HF + CO_2(000)$; $k = 3.6 \pm 0.3 \times 10^4\ sec^{-1}\ torr^{-1}$

(f) $HF\ (v=1) + nF\ (v=0) \rightarrow 2HF\ (v=0)$; $k = 5.25 \pm 0.30 \times 10^4\ sec^{-1}\ torr^{-1}$

The experimental results for HF and DF vibrational deactivation exhibit good qualitative agreement with the vibration-rotation theory of Shin, when the effects of strong attractive interactions are considered[7].

The rates of vibrational energy transfer from HF and DF to CO_2 are too large to be accounted for with present approximate theories. Interpretation of the above results[6] suggests that the magnitude of these rates may be explained in terms of a hydrogen bonded attractive intermolecular potential

well for HF-CO_2 and DF-CO_2 collision pairs which leads to enhanced repulsion at close ranges. A successful theory must necessarily allow the major portion of the vibrational energy defect between initial and final states to be taken up as rotational motion of the collision partners.

The approximations inherent in the first order perturbation theory of multipole moment interactions are invalid for treatment of the energy transfers to CO_2(001) from HX (v=1) and DX (v=1) molecules. We have been successful, however, in calculation of the previously measured[8] rate of energy transfer between D_2 (v=1) and CO_2(001).[6] For this case an interaction between the quadrupole moment of ortho-deuterium and the transition dipole moment of the CO_2 asymmetric stretching vibration is responsible for the observed rate of transfer.

Our apparatus is currently being used for measurements of V → V coupling between HF and H_2 and DF and D_2. We plan on detailed studies of the above processes over the temperature range 200 - 700°K during the coming year to further elucidate the energy transfer mechanisms.

A brief description of the apparatus we have used is given in reference 4 which is also included in the appendix to this report.

REFERENCES

1. J. R. Airey and S. F. Fried, Chem. Phys. Lett. 8, 23 (1971).
2. W. C. Solomon, J. A. Blauer, F. C. Jaye, and J. G. Hnat, Intl. J. of Chem. Kinetics 3, 215 (1971).
3. J. F. Bott and N. Cohen, "Shock Tube Studies of HF Vibrational Relaxation" (to be published) J. Chem. Phys.
4. R. R. Stephens and T. A. Cool, Rev. Sci. Inst. 42, 1489 (1971).
5. R. R. Stephens, "Vibrational Energy Transfer Processes in the DF, HF, DF-CO_2 and HF-CO_2 Chemical Lasers", Ph.D. Thesis, Cornell University, submitted Sept. 1971.
6. R. R. Stephens and T. A. Cool, "Vibrational Energy Transfer and Deexcitation in the HF, DF, HF-CO_2, and DF-CO_2 Systems" submitted to J. Chem. Phys.; T. A. Cool and J. C. Kershenstein (unpublished).

7. H. K. Shin, Chem. Phys. Letters, 10, 81 (1971).

8. C. B. Moore, Fluorescence, edited by C. G. Guilbault (Marcel Dekker, New York, 1967), p. 133.

SHOCK TUBE STUDIES

S. H. Bauer

A substantial effort has been devoted to the study of vibrational relaxation in CO_2 induced by a selected sequence of colliders. Density gradients at shock fronts were measured with a laser-schlieren arrangement. These data provide vibrational-translation relaxation times for the (010) state. The experimental set up is shown in Figure 5; operating conditions are listed below.

SHOCK TUBE OPERATING CONDITIONS

Shock speed: measured to $\pm$ 1 mm/μsec
raster accuracy $\pm$ 0.5 μsec
} $\delta T_{unrelax} \approx \pm$ 20°K

Background pressure: 7×10^{-6} torr
Leak rate: 4×10^{-5} torr/min
} sample pressures (5-150 torr)

Degassing minimized by flushing tube with sample
CO_2 -- research grade [N_2 (7.4 ppm); O_2 (1.7 ppm); others ($\approx$ 1 ppm)]
Estimated impurity level (incl. degass) $\approx$ 20 ppm
D_2O -- 99.82% level; other gases of high quality
Driver gases; He and N_2 (100 - 200 psi)
Rise time of optical-electronic system: $\approx$ 200 n sec
Correction for finite rise time inserted in program

The most difficult problem encountered in this investigation, when H_2O and D_2O served as catalyst gases was the determination of the actual water content in the shocked gas. After testing several analytical devices Mr. M. Buchwald finally obtained consistent results with a vapor phase chromatograph. He calibrated the system, which included flow controls, a portion of tube identical with that used in the construction of the shock tube, and the handling procedures by means of the arrangement shown in Figure 6. His results are summarized in

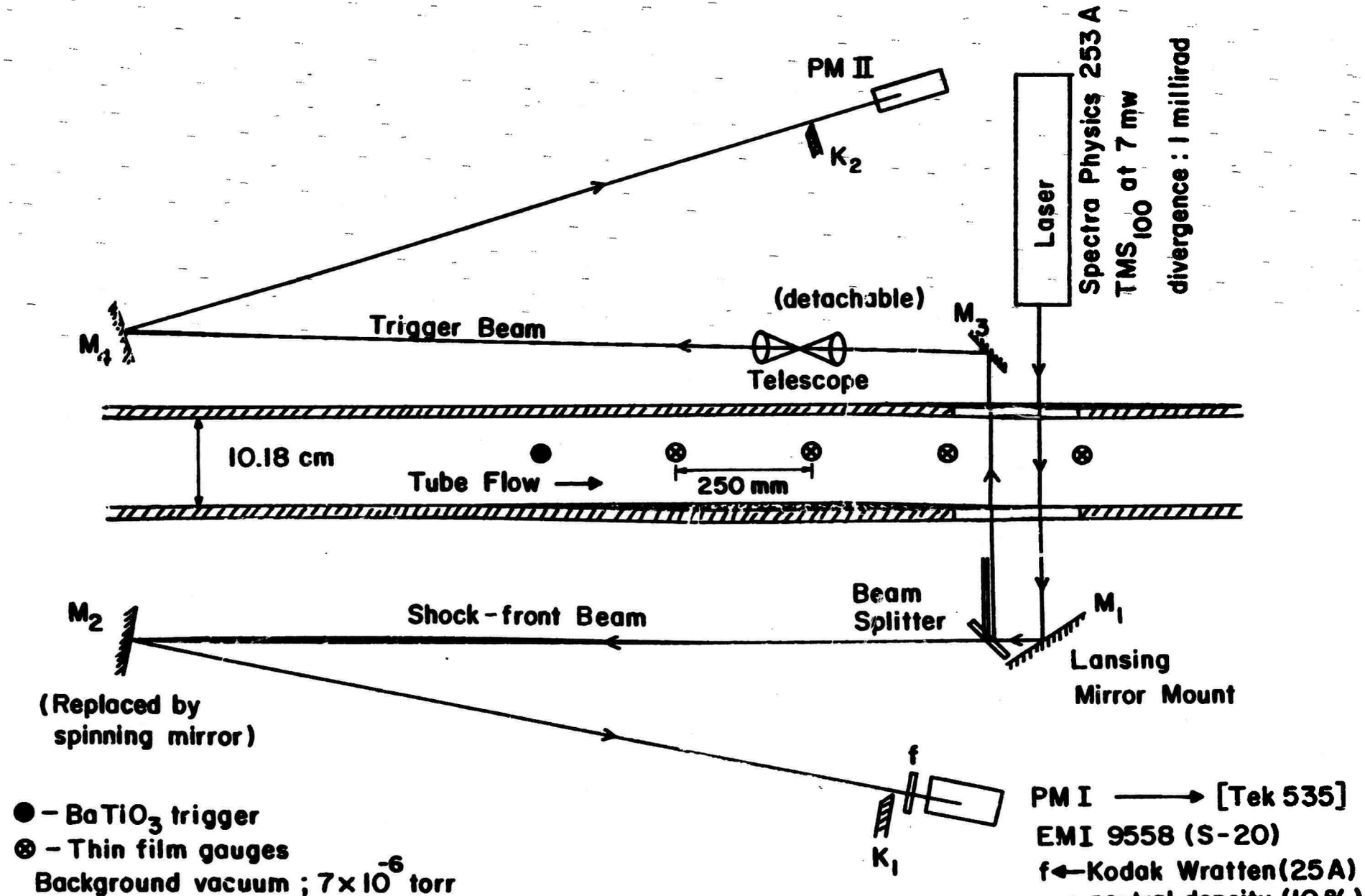

Shock-front Density gradient (Schlieren Optical Arrangement)

FIGURE 1

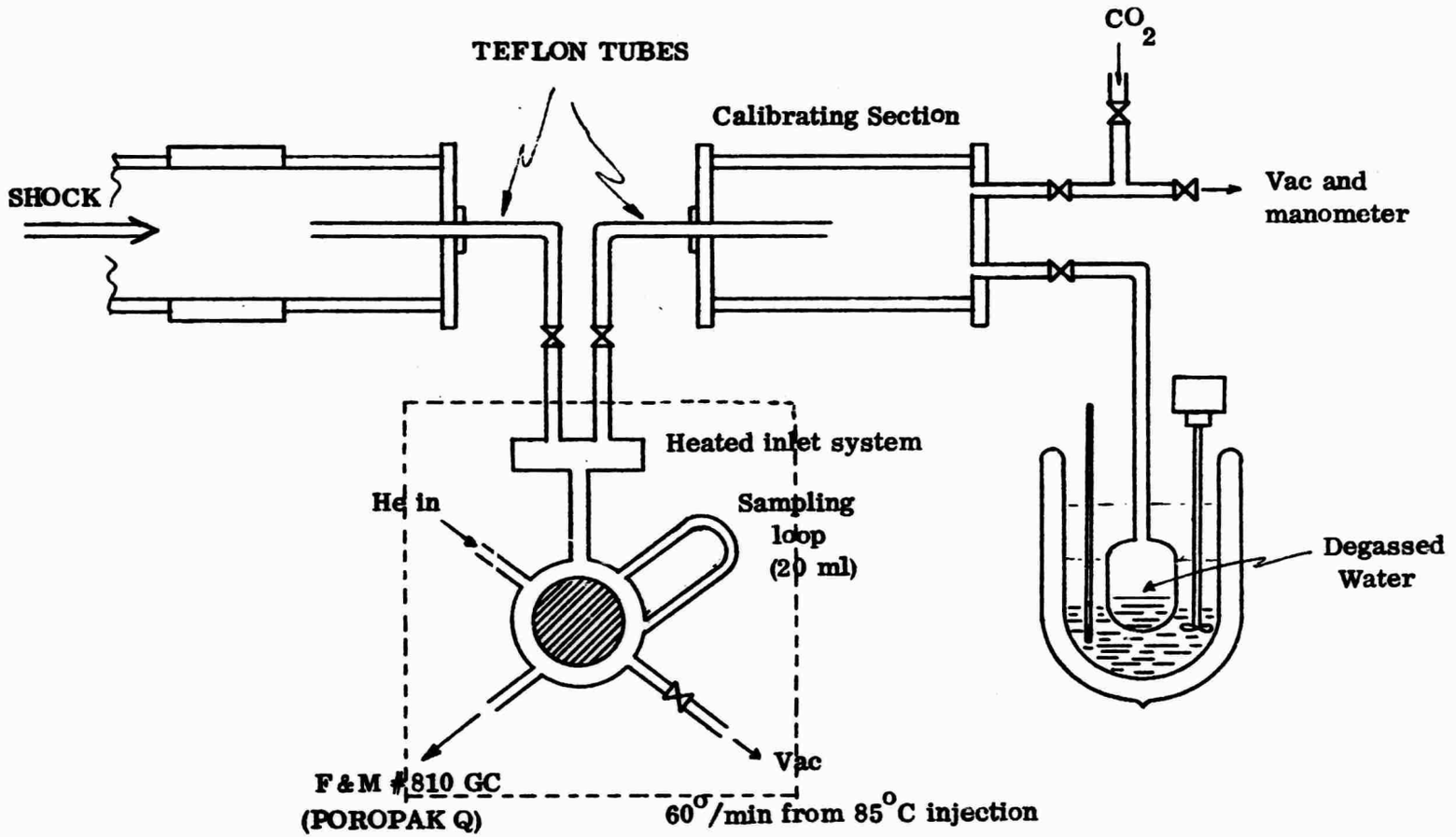

Repeated samplings over 10-15 minute residence period in shock tube

WATER CONCS: 0.5% to 5.0%

FIGURE 2

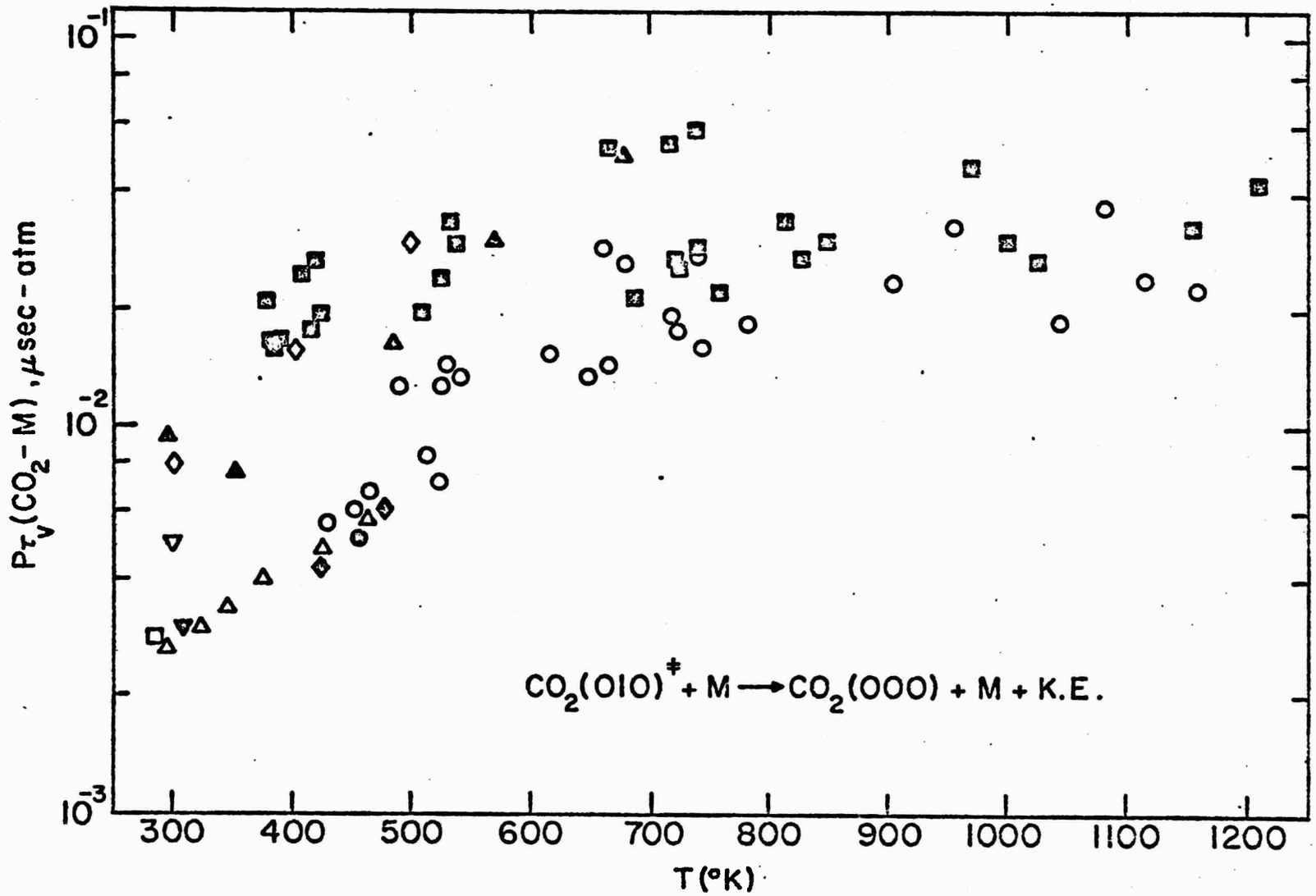

CO_2-D_2O (OUR MEASUREMENTS)

CO_2-H_2O (OUR MEASUREMENTS)

CO_2-D_2O SHIELDS AND BURKS

LEWIS AND LEE; CO_2-H_2O

HIGGS AND TORBORG; CO_2-H_2O

EUCKEN AND NÜMANN; CO_2-H_2O

FIGURE 3

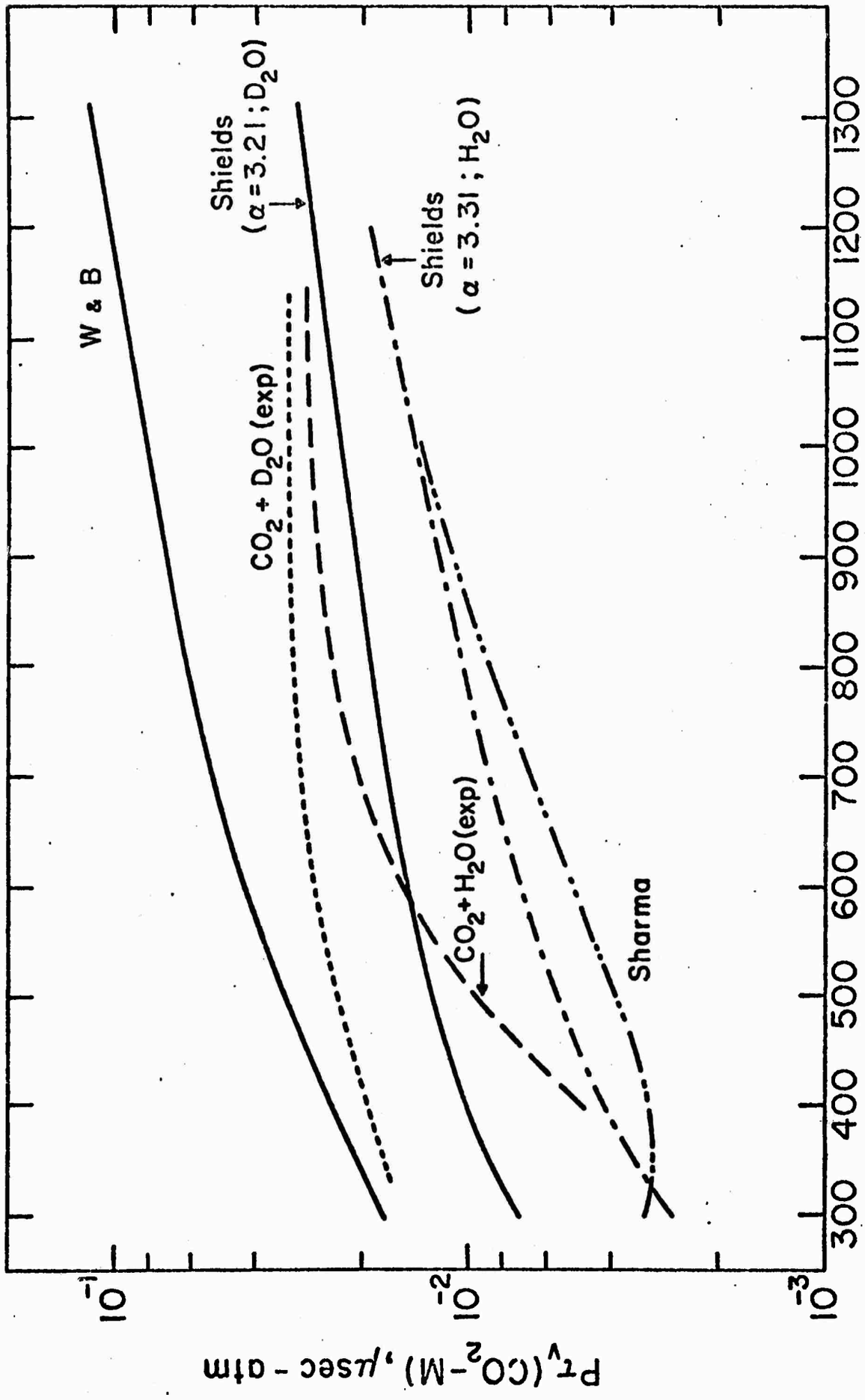
W & B
Shields
(α=3.21; D2O)
CO2 + D2O (exp)
Shields
(α = 3.31 ; H2O)
CO2+H2O(exp)
Sharma
T(°K)
300
400
500
600
700
800
900
1000
1100
1200
1300
10-1
10-2
10-3
Pτν(CO2-M), μsec - atm

FIGURE 4

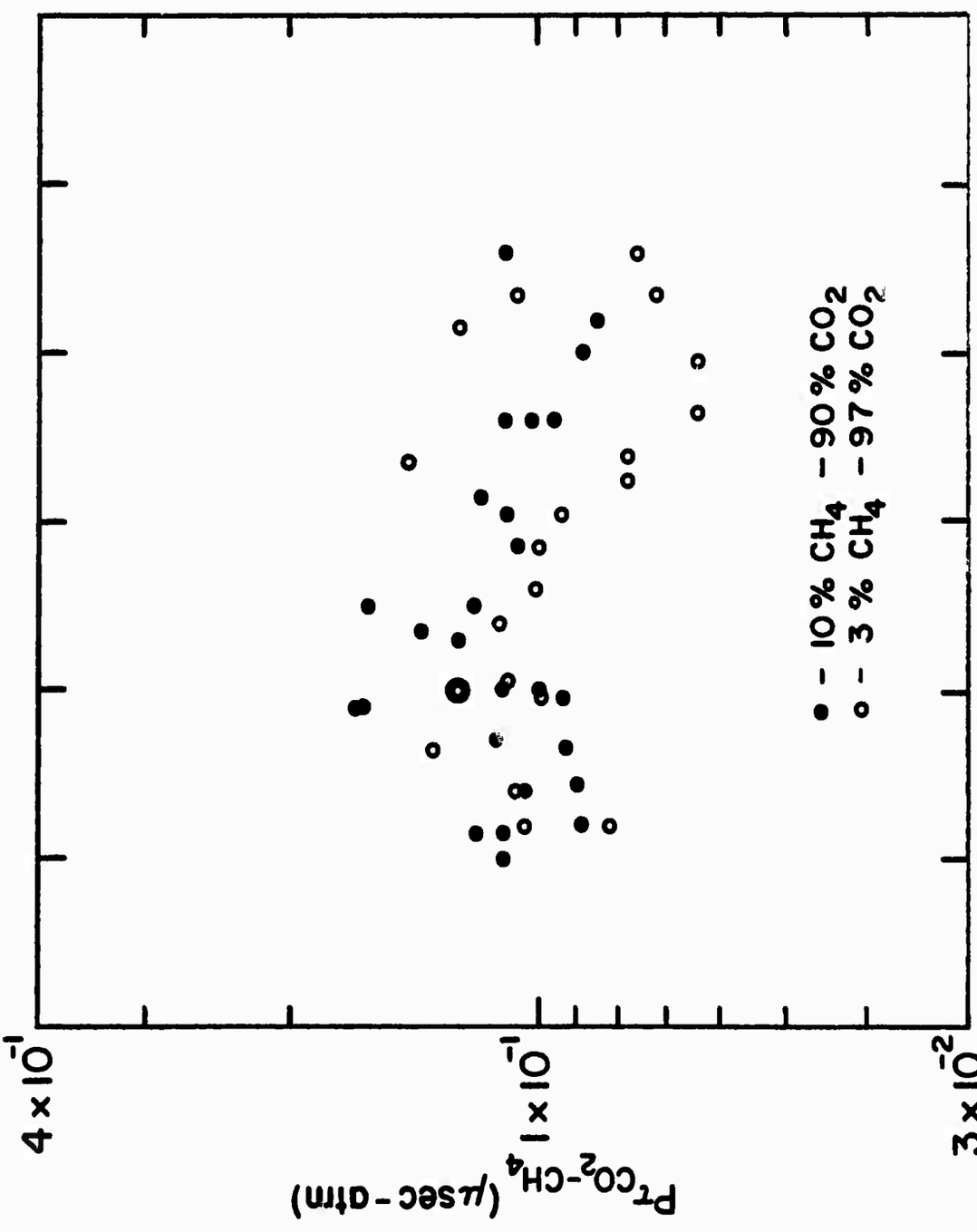
$P_{\tau CO_2\text{-}CH_4}$ (μsec-atm)
4×10^{-1}
1×10^{-1}
3×10^{-2}
400
600
800
1000
1200
T(°K)
● - 10% CH_4 - 90% CO_2
○ - 3% CH_4 - 97% CO_2

FIGURE 5

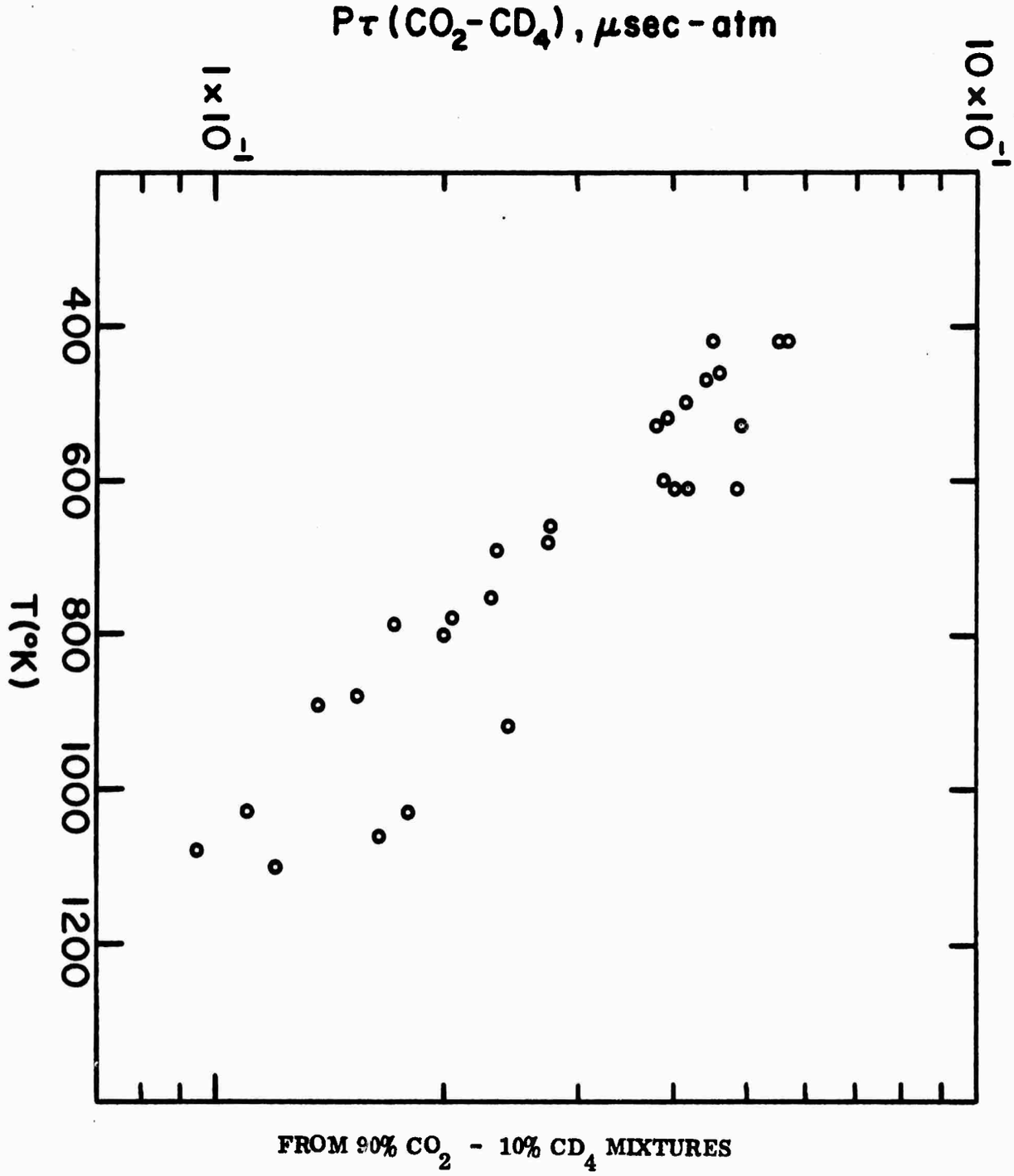

FIGURE 6

FROM 90% CO_2 - 10% CD_4 MIXTURES

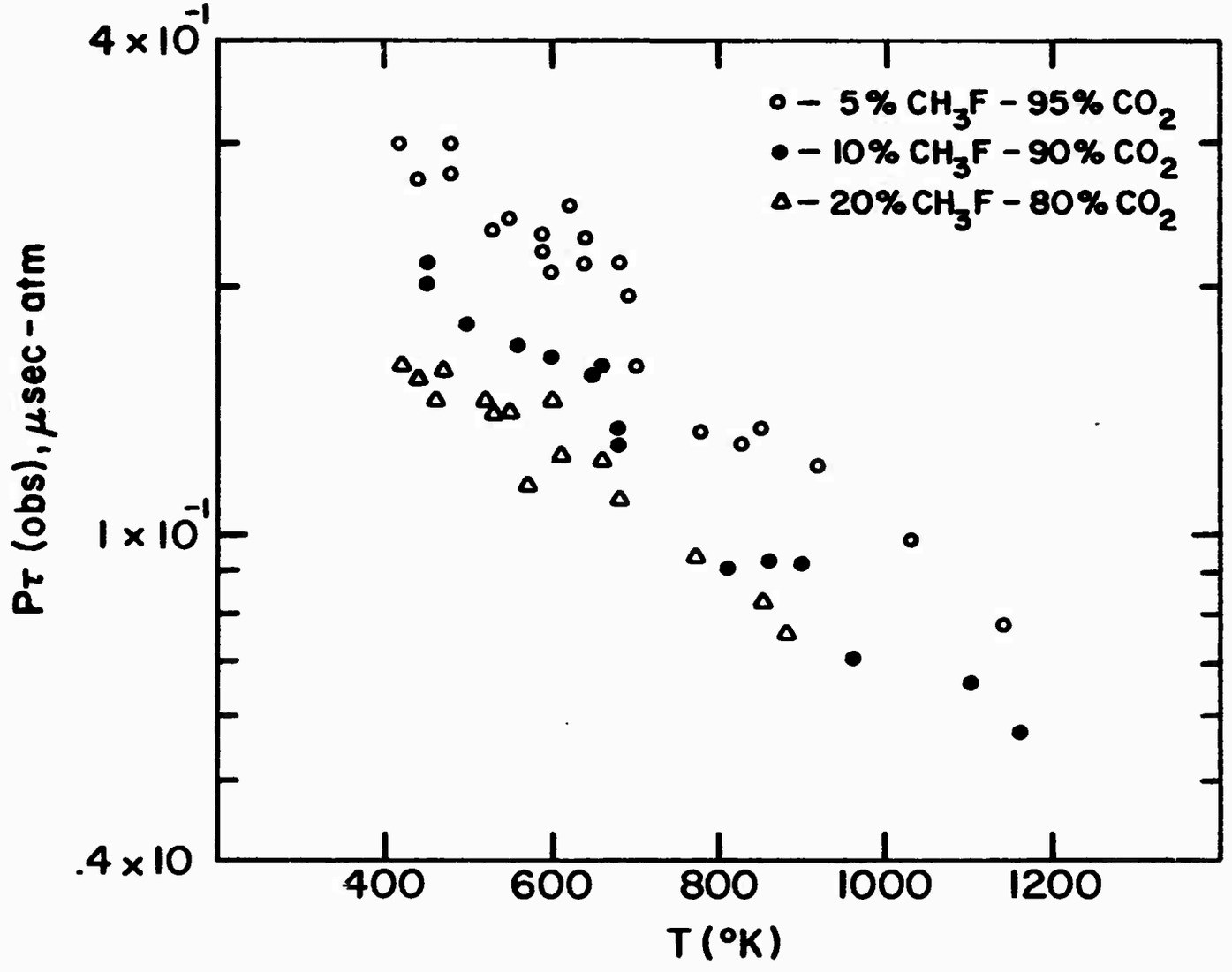
4 x 10⁻¹
1 x 10⁻¹
.4 x 10
Pτ (obs), μsec-atm
400
600
800
1000
1200
T (°K)
○ – 5% CH3F – 95% CO2
● – 10% CH3F – 90% CO2
△ – 20% CH3F – 80% CO2

FIGURE 7

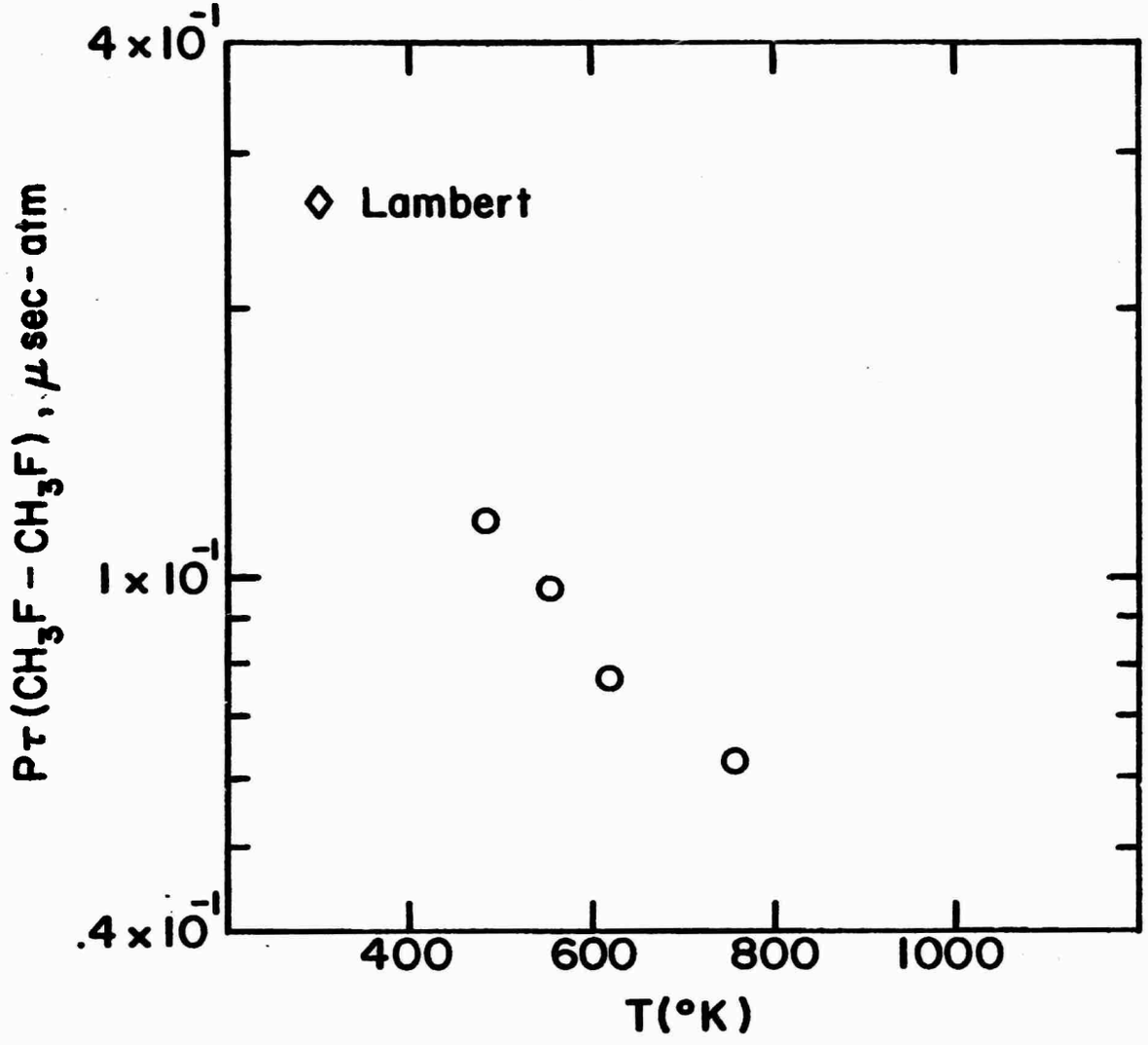
4 x 10⁻¹
1 x 10⁻¹
.4 x 10⁻¹
◇ Lambert
Pτ(CH3F - CH3F), μsec-atm
400
600
800
1000
T(°K)

FIGURE 8

Figure 3, both for CO_2 - H_2O and CO_2 - D_2O. Comparisons are also made in this figure with selected data taken from the literature. These experimental results for the relaxation of the (010) state of CO_2 with H_2O and D_2O as collision partners, were replotted in Figure 4 for comparison with predictions based on the theory of Sharma, the expression proposed by Shields (for H_2O and D_2O) and the theory of Widom-Bauer for H_2O. The effect of isotopic substitution is best reproduced by the Shields equation as is also the general trend with temperature. The precise magnitudes for the relaxation times are subject to adjustment with the α parameter. Similar shock front density gradient data for mixtures of CO_2 with CH_4, CD_4 and CH_3F were obtained by Mr. Peter Walsh; these are reproduced in Figures 5, 6, and 7. As an overall check on the technique Mr. Walsh also determined the vibrational relaxation time in pure CH_3F as a function of temperature. As can be seen from his curve, Figure 8 his values extrapolate to the room temperature value report by Lambert, based on sound dispersion measurements. Finally, these results along with appropriately selected values from the literature were summarized in a series of plots. For each catalyst molecule the de-excitation probability for CO_2 (010) + M → CO_2 (000) + M and the vibrational de-excitation CO_2 (001) + M → CO_2(m,n,0) + M were compared (i) to ascertain which collision partner would be most suitable for facilitating laser operations, such that the lower lasing state is preferentially de-excited, and (ii) to call attention to intrinsic molecular parameters, such as moments of inertia, dipole moments, etc., for the various collision partners which would provide essential parameters for any theory which accounts for the different efficiencies for energy transfer.

In another shock tube experiment Mr. R. Jones is measuring the (010) relaxation time in pure CO_2 as a function of the translation temperature, in the low temperature regime. His tube can be cooled to about -40°C. By now the serious problems of reliable temperature control and clean operation appear to have been solved; a series of runs, from about 600°K and down, are being made.

The discovery by Mr. Miller that on shock heating a mixture of N_2O with CO to a temperature around 2500°K, CO_2 is produced in an inverted population, as demonstrated by gain in an incident beam of 10.6 μ radiation, is most intriguing. If confirmed, this is indeed a very novel process. To date three experiments under varying conditions indicate some degree of gain. Also, more than a half dozen experiments have been run with N_2O and CO_2, where no gain was observed. The tentative assumption is that at these high temperatures the N_2O dissociates rapidly to produce vibrationally excited N_2 and $O(^1D)$; that these ^1D atoms combine with CO to produce $CO_2(^1B_2)$, which then must get de-excited to the $CO_2(^1\Sigma_g^+)$ by collision with another molecule. The latter process leads to preferential population of the (001) state. This is consistent with a paper published in 1967 by Clerc and Barat on the reaction between CO and $O(^1D)$ for which they report a very large association rate constant. The surprising feature, of course, is that the product CO_2 is in a non-Boltzmannian distribution. Further work is in progress.

Very briefly I wish to mention our pre-occupation with chemical effects induced by laser irradiation. The experiments to date on the reaction between NO_2 and CO to produce NO + CO_2 have led nowhere. At present we are convinced that no augmentation of the reaction by CO_2 laser radiation occurs. This ends (I hope) a long list of inconclusive experiments, where we finally traced the difficulties to variations in the method of analysis. We may return to it after we set up a laser which will provide a much closer coincidence between the incident and the absorption spectrum. In order to select appropriate systems for such studies we set up a spectrophone, as shown in Figure 13. This will permit us to determine relatively easily which substances have strong absorptions for particular lines in the CO_2 spectrum. Following such scans we should be in a good position to select those species which are good candidates for selectively induced reactions based on their high absorption and long vibrational translation relaxation times.

REFERENCES

For Figure 7

$CO_2 + D_2O$: Shields and Burks, J. Acoust. Soc. Am. 43, 510 (1968).

$CO_2 + H_2O$: Lewis and Lee, J. Acoust. Soc. Am. 38, 813 (1965).

$CO_2 + H_2O$: Higgs and Torborg, J. Acoust. Soc. Am. 42, 1038 (1967).

$CO_2 + H_2O$: Eucken and Nümann, Z. Phys. Chem. 36B, 163 (1937).

For Figure 8

$CO_2 + H_2O$ (theory): Widom and Bauer, J. Chem. Phys. 21, 1670 (1953).

$CO_2 +$ $\begin{matrix} H_2O & H_2S \\ D_2O & D_2S \end{matrix}$: Shields and Carney, J. Acoust. Soc. Am. 47, 1269 (1970).

$CO_2 + H_2O$ (theory): Sharma, J. Chem. Phys. 54, 810 (1971).

For Figure 12

H_3CF : Corran and Lambert, Proc. Roy. Soc., A244, 212 (1952).

BIBLIOGRAPHY FOR CO_2(001) RELAXATION

Collision Partner	Source
Helium	J. J. Hinchen (umpublished)
CO_2	"
CF_4	"
CH_4	"
H_2	"
D_2	"
HD	"
N_2	W.A. Rosser, A.D. Wood, E.T. Gerry, JCP, 50, 4996 (1969).
CO	W.A. Rosser, R.D. Sharma, E.T. Gerry, JCP, 54, 1196 (1971).

Collision Partner	Source
H_2O	D.F. Heller, C. Bradley Moore, JCP, 52, 1005 (1970).
D_2O	"
HDO	"
Ar	G. Kamimoto, H. Matsui, JCP, 53, 3990 (1970).
SF_6	J.C. Stephenson, C. Bradley Moore, JCP, 52, 2333 (1970).
C_2H_4	"
$BC\ell_3$	"
CH_3F	"
$CH_3C\ell$	"
CH_3Br	"
CH_3I	"
Ar, Ne	J.C. Stephenson, R.E. Wood and C. Bradley Moore, JCP, 54, 3097 (1971).

RELAXATION TIMES AT ROOM TEMPERATURE FOR

$CO_2(001) + AB(v=0) \rightarrow CO_2(001) + AB(v=1)$

J. C. Stephenson, AVCO Corporation

AB	τ (sec-atm)
HBr	4.74×10^{-9}
HI	6.33×10^{-9}
HCℓ	1.54×10^{-8}
DCℓ	1.32×10^{-8}
DBr	2.54×10^{-7}
DI	1.03×10^{-6}
^{14}NO	2.29×10^{-6}
^{15}NO	2.30×10^{-6}
$^{14}N_2$	6.78×10^{-8}
$^{15}N_2$	9.25×10^{-8}
^{12}CO	2.16×10^{-7}
^{13}CO	8.47×10^{-7}

AB = DCℓ

T	τ (sec-atm)
300°K	1.32×10^{-8}
390°K	1.64×10^{-8}
630°K	2.78×10^{-8}

ATOM SOURCES

Y. S. Liu, R. A. McFarlane and
G. J. Wolga

To provide atomic species for use in laser systems employing exothermic reactions of the type

$$A + BC \rightarrow AB^{*} + C$$

the molecules A_2 is usually dissociated in an electrical discharge source consisting of one of

(a) C. W. direct current discharge between internal metal electrodes.
(b) High current capacitor discharge.
(c) Microwave discharge in a resonant cavity.
(d) Electrodeless radio-frequency discharge.

Where relatively small flow rates of atomic hydrogen, nitrogen, oxygen or the several halides are required any of these sources is adequate.

In general however, d.c. discharges provide a smaller percentage of dissociation and can give rise to gas contamination because of the presence of metal electrodes. The high electric fields employed in capacitor discharge sources can be beneficial for dissociating molecular species requiring larger amounts of energy such as N_2 but the flow of atoms is not continuous in fast flow systems except under high repetition rate conditions.

The efficiency of atom production can be very high for radio-frequency sources, and generators operating at 10 - 30 MHz with kilowatt power levels have been applied with success. Efficient coupling of the available energy to the gas column is at best difficult, particularly under varying conditions of gas pressure and excitation level. Impedance mismatch between the r.f. generator and the gas column can give rise to substantial radiation of energy at the operating wavelength and high intensity r.f. fields can seriously influence the operation of optical detectors and electronic signal processing apparatus being used in the vicinity.

Similarly high efficiencies of atom production can be achieved with microwave excitation and the Evenson-Broida cavity driven by an 80 W c.w. S band magnetron has been widely applied. This type of source has the advantage of inherently clean operation -- a 1 cm. diameter quartz tube carrying the gas passes through the cavity -- and is capable of operating over a wide pressure range. Early measurements which we made on such a source for atomic oxygen production indicated that in a fast flow system the rate of atom production

was continuing to rise at the maximum available microwave operating power.

The availability of relatively inexpensive C.W. magnetrons capable of producing powers in excess of 1 kw. at 2450 MHz led to the discharge source shown in Figure 1. The microwave power tube is a Litton Type L-5001 normally employed for microwave heating and cooking. This tube is E-probe coupled to a section of 3" X 1½" C band waveguide and an adjustable shorting plunger is arranged to present the appropriate high impedance plane at the probe position. The waveguide size employed is smaller than normally used at 2,450 MHz but the cutoff wavelength of 15.2 cms. is more than adequate for an operating wavelength of 12.2 cms.

A 100 c.f.m. blower provides cooling for the anode fin structure and cathode terminals. The required heater power depends upon the operating power level because of back bombardment of the cathode. We have found that for D.C. anode currents between 500 ma. and 750 ma. a voltage of 4.3 volts as measured at the magnetron terminals and a heater current of 18 amperes is adequate. High voltage is supplied by a full wave three phase bridge rectifier power supply and no filtering is required as the inherent ripple on such a system is only about 4%. The rated power output to a flat load for anode currents of 500-750 ma. is 1300-1700 watts. No direct measurements have been made of the power delivered by the source to the gas column during operation. The absence of a substantial temperature rise of the fin structure suggests that 70-80% of the available power is deposited in the gas.

For initial studies of this source a quartz discharge tube 2 cm. I.D. was passed through the broad face of the waveguide section at an angle of 10° to the propagation direction. A microwave noise source waveguide section was used for these experiments and the quartz tube was simply substituted for the fluorescent lamp noise generator. The waveguide section was closed by a second adjustable shorting plunger.

During operation the high voltage is increased until the indicated anode current is within the range discussed above. For gas pressures in the range of 1 Torr a discharge will have been initiated by this time in the quartz tube, the exact point of onset being somewhat dependent upon the position of the second shorting plunger. This occurs of course because in the absence of gas breakdown the waveguide structure can be tuned as a resonant cavity near to the operating frequency. The attendant large E fields then lead to breakdown

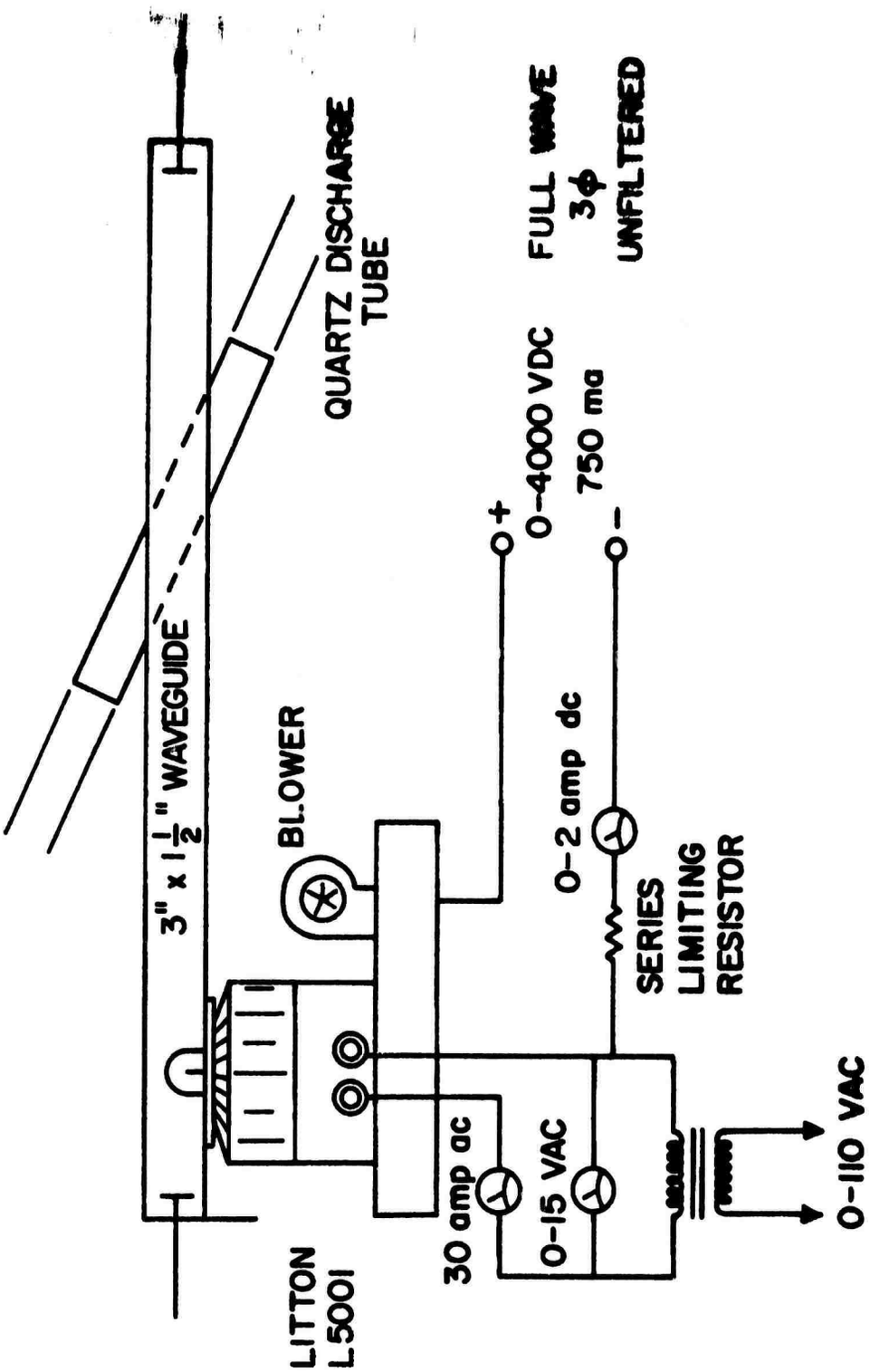
3" x 1 1/2" WAVEGUIDE
QUARTZ DISCHARGE TUBE
BLOWER
LITTON L5001
30 amp ac
0-15 VAC
0-2 amp dc
SERIES LIMITING RESISTOR
0+
0-4000 VDC
750 ma
0-
FULL WAVE 3φ UNFILTERED
0-110 VAC

FIGURE 1

in the quartz tube. The plunger position is not critical and once the discharge is operating, variation in its position has no effect. It is concluded therefore that little or no microwave energy is transmitted beyond the discharge tube after breakdown takes place. The angle of 10^{o} is sufficiently small that microwave power reflected from the discharge column back toward the magnetron should be unimportant. The only adjustment required therefore is the position of the first shorting plunger near the magnetron and it is simply set for maximum gas column brightness. Once set it needs no further adjustment.

Measurements were made to determine if leakage of microwave energy from such a high power source could present a hazard to any nearby experimenter. Where the discharge tube leaves the waveguide structure, radiation levels of 10 mw/cm^2 were detected, falling rapidly to less than 1 mw/cm^2 at a distance of six to eight inches. A second waveguide structure described below employs cylindrical metal tube sections beyond cutoff surrounding the quartz tube and even lower levels of radiation were found for that system. It is concluded that no hazard exists for normal operating procedures but the experimenter should be aware that 10 mw/cm^2 is an upper limit to avoid cornea damage and some caution should be exercised when viewing the discharge column at very close distances.

To evaluate the performance of the discharge source, measurements were made of the dissociation of molecular oxygen at pressures up to 2.3 Torr using initially a relatively low capacity pumping system. Gases were introduced into the discharge tube via Matheson Type 602 flowmeters and exhausted by a Precision Scientific pump with a rated speed of 6 litres/sec at 1 micron. Atomic oxygen concentration was measured at a point 50 cm. from the discharge region by titration with NO_2. The atomic oxygen flow rate is equal to the NO_2 flow rate required to cause the disappearance of the green fluorescence produced as a result of the second reaction below -

$$O + NO_2 \longrightarrow NO + O_2 \qquad (1)$$

$$NO + O \longrightarrow NO_2^{*} \longrightarrow NO_2 + h\nu \qquad (2)$$

At that time reaction (1) has removed all atomic oxygen and none is available for reaction (2).

It is known that the presence of helium or trace amounts of nitrogen can strongly influence the rate of atomic oxygen production and this is demonstrated

in Figure 2 where the production rate of atomic oxygen is shown as a function of the flow rate of molecular oxygen. Figure 3 shows that the pumping rate was essentially constant over the pressure range employed and Figure 4 shows the percent dissociation observed as a function of molecular oxygen flow rate.

The maximum atom production rate was 1.4×10^{20} atoms/sec. at a molecular oxygen pressure of 2.3 Torr and approximately 4 litres/sec. pumping speed. For a fixed pressure this will scale directly with pumping speed and a two order of magnitude increase should easily be obtained. The percentage of dissociation approached 20% at the higher pressures used. The excitation source will operate up to pressures of 10 Torr and additional increase of atom production rate should be possible at higher pressures than shown in Figure 3. However recombination effects will have to be considered as the pressure is increased and it is to be expected that an optimum pressure will be determined for any particular system.

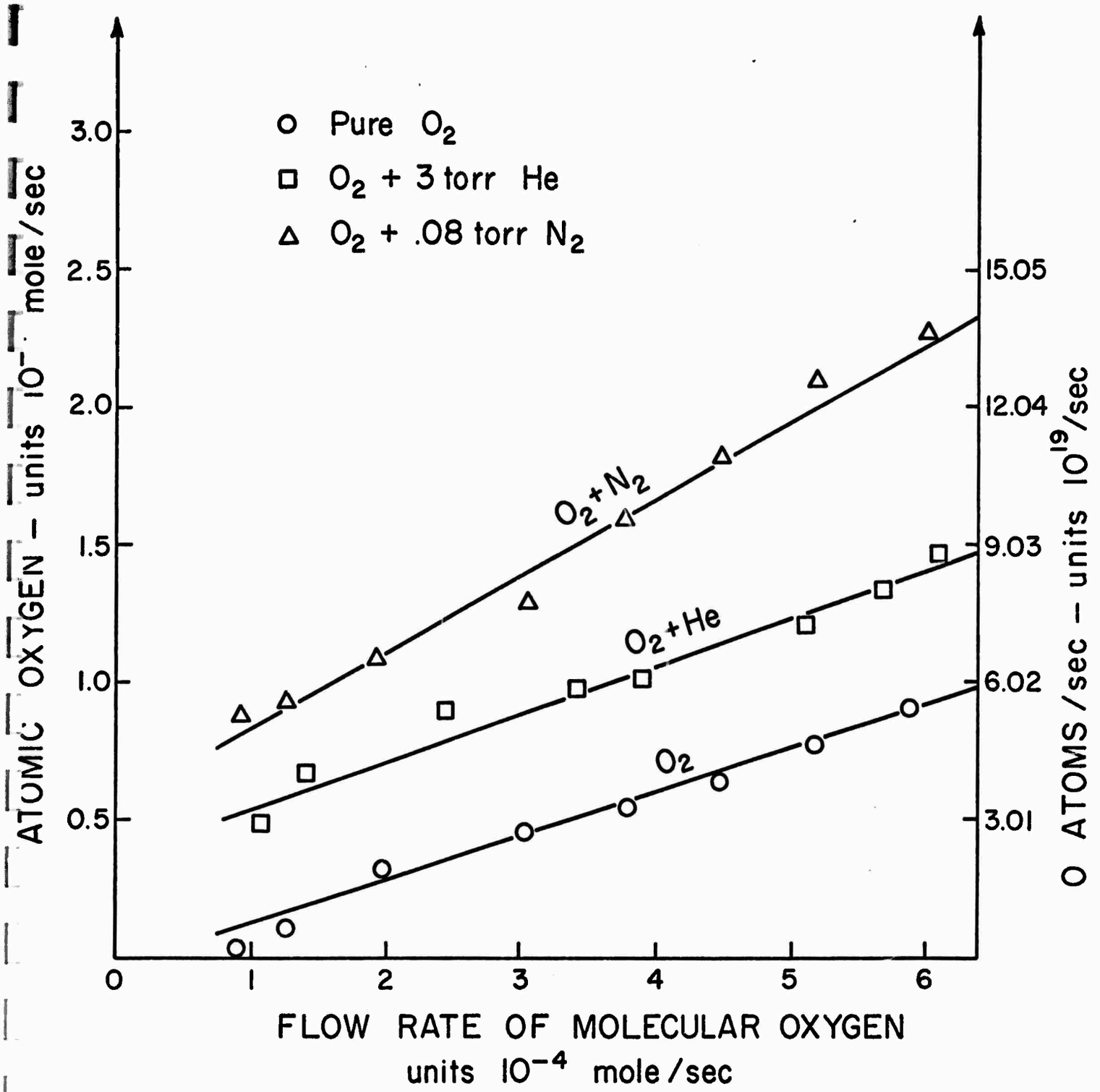
Pure O_2
O_2 + 3 torr He
O_2 + .08 torr N_2
O_2+N_2
O_2+He
O_2
ATOMIC OXYGEN – units 10^{-4} mole/sec
O ATOMS/sec – units 10^{19}/sec
3.0
2.5
2.0
1.5
1.0
0.5
0
15.05
12.04
9.03
6.02
3.01
1
2
3
4
5
6
FLOW RATE OF MOLECULAR OXYGEN
units 10^{-4} mole/sec

FIGURE 2

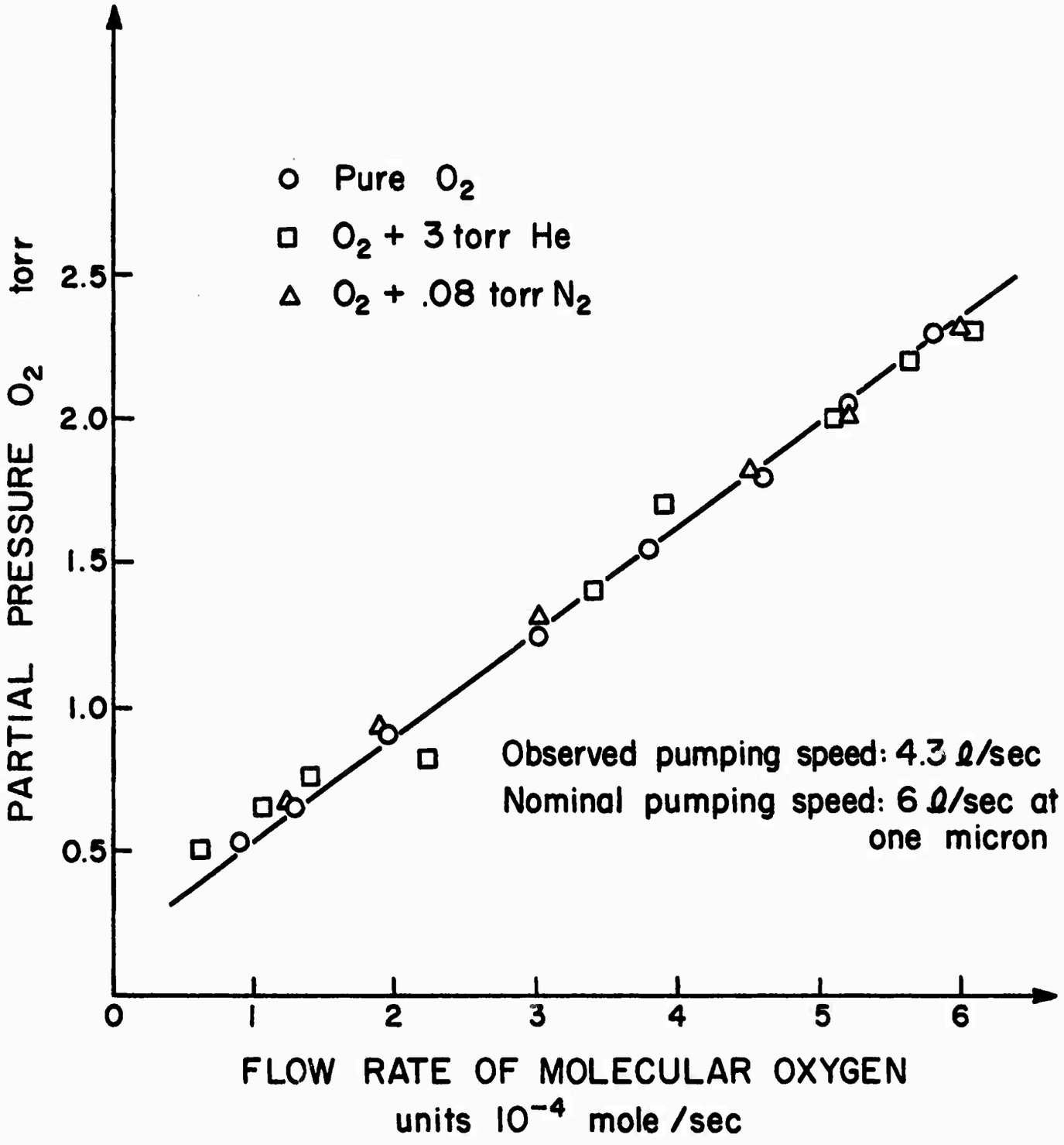
Pure O_2
O_2 + 3 torr He
O_2 + .08 torr N_2
PARTIAL PRESSURE O_2 torr
0.5
1.0
1.5
2.0
2.5
0
1
2
3
4
5
6
Observed pumping speed: 4.3 ℓ/sec
Nominal pumping speed: 6 ℓ/sec at one micron
FLOW RATE OF MOLECULAR OXYGEN
units 10^{-4} mole /sec

FIGURE 3

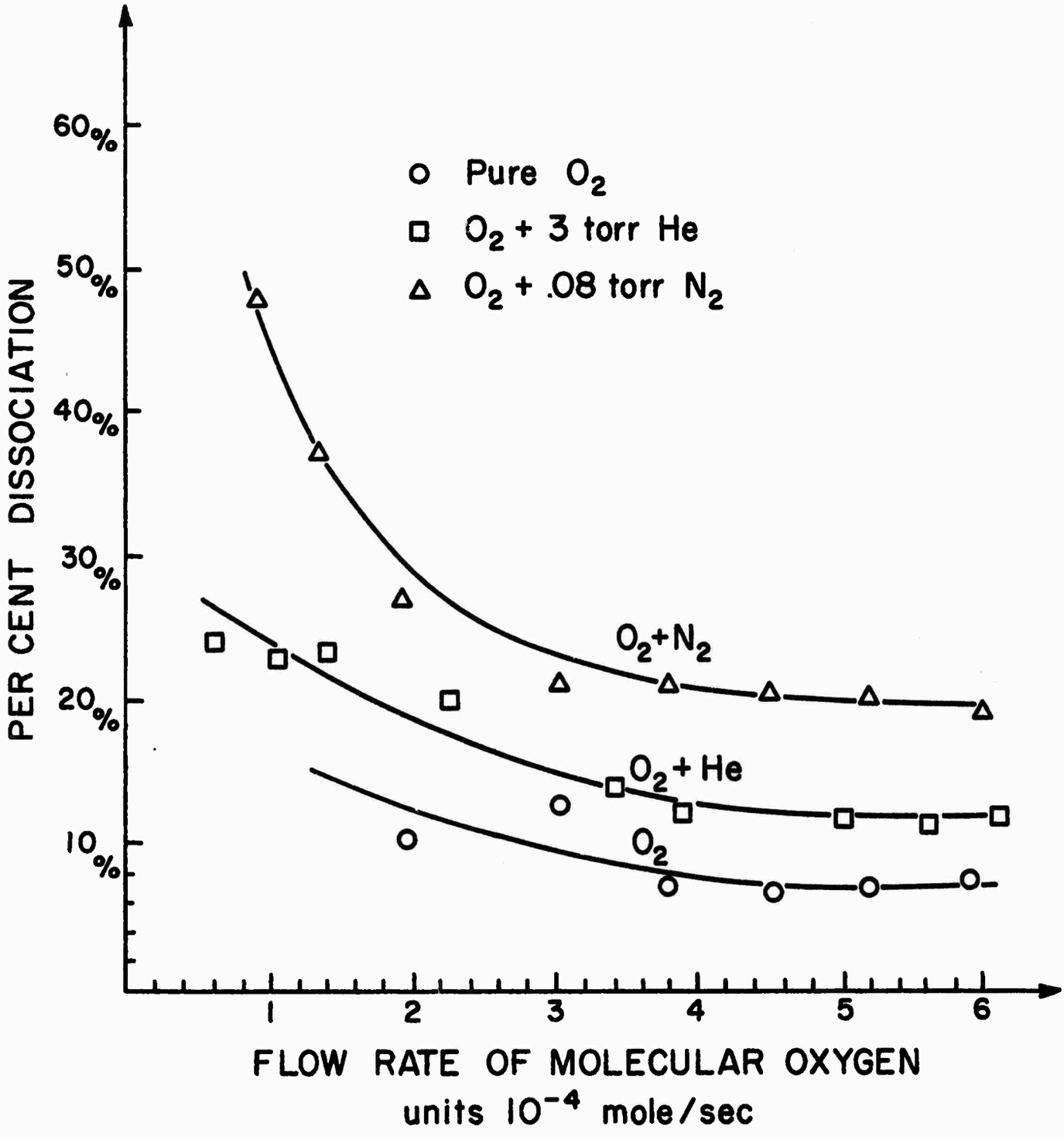
60%
50%
40%
30%
20%
10%
PER CENT DISSOCIATION
Pure O_2
O_2 + 3 torr He
O_2 + .08 torr N_2
O_2+N_2
O_2 + He
O_2
1
2
3
4
5
6
FLOW RATE OF MOLECULAR OXYGEN
units 10^{-4} mole/sec

FIGURE 4

NEW LASER SYSTEM STUDIES - C_2H_2 + O

Y. S. Liu, R. A. McFarlane and
G. J. Wolga

The capability of producing large flow rates of atomic oxygen makes possible the exploration of reactions which are sufficiently exothermic to allow the formation of vibrationally excited products which correspond to very high vibrational temperatures. If the rotational to vibrational temperature ratio can be maintained adequately small, partial inversion and laser oscillation can be established with the excited products. A particularly attractive candidate for the production of vibrationally excited carbon monoxide is the reaction of oxygen with acetylene. Recent measurements have been reported on infrared chemiluminescence for this system[1,2] at relatively low pressures (20-300 microns). The primary reactions are

$$O + C_2H_2 \longrightarrow CO + CH_2 + 51 \text{ kcal./mole} \qquad (1)$$

$$O + CH_2 \longrightarrow CO + 2H + 71 \text{ kcal./mole} \qquad (2)$$

for low fuel flows, and excitation of CO up to $v' = 14$ is observed. With increased fuel flow or the addition of H atoms, changes in vibrational distribution above $v' = 8$ occur and emission corresponding to $v' = 33$ has been identified.[1] This is ascribed to the reaction

$$O + CH \longrightarrow CO + H + 176 \text{ kcal./mole} \qquad (3)$$

and is clearly an additional potential source process for populating higher vibrational levels for utilization as initial laser states.

Measurements of the relative populations of the vibrational levels of the CO molecule which have been reported in the literature[2] indicate that at low pressures (25 microns) the population of levels up to $v' = 13$ can be characterized by a Boltzmann distribution with a vibrational temperature of approximately 7500°K. Above $v' = 13$ the population fell off more rapidly with vibrational quantum number but could be enhanced by operation at higher pressures (150 microns). The result can be understood in terms of a preferential V-V pumping mechanism examined by Rich, Watt and Thomson and shown to be of crucial importance in electrically excited CO lasers.[3] A striking increase in the population of higher vib-

rational levels was observed by Thrush and co-workers[1] with fuel rich mixtures and this can be interpreted as a direct consequence of V-V pumping at increased levels of CO* concentration. The data for fuel lean and fuel rich operation were analysed by Thrush to show that in the latter case a non equilibrium distribution of population was present in CO* for vibrational levels higher than $v' \cong 13$. This corresponds directly to the appearance of the plateau in the $N_{v'}$ versus v' curve in the analysis of Rich, Watt and Thomson.[3]

If it were possible to obtain a sufficiently high "local" vibrational temperature characterizing adjacent vibrational levels while maintaining a low rotational temperature, laser oscillation could be obtained in the chemically formed CO species. Vibrational temperatures near 8000°K for $v' = 8,9$ have been determined for the electrical CO laser[3] increasing to greater than 20,000°K for vibrational levels above $v' = 13$. For laser oscillation near 5.2 microns ($v' = 8,9$) the required vibrational temperatures are apparently available from the $O + C_2H_2$ reaction. There are however other temperatures which must be examined and controlled.

The V-V pumping rates decrease with increasing translational temperature[3] and losses due to V-T processes increase. It will be necessary therefore to operate at the lowest possible translational temperatures in such a laser and it is expected that the addition of helium can be used to lower the translational and rotational temperatures by increasing the rate of heat conduction to the tube walls. While CO*-He collisions will contribute additional V-T losses the effect is expected to be small in comparison with the enhancement due to the lowering of $T_{trans.}$ and $T_{rot.}$

A series of measurements has been undertaken to examine the $O + C_2H_2$ reaction in a laser configuration as shown in Figure 1. Atomic oxygen is formed in the source described above using a 3 cm. I.D. quartz discharge tube and the acetylene is injected radially into the flow in a teflon reaction tube 18" long and with a $\frac{1}{2}$" central bore. A laser cavity is formed by two gold mirrors and output coupling is provided by a 1 mm central hole in one of the mirrors. Slots in the teflon tube permit observation of the IR emission from the chemically formed excited species. The system is pumped with a 100 cfm blower backed by a Model 1397B Welch forepump.

Measurements of atomic oxygen production rate in this system were essentially in agreement with observations on the smaller source. To avoid

A SCHEMATIC DIAGRAM OF THE EXPERIMENTAL SET UP:

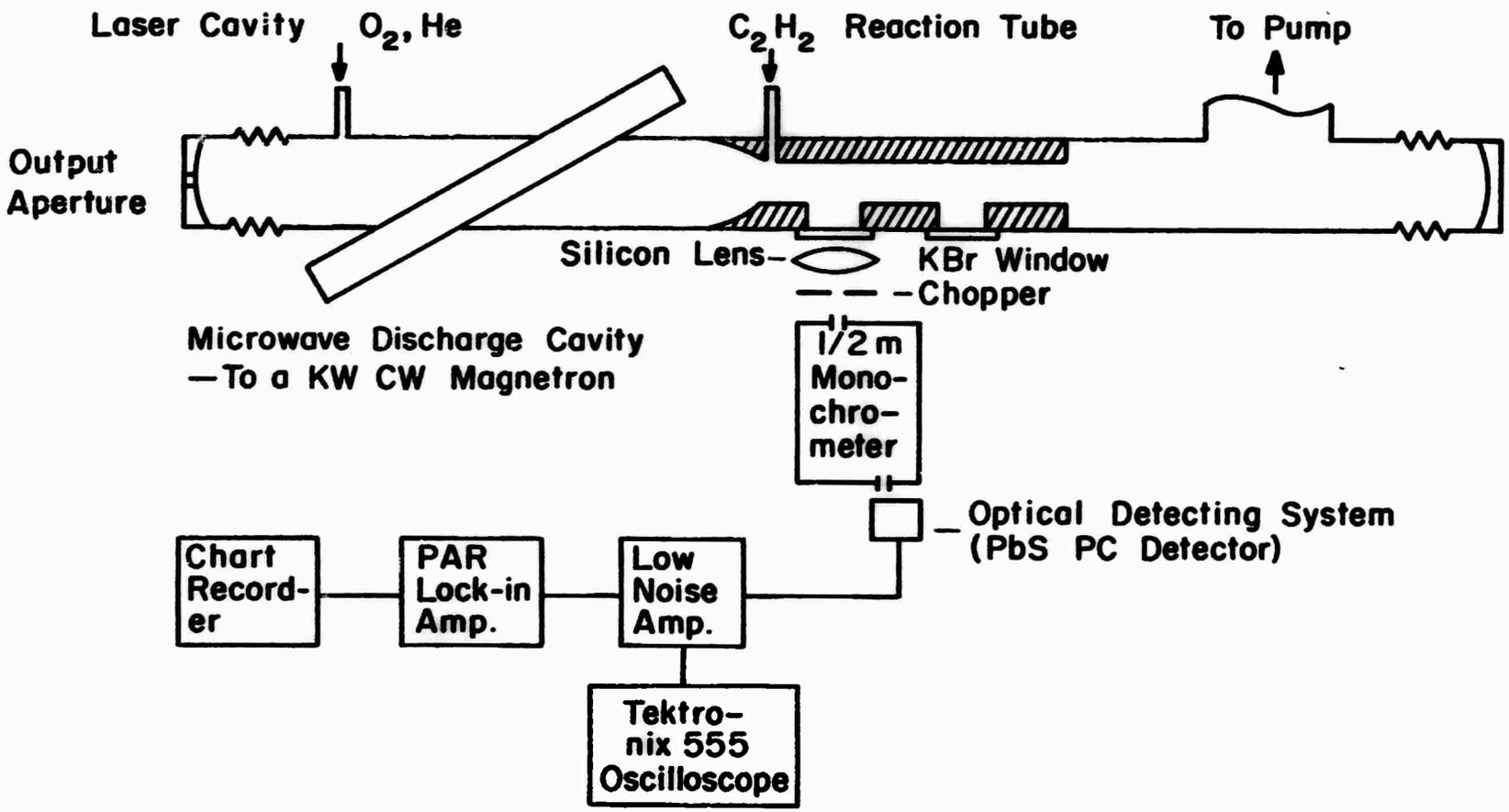

FIGURE 1

the influence of vibrationally excited nitrogen on the chemiluminescence studies, trace amounts of hydrogen were substituted for the nitrogen previously employed to enhance the dissociation of O_2. Figures 2 and 3 summarize the performance with hydrogen. The long narrow-bore reaction channel limited the pumping speed to about one-third the capacity of the pump system and rates of 13 litres/sec were observed at the location of the pressure tap in the reaction tube. This corresponds to a flow velocity of 83 meters/second.

The optical detection system consists of a Jarrell-Ash one-half meter Ebert monochromator employing several detectors--a room temperature lead sulphide photoconductive detector, a liquid N_2 cooled InSb photovoltaic detector and a liquid N_2 cooled Au:Ge photoconductive detector. Radiation from the reaction tube is focused with a silicon lens through a 400 c.p.s. chopper onto the entrance slit of the monochromator and the detector output is amplified by a Keithley Model 103 Low Noise Amplifier. The signal is synchronously detected using the chopper as reference with a Princeton Applied Research Model JB-5 Lock-in amplifier.

The spectrometer employs a grating with 105 lines/mm blazed at 8.6 μ in first order. It was intended to observe the CO fundamental spectral region in first and second order, isolated by a 4 micron long-pass filter. The measured spectrum and a 600°C blackbody response is shown in Fig. 4. No well defined features attributable to the CO fundamental are apparent. These would be expected to fall in the spectral region 4.6 - 4.9 microns. The spectrometer slit width of 1.5 mm. should permit the resolution of features approximately .025 μ apart. A similar failure to observe a structural spectral feature due to the CO fundamental was experienced when operating in second order of the spectrometer and in first order at one-half the initial slit width. It is concluded that in addition to any CO fundamental emission present, there was also present a broadband emission of substantial intensity throughout this region. The 4 micron long pass filter distorted the apparent intensity at short wavelengths on the scan shown. Radiation is present however out to at least 6.5 microns and other scans have shown similar emission at wavelengths down to below 3.5 microns. As dry nitrogen was used to flush the spectrometer and all external optical paths, little or no water vapour absorption is apparent on the blackbody scan. There does appear however, against the broadband radiation from the

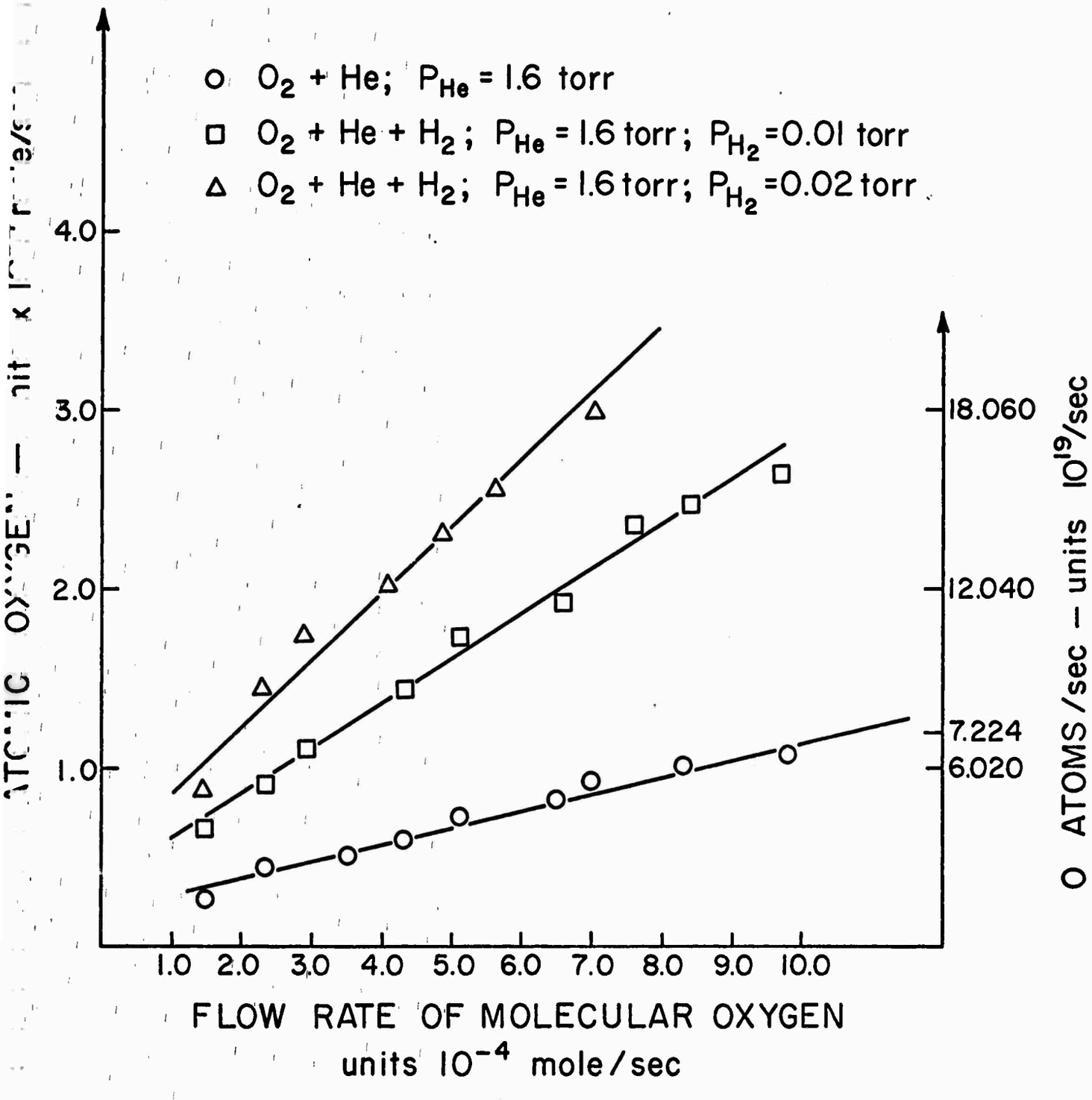
O O_2 + He; P_{He} = 1.6 torr
□ O_2 + He + H_2; P_{He} = 1.6 torr; P_{H_2} = 0.01 torr
△ O_2 + He + H_2; P_{He} = 1.6 torr; P_{H_2} = 0.02 torr
4.0
3.0
2.0
1.0
18.060
12.040
7.224
6.020
O ATOMS/sec – units 10^{19}/sec
1.0 2.0 3.0 4.0 5.0 6.0 7.0 8.0 9.0 10.0
FLOW RATE OF MOLECULAR OXYGEN
units 10^{-4} mole/sec

FIGURE 2

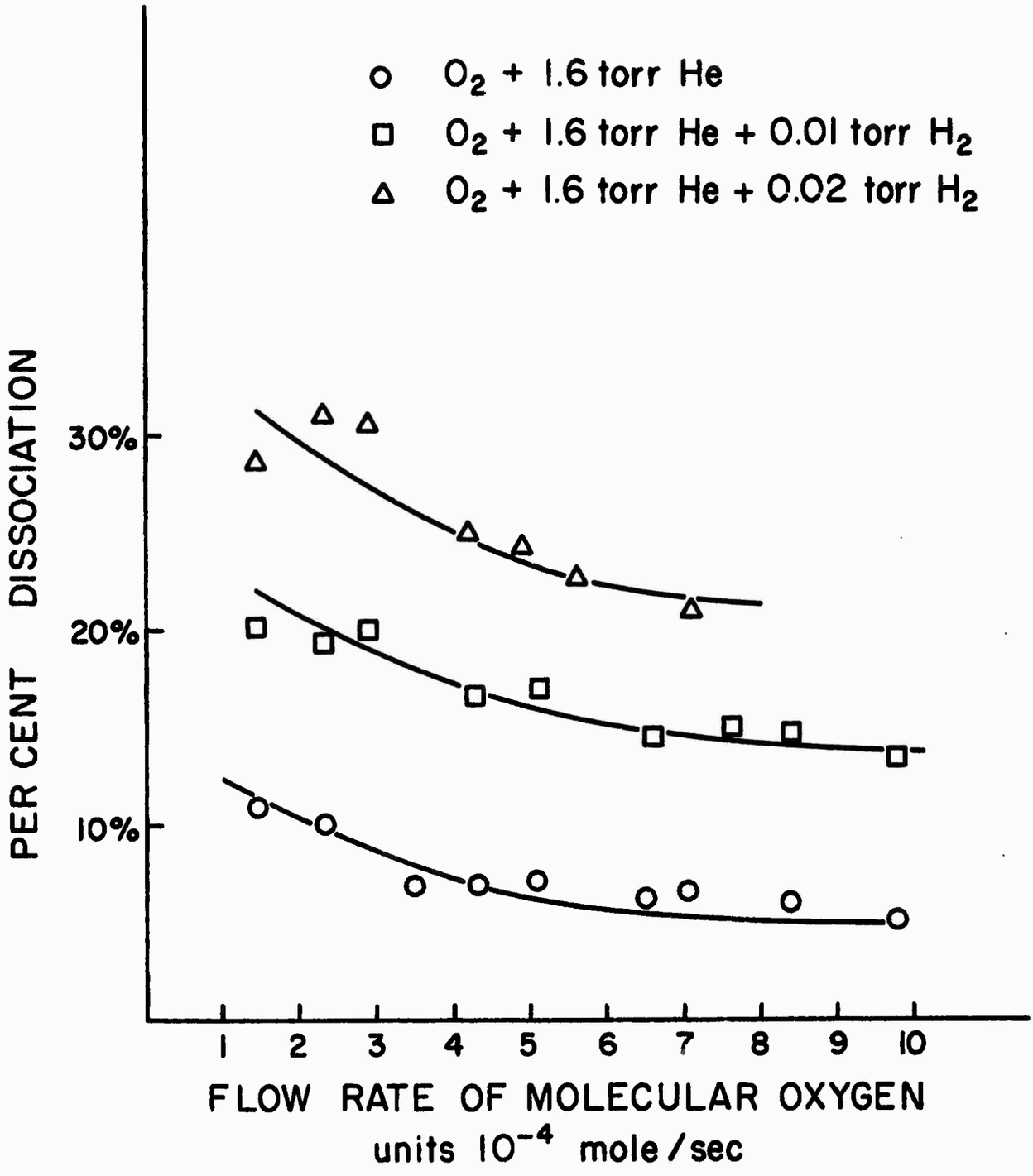
○ O_2 + 1.6 torr He
□ O_2 + 1.6 torr He + 0.01 torr H_2
△ O_2 + 1.6 torr He + 0.02 torr H_2
PER CENT DISSOCIATION
30%
20%
10%
1 2 3 4 5 6 7 8 9 10
FLOW RATE OF MOLECULAR OXYGEN
units 10^{-4} mole/sec

FIGURE 3

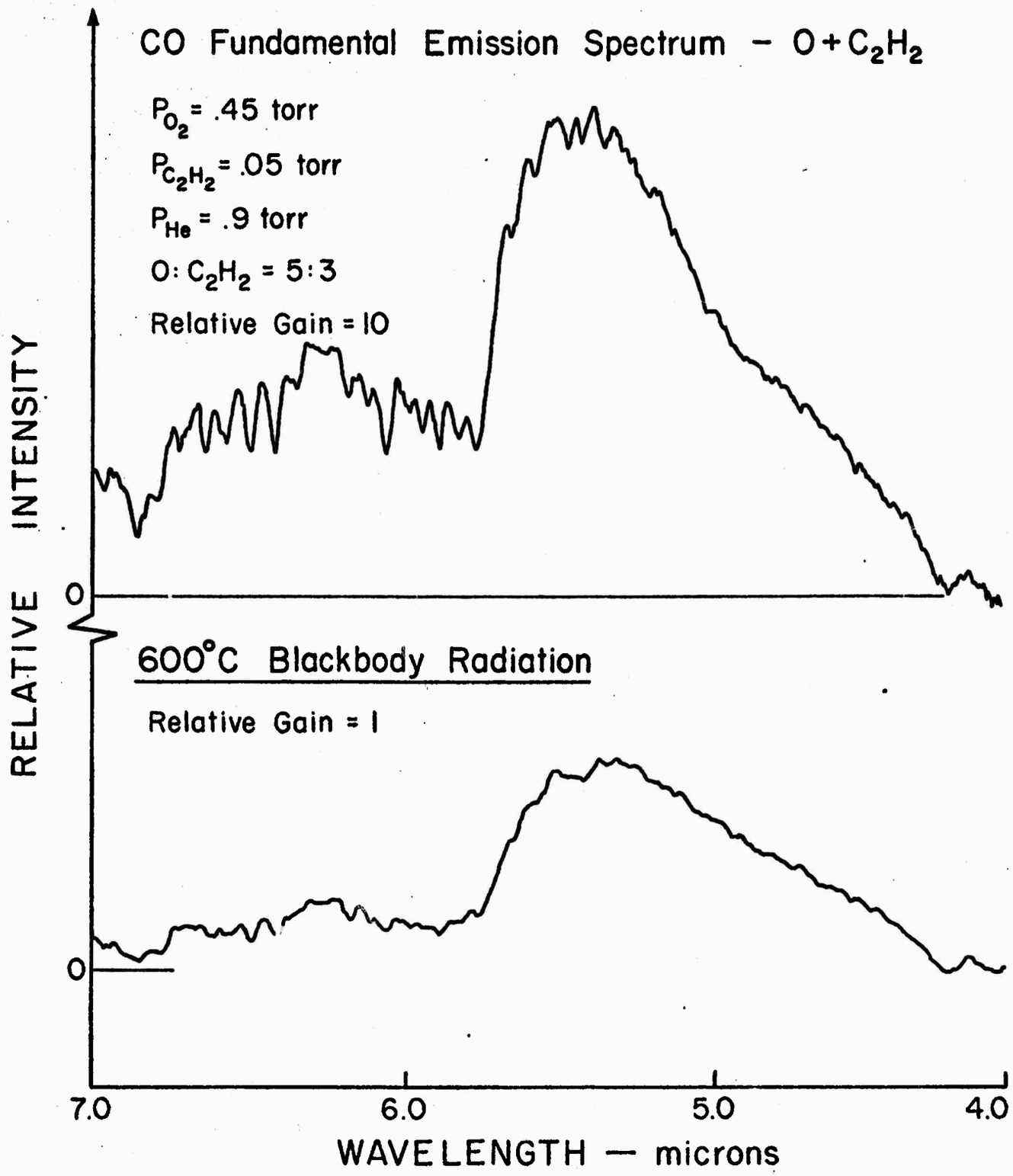
CO Fundamental Emission Spectrum – O+C2H2
PO2 = .45 torr
PC2H2 = .05 torr
PHe = .9 torr
O: C2H2 = 5:3
Relative Gain = 10
0
600°C Blackbody Radiation
Relative Gain = 1
0
RELATIVE INTENSITY
7.0
6.0
5.0
4.0
WAVELENGTH — microns

FIGURE 4

$O + C_2H_2$ reaction, sharp absorption features identifiable as due to water formed in the reaction. These features do exhibit the resolution estimated above. The source of this excess radiation has not been identified for the present experiment but makes extremely difficult any determination of vibrational population distribution based on observations of CO fundamental emission. It is also true that significant absorption due to water could drastically modify the spectrum of any laser which might be operated based on the $O + C_2H_2$ reaction.

A series of spectral scans were made in the CO first overtone region in the vicinity of 2.5 microns using the spectrometer in third order. The spectral response was limited by a 2.3 micron long pass filter and the rapid decrease in sensitivity of the lead sulphide detector at wavelengths greater than 2.8 microns. This decrease will be seen to be unfortunate for the observation of the higher vibrational levels but the operation of the monochromator in third order required a long wavelength cutoff for unambiguous measurements.

Figure 5 shows a spectral scan for conditions where the oxygen dissociation was only about 10%, providing a ratio of oxygen atoms to fuel molecules of 2.3:1. The band centers for the indicated $\Delta v = 2$ transition are shown above the wavelength scale. Emission from $v' = 14$ is apparent although its relative intensity is distorted by the falling detector response. A computer program is being set up with temperature and population parameters to establish the relative distribution of CO* over the vibrational levels by comparing observed and synthetic spectra. At the present time this is not yet running but nevertheless a qualitative comparison of the overtone emission under a variety of conditions is significant.

The addition of a trace of H_2 to the oxygen source increased the dissociation to above 30% and the O/C_2H_2 ratio to 8:1. A twenty fold increase in overall signal level was observed as shown in Figure 6. There is a water vapour absorption structure in the vicinity of 2.58 and 2.68 microns but the disappearance of vibrational structure compared to that in Figure 5 indicates a substantial increase in rotational temperature, certainly in excess of $600^{\circ}K$. Lacking the synthetic spectra it is not possible to establish exactly any changes in the population of higher vibrational levels. Such changes in

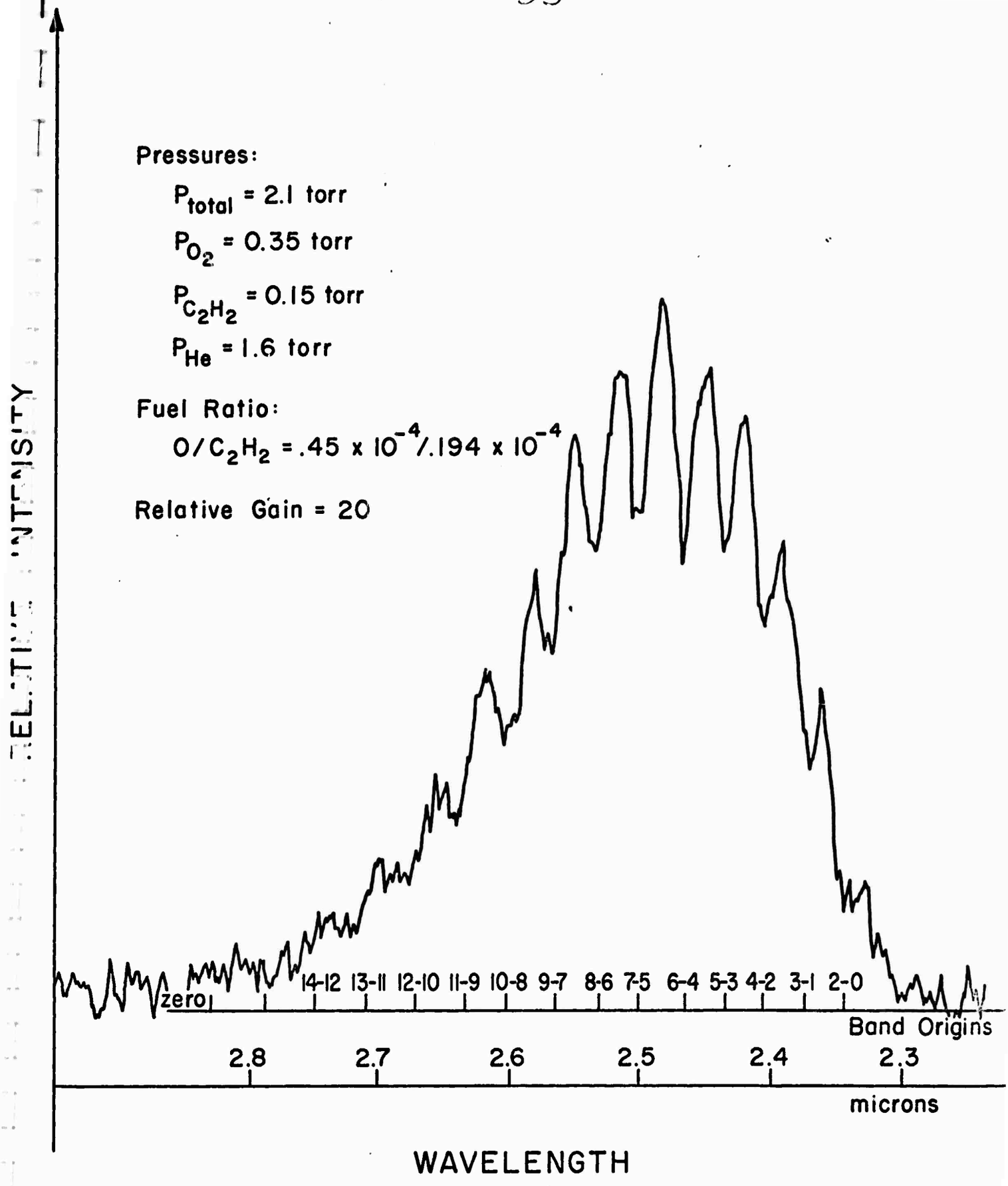
Pressures:
P_{total} = 2.1 torr
P_{O_2} = 0.35 torr
$P_{C_2H_2}$ = 0.15 torr
P_{He} = 1.6 torr
Fuel Ratio:
O/C_2H_2 = .45 x 10^{-4}/.194 x 10^{-4}
Relative Gain = 20
zero
14-12 13-11 12-10 11-9 10-8 9-7 8-6 7-5 6-4 5-3 4-2 3-1 2-0
Band Origins
2.8 2.7 2.6 2.5 2.4 2.3
microns
WAVELENGTH

FIGURE 5

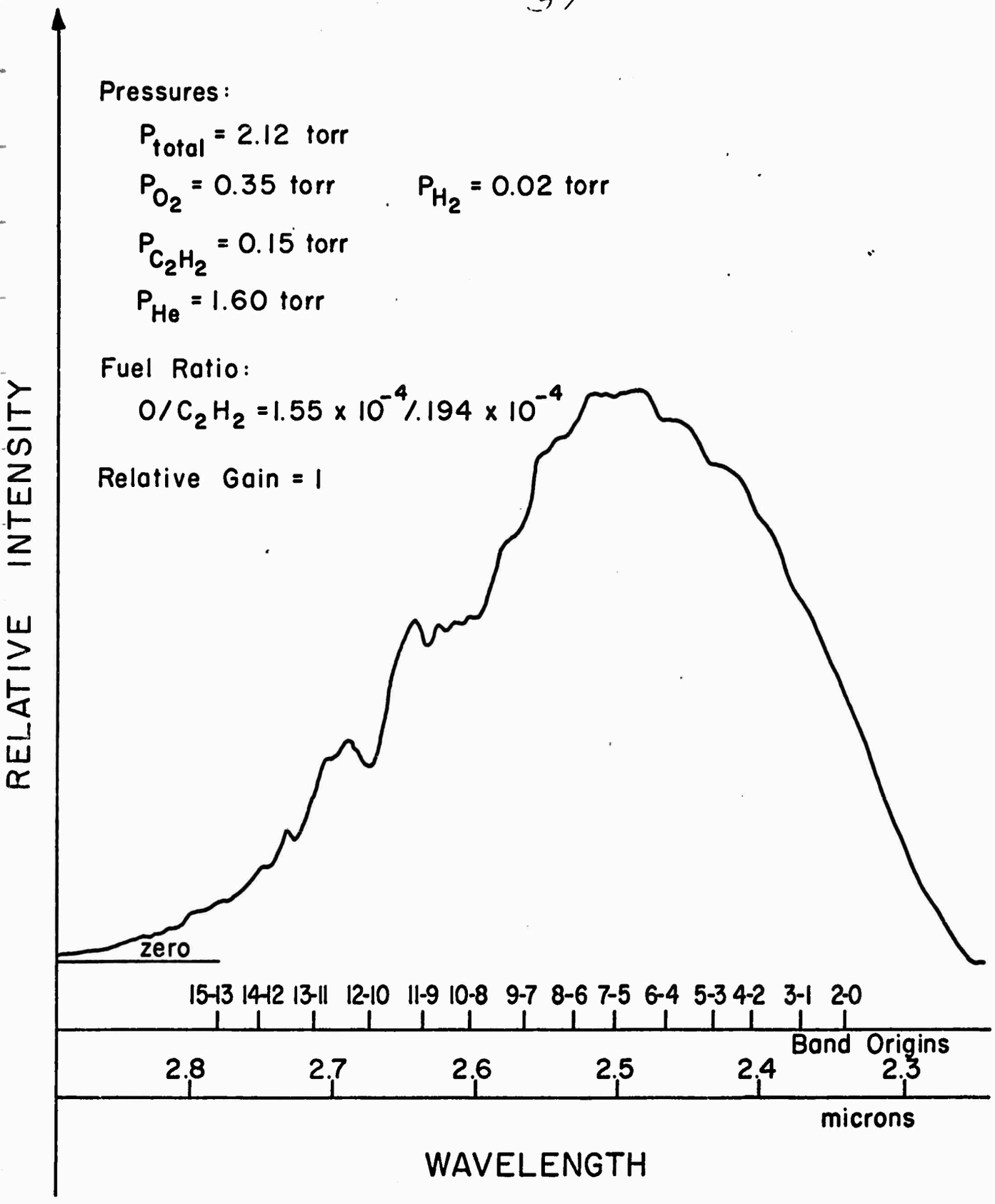
Pressures:
P_{total} = 2.12 torr
P_{O_2} = 0.35 torr
P_{H_2} = 0.02 torr
$P_{C_2H_2}$ = 0.15 torr
P_{He} = 1.60 torr
Fuel Ratio:
$O/C_2H_2 = 1.55 \times 10^{-4}/.194 \times 10^{-4}$
Relative Gain = 1
RELATIVE INTENSITY
zero
15-13 14-12 13-11 12-10 11-9 10-8 9-7 8-6 7-5 6-4 5-3 4-2 3-1 2-0
Band Origins
2.8 2.7 2.6 2.5 2.4 2.3
microns
WAVELENGTH

FIGURE 6

relative population do not appear to be large as judged from a comparison of Figures 5 and 6 at the longer wavelengths.

Figure 7 shows that an increase in He pressure from 1.6 Torr to 3.1 Torr lowers the rotational temperature as expected, with little effect on the vibrational distribution. The overall signal level has however decreased an order of magnitude compared to Figure 6.

Figure 8 shows that an increase in fuel flow by a factor of three over the conditions in Figure 7 increases the overall signal level by a factor of 2 compared to Figure 6 and increases slightly the rotational temperature. More significant is the increase in relative emission from vibrational levels with v' = 9 and greater. The increase is substantial for v' > 12 and is indicative of the plateau in the $N_{v'}$ versus v' dependence mentioned above. Such a distribution is exactly that found for electrically excited CO lasers. It is to be expected that optical gain should be present under operating conditions similar to those employed in the experiment of Figure 7 if a further decrease of T_{trans} and T_{rot} could be brought about. This might be accomplished by liquid N_2 cooling of the reaction chamber or more directly by employing a supersonic expansion of the reaction products. Calculations will be initiated shortly to examine this latter possibility.

References

1) P. N. Clough, S. E. Schwartz and B. A. Thrush. Proc. Roy. Soc. Lond. A 317, 575, 1970.

2) D. M. Creek, C. M. Melliar - Smith and Neville Jonathan. J. Chem Soc - 646, 1970.

3) J. W. Rich, W. S. Watt, and H. M. Thomson. Technical Report AFAL-TR-71-152 Air Force Avionics Laboratory, Wright-Patterson Air Force Base, Ohio, March 1971.

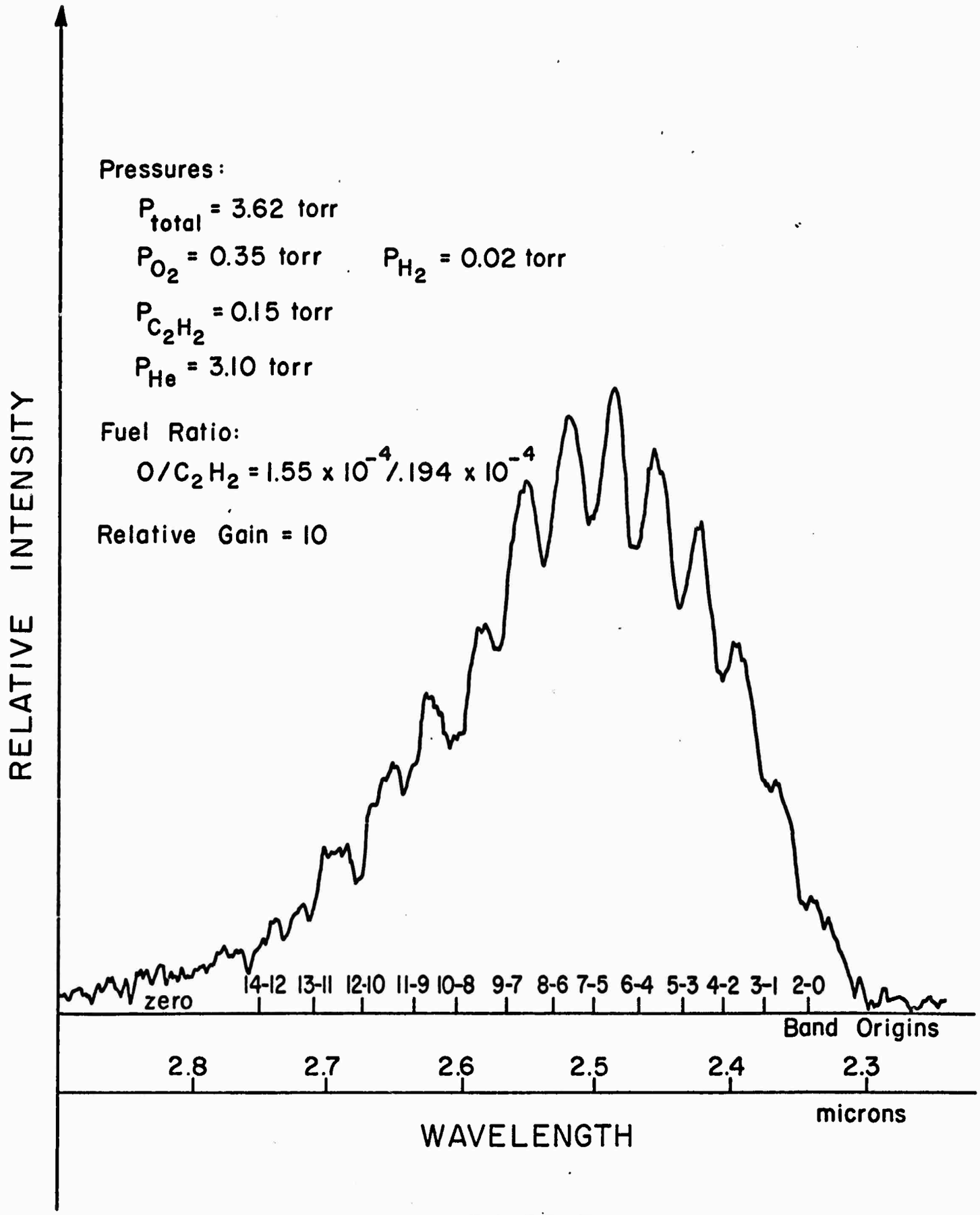
Pressures:
P_{total} = 3.62 torr
P_{O_2} = 0.35 torr
P_{H_2} = 0.02 torr
$P_{C_2H_2}$ = 0.15 torr
P_{He} = 3.10 torr
Fuel Ratio:
$O/C_2H_2 = 1.55 \times 10^{-4}/.194 \times 10^{-4}$
Relative Gain = 10
RELATIVE INTENSITY
zero
14-12 13-11 12-10 11-9 10-8 9-7 8-6 7-5 6-4 5-3 4-2 3-1 2-0
Band Origins
2.8 2.7 2.6 2.5 2.4 2.3
microns
WAVELENGTH

FIGURE 7

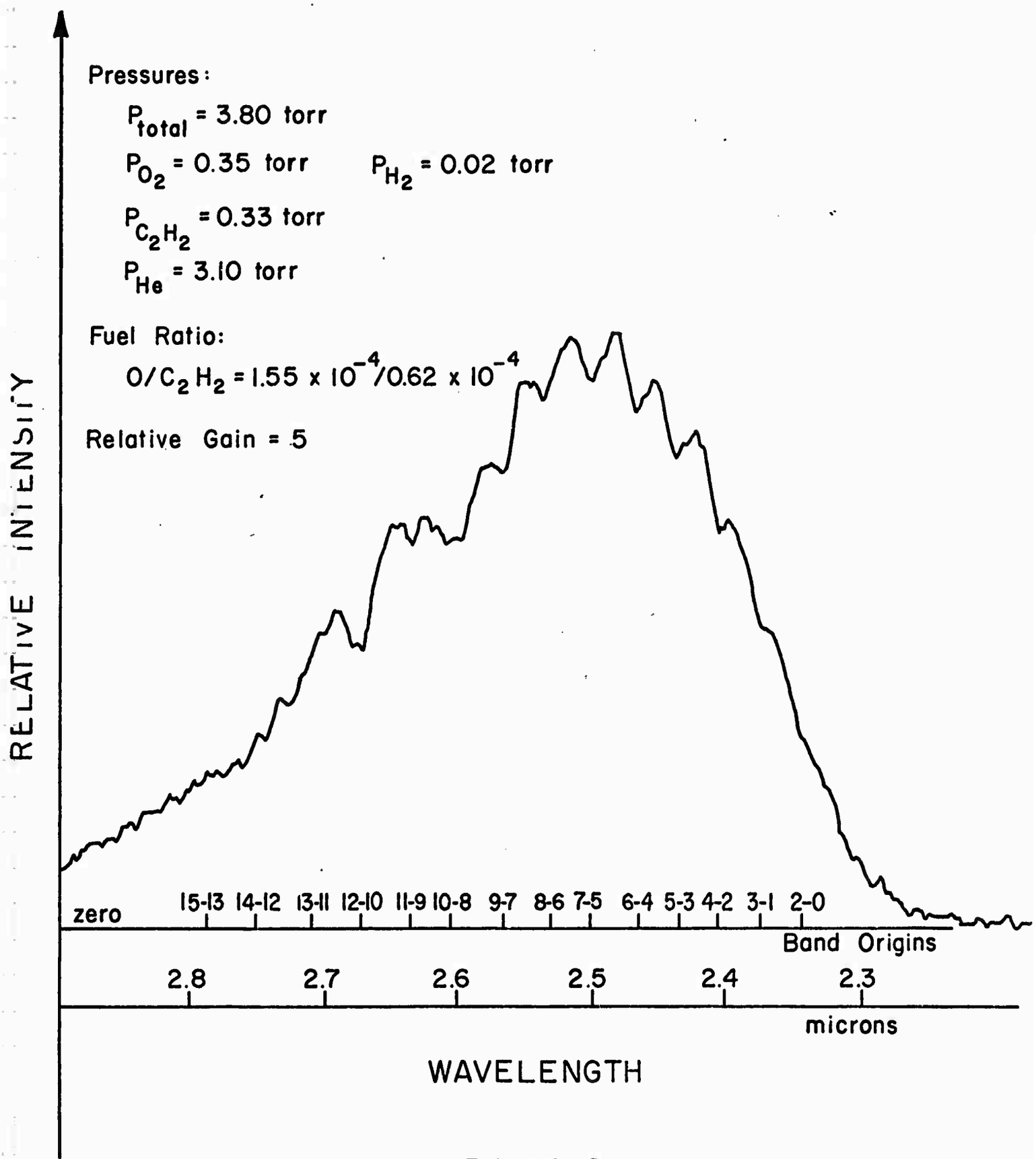
Pressures:
P_{total} = 3.80 torr
P_{O_2} = 0.35 torr
P_{H_2} = 0.02 torr
$P_{C_2H_2}$ = 0.33 torr
P_{He} = 3.10 torr
Fuel Ratio:
$O/C_2H_2 = 1.55 \times 10^{-4}/0.62 \times 10^{-4}$
Relative Gain = 5
RELATIVE INTENSITY
zero
15-13 14-12 13-11 12-10 11-9 10-8 9-7 8-6 7-5 6-4 5-3 4-2 3-1 2-0
Band Origins
2.8 2.7 2.6 2.5 2.4 2.3
microns
WAVELENGTH

FIGURE 8

MECHANISMS IN THE CS_2 + O REACTION

S. H. Bauer, S. Tsuchiya, and N. Nielsen

A longitudinally excited pulse discharge has been set up in a 1" I.D. glass tube, about one meter in length, for the study of the $CS_2 + O_2$ reaction in a flow system. The laser output is controlled with a grating with sufficient resolution so that individual rotation-vibration lines can be observed. The block diagram for the set up is given in Figure 1. Dr. Tsuchiya and Mr. Nielsen measured the dependence of total power produced on the following parameters: CS_2, O_2 and He pressures for a range of exciting voltages. The half widths of the pulses range from 0.3 to 4.0 μ sec. The current is measured by the voltage drop across a resistor of 0.27-40 ohms, depending on the current levels, which range from 5 to 500 amps. Plots that show the effect of oxygen pressure on the integrated power for various voltages are shown in Figure 2. Similar graphs were obtained by varying the CS_2 and He pressures. For example, the laser power increases monotonically with CS_2 content for voltages higher than about 9 Kv. The laser pulses appear 20-250 μ sec. after the discharge. In the O_2 rich case the power peaks rapidly and then decreases in an oscillatory manner. These oscillations have been correlated with sound speeds appropriate for the gas mixture, for waves propagating in a direction perpendicular to the tube axis. The distribution of laser light intensity over the various vibrational transitions is shown in Figure 3, for three peak voltages. The intensity was integrated over a period of about 10 seconds in these measurements.

About 100 lines have been observed and assigned to their respective vibration-rotation transitions covering the range Δv(14-13) to (2-1). Of most interest are the measurements of delay in lasing subsequent to pulse initiation, as dependent on the vibrational transition (for three rotational lines); this is shown in Figure 4. It is anticipated that these data plus the relative intensities of chemiluminescent

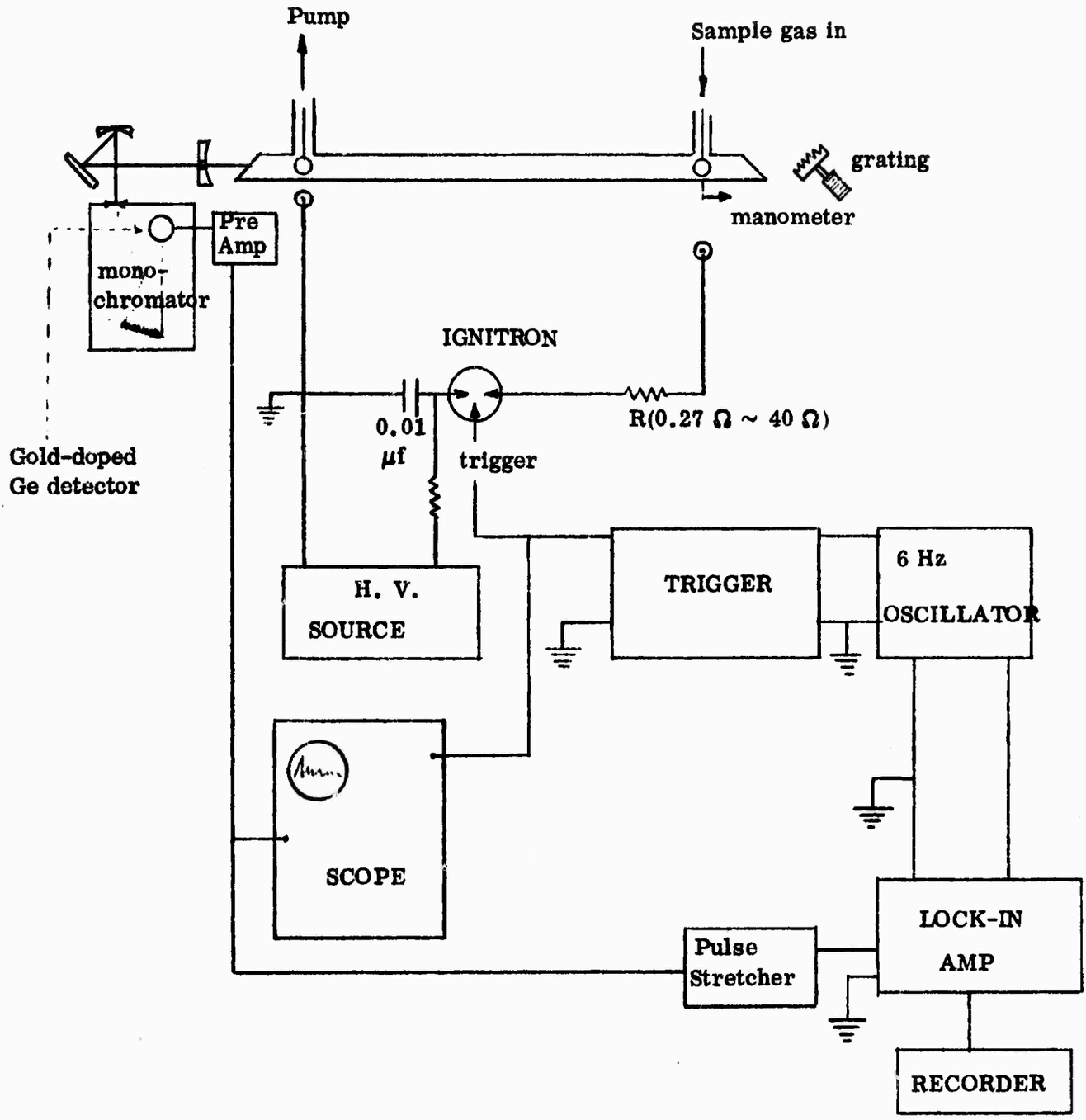

BLOCK DIAGRAM

FIGURE 1

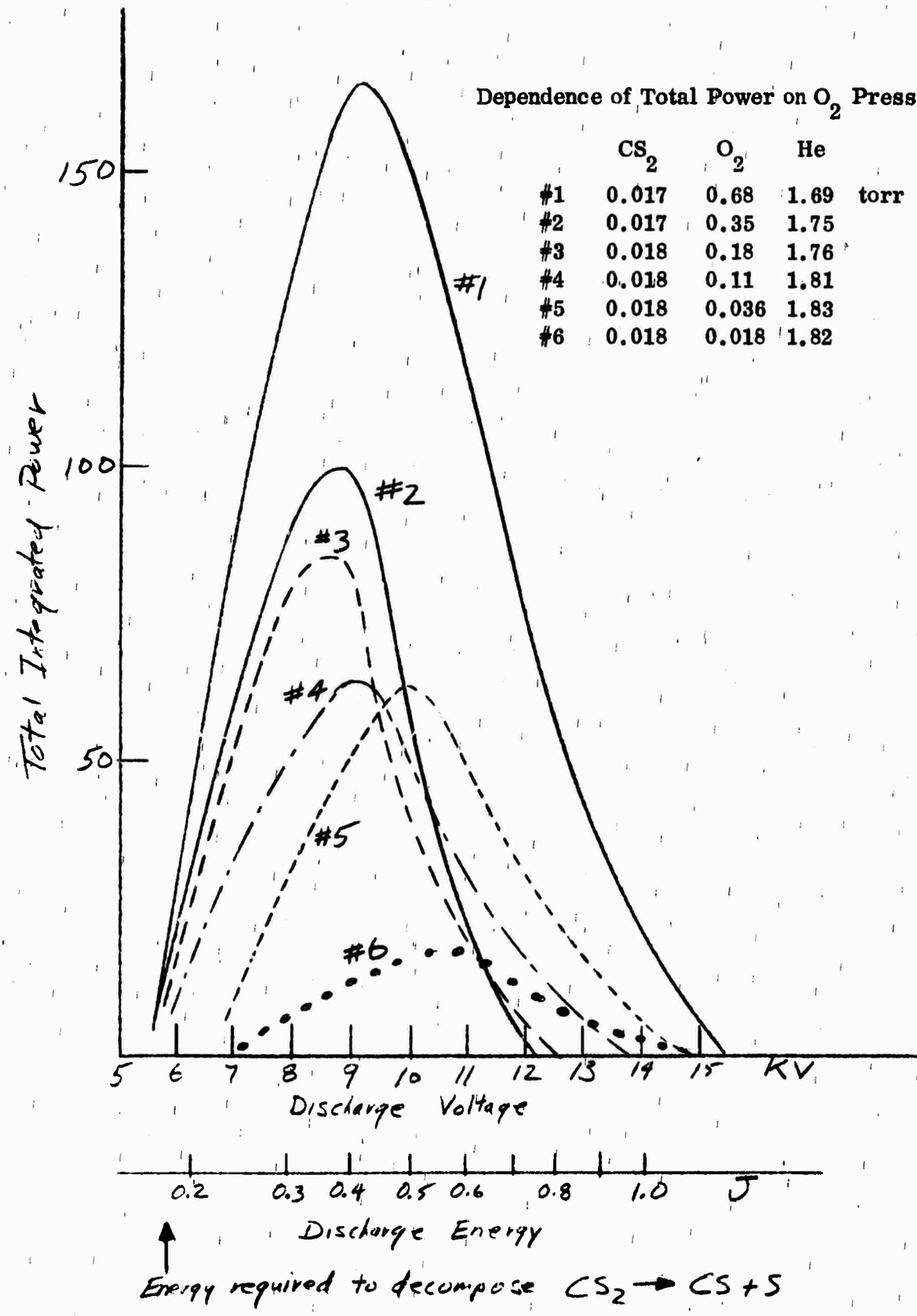
Dependence of Total Power on O_2 Pressure
CS_2 O_2 He
#1 0.017 0.68 1.69 torr
#2 0.017 0.35 1.75
#3 0.018 0.18 1.76
#4 0.018 0.11 1.81
#5 0.018 0.036 1.83
#6 0.018 0.018 1.82
Total Integrated Power
150
100
50
#1
#2
#3
#4
#5
#6
5 6 7 8 9 10 11 12 13 14 15 KV
Discharge Voltage
0.2 0.3 0.4 0.5 0.6 0.8 1.0 J
Discharge Energy
Energy required to decompose $CS_2 \rightarrow CS + S$

FIGURE 2

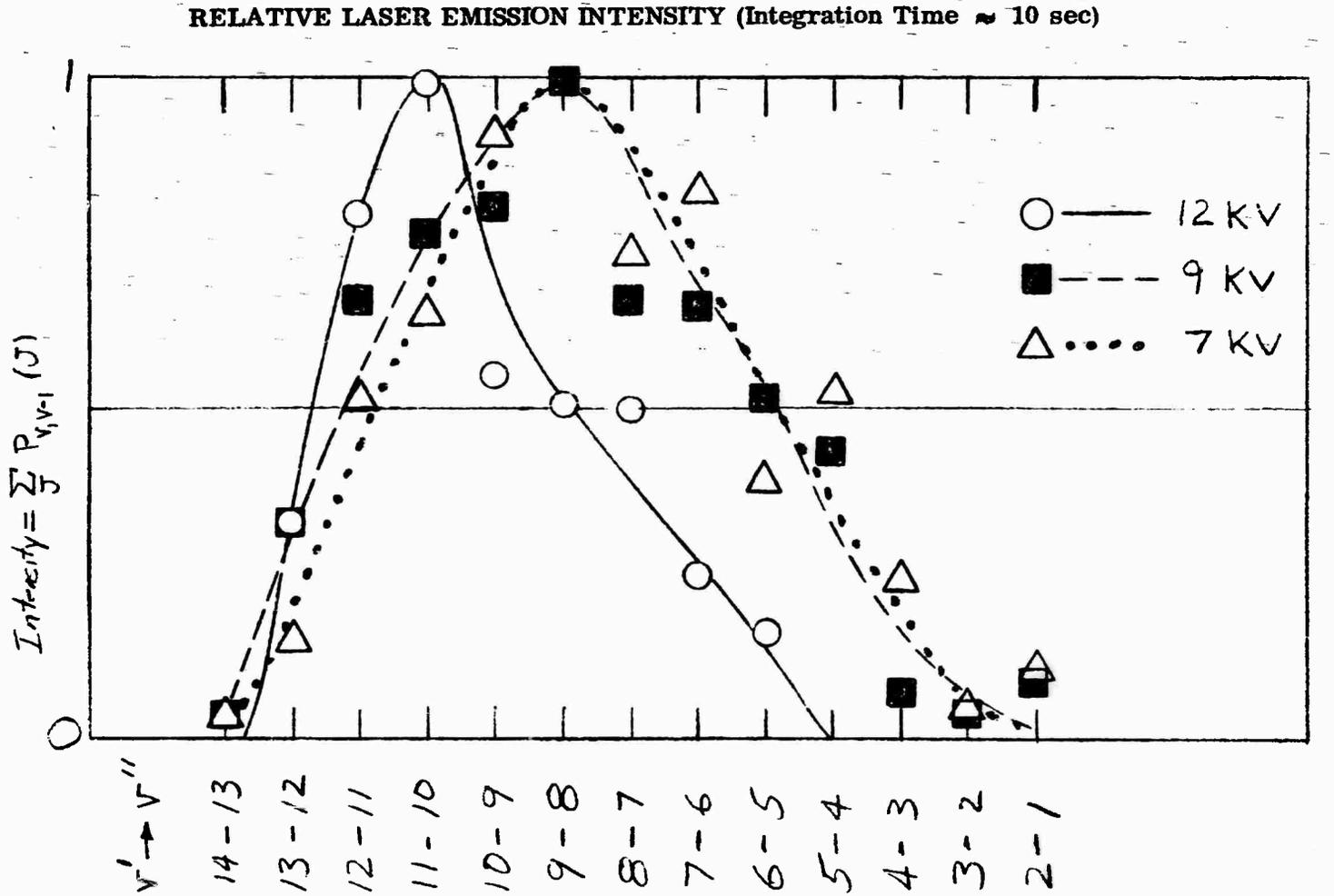
RELATIVE LASER EMISSION INTENSITY (Integration Time ≈ 10 sec)
Intensity = $\sum_J P_{v,v-1}(J)$
1
0
12 KV
9 KV
7 KV
v' → v''
14-13
13-12
12-11
11-10
10-9
9-8
8-7
7-6
6-5
5-4
4-3
3-2
2-1
CS2 0.017 torr
O2 0.68
He 1.69
Total pressure 2.39 torr
Flow speed: 10m/sec

FIGURE 3

DELAY (AFTER PULSE INITIATION) --- GRATING IN CAVITY

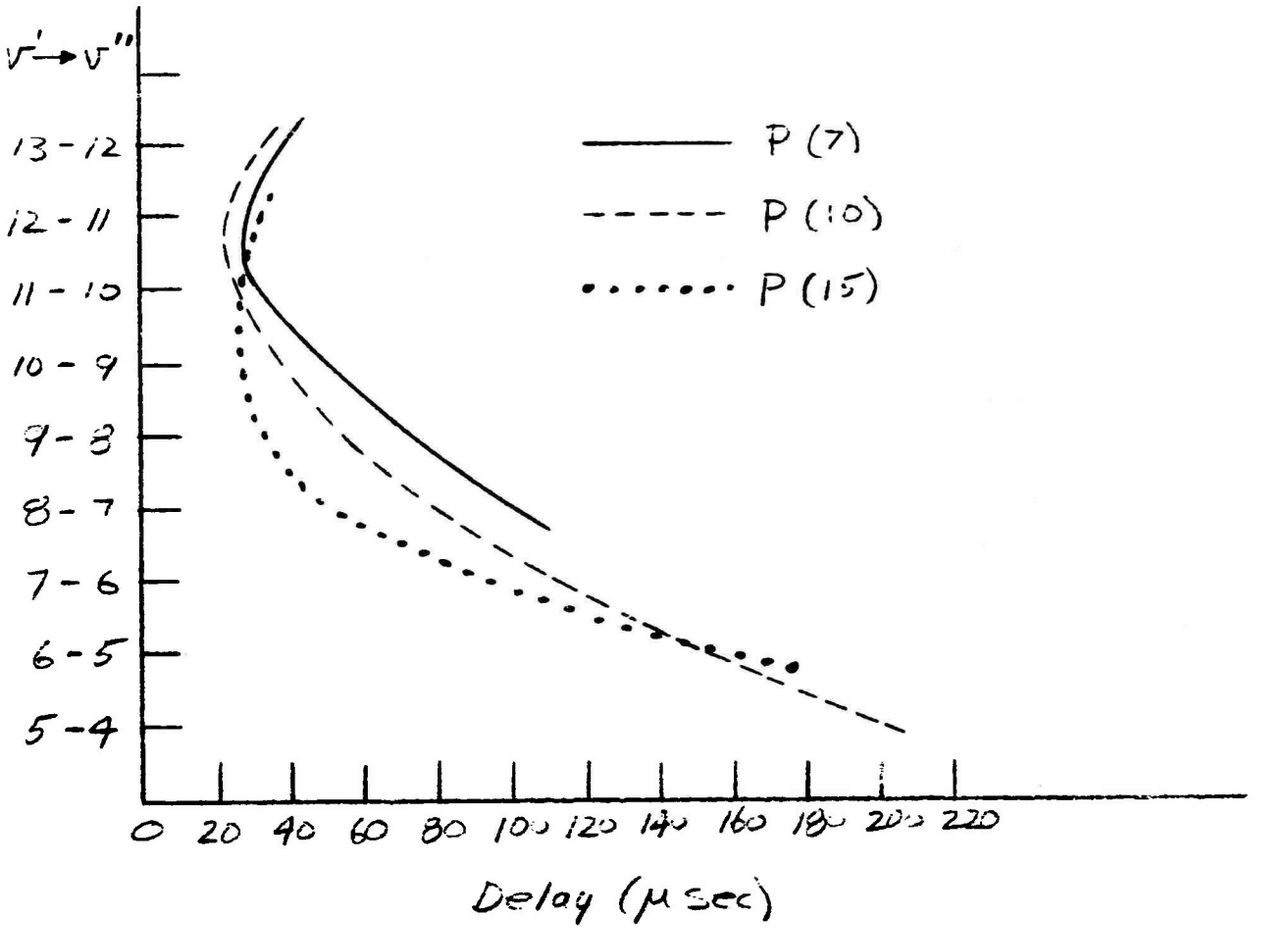

CS_2	0.035 torr
O_2	0.68
He	1.69

9 KV Excitation

FIGURE 4

42

radiation in the infrared (non-lasing condition), which are now being measured as a function of the time after initiation, will provide the necessary information to permit the unambiguous formulation of a mechanism and values for the rate constants. At present we are operating under the assumption that the high voltage discharges dissociate both the $O_2 \rightarrow 2O$ and $CS_2 \rightarrow CS + S$; and that the subsequent reaction $CS + O \rightarrow CO^{\dagger} + S$ leads to the vibrationally excited CO. However, in the low voltage discharges a chain mechanism must be present. This is represented as follows:

$$O_2 \xrightarrow[\text{discharge}]{\text{pulse}} 2O$$

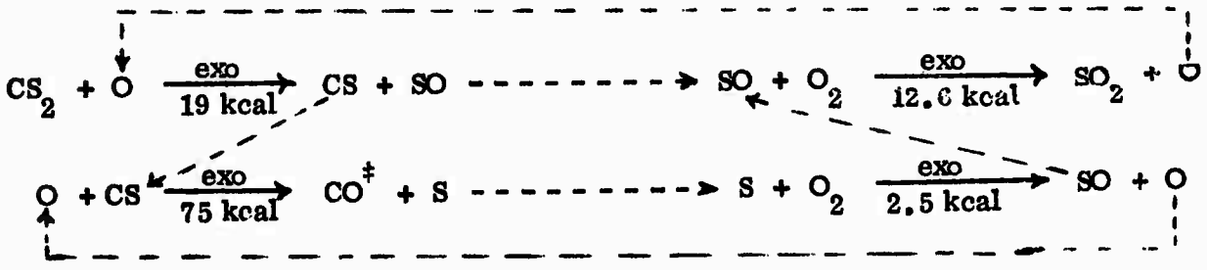

Whether the four center reaction:

$$CS + O_2 \xrightarrow[81\ \text{kcal}]{\text{exo}} CO + SO$$

plays a role is yet to be determined; this is one of the important questions we hope to answer. After completing recording of the chemiluminescence in the infrared, we plan to measure the absorption by CS (in the UV), both under lasing and non-lasing conditions, and thus to correlate the production of CS with its destruction during $CO^{\dagger}$ lasing.

EPR CHEMICAL KINETIC RATE DETERMINATION

The kinetics of chemical reaction rates may be studied and absolute reaction rates determined by use of Electron Paramagnetic Resonance (EPR) techniques. The types of reactions that may be studied with this method are those in which free atoms are present as either reactants or products or both since most free atoms in their ground states possess a magnetic moment and are therefore paramagnetic. Certain molecules such as O_2, NO are also paramagnetic and reactions involving them can also be studied. In addition, when atoms or paramagnetic molecules are present in excited electronic states with sufficient number density ($n > 10^{12} cm^{-3}$) they may be distinguished from their ground state counterparts since their magnetic properties are nearly always different. Many reactions of interest to chemical lasers can be studied with EPR techniques and we have begun a program of absolute reactions rate determination for a series of these reactions whose rates are unknown or in doubt.

An EPR spectrometer defects the absorption of microwave power by the paramagnetic species in a microwave cavity. Maximum power absorption occurs for fixed microwave frequency when the relevant energy levels are split by the Zeeman effect such that the microwave photon energy equals the Zeeman energy splitting. If several paramagnetic species are simultaneously present in the microwave cavity they are separately distinguishable since each will display a absorption resonance at a different magnetic field value. A good EPR spectrometer has high sensitivity and S/N >1 can be observed at specie densities of 10^{11}-$10^{12} cm^{-3}$ at pressures of approximately 1 Torr and T=300°K. Moreover, by comparing the absorption strength of the sample specie with that of a reference specie (frequently taken to be O_2) absolute density determinations are routinely made.

Chemical reactions are studied in the following way for a reaction of the type $A+BC \xrightarrow{k_2} AB+C$. Atoms A are produced upstream of the cavity in a rapidly flowing gas stream and their absorption strength S at the cavity is determined. The signal S is directly proportional to the concentration of A, [A]. Molecules BC are rapidly mixed into the flowing stream of A at different points upstream of the cavity and for each location of gas mixing [A] or S is determined at the cavity. The farther

upstream the injection occurs the longer the reaction can proceed before [A] is determined. The gas flow velocity is measured so that distance upstream is equivalent to time of flight. If [A] = αS then $\frac{d[A]}{dt} = -k_2[A][BC]$ and $S = \frac{[A]_o}{\alpha} e^{-k_2' t}$ where $k_2' = k_2[BC]$ and the reaction is run under conditions that [BC] is much greater than [A] and thus can be considered essentially constant. A plot of S vs. distance upstream on semi log paper yields a straight line (for the assumptions stated) whose slope gives k_2' and therefore k_2. Under the assumptions stated, only relative concentration determinations are required. More sophisticated variations upon the above method will be discussed later.

We have assembled a high sensitivity EPR spectrometer ($n_0 \geq 10^{11}$ can be measured) from existing parts and coupled it to a 400 cfm pumping facility. Means for gas injection at continuously variable upstream locations have been established and calibration procedures for gas flow and paramagnetic specie density have been developed. We are equipped to handle most gases including reactive species such as NO, HF and the halogens. Atoms are produced by molecular dissociation in a 2.45 GHz microwave discharge energized by a 80 watt CW magnetron. The following paramagnetic species have been observed with excellent signal to noise: H, N, O, Cl, F, NO, O_2. The reactions chosen for initial study were

$$H + F_2 \xrightarrow{k_2} AF + F, \quad (1)$$

$$H + Cl_2 \xrightarrow{k_2} HCl + Cl, \quad (2)$$

$$NO + F_2 \xrightarrow{k_2} NOF + F. \quad (3)$$

Reactions (1) and (2) are of course half of a chain reaction with corresponding chain partners

$$F + H_2 \xrightarrow{k_3} HF + H \quad (1')$$

$$Cl + H_2 \xrightarrow{k_3} HCl + H \quad (2')$$

Our initial studies attempted to use the method of data analysis obtained above in which reactions (1') and (2') were ignored since under the assumptions previously discussed the data analysis is particularly simple. Linear semi log plots of S vs. distance were indeed obtained under typical flow conditions, for reaction (1), for example:

$QF_2 = 7.32 \times 10^2 cm^3$ torr sec^{-1}
$QH_e = 4.72 \times 10^3 cm^7$ torr sec^{-1}
$QH_2 = 23.2 cm^3$ torr sec^{-1}
$v = 61.8$ m/sec
$[f_2] = 4.85 \times 10^{15}$ molecules cm^{-3}

The hydrogen flow was chosen very much less than that of F_2 to help validate the assumptions required to neglect (1'). The average of many determinations analyzed with this method are:

Reaction (1) : $k_2 = 4.69 \times 10^{-13}$ molecules^{-1}cm^{3}sec^{-1}
Reaction (2) : $k_2 = 3.27 \times 10^{-12}$ molecules^{-1}cm^{3}sec^{-1}

These rates are somewhat slower than those quoted by Albright, et al J. Chem. Phys. 50, 3632 (1969) who find

Reaction (1) : $k_2 = 3.56 \times 10^{-12}$ molecules^{-1}cm^{3}sec^{-1}
Reaction (2) : $k_2 = 3.04 \times 10^{-11}$ molecules^{-1}cm^{3}sec^{-1}

We have therefore undertaken to refine our data analysis procedure by taking into account both reactions (1) and (1') and (2) and (2') in the following manner. We can find operating conditions such that $\frac{d[H]}{dt} = -k[H]$ ie a linear plot of S vs. x on semi log paper is obtained. Using (1) and (1') we have $k = k_2[F_2] - k_3[F][A_2][H]^{-1}$. We shall determine $[A_2]$ and $[F_2]$ from flow measurements and [F] and [A] from absolute EPR density determinations. Knowing K and S at two points on the semi log plot we can determine both k_2 and k_3. We are currently completing this series of measurements.

We are also partway into the determinations of k_1 for reaction (3). By operating at low [NO] we can avoid consideration of the competing reaction NO+F → ONF since both [NO] and [F] can be made small compared to $[F_2]$. While we have observed F production by reaction (3) and have observed paramagnetic absorption by NO we are currently fabricating another microwave cavity in which a larger electric field component will interact with the gas as compared with our present cavity that is optimum for magnetic dipole transitions. Resonant obsorption by NO can be observed with greater sensitivity using electric dipole transitions and thus operation at smaller [NO] will be possible.

After completion of these studies we would like to study the O+CS_2 reaction in which O, S and SO are observable paramagnetic species. The rates for this reaction(s) are not known.

STUDY OF RAPID GAS MIXING

Donald L. Turcotte

A mixing wind tunnel has been built to study turbulent diffusion at low pressures and to test mixing devices. The mixing tunnel is illustrated in Fig. 1. The plenum is divided into two parts by a splitter plate. The two gases that are to be mixed are metered into the two plenums. For the experiments reported here the two gases used were helium and argon. The splitter plate ends with a sharp edge at the entrance to the mixing section. The mixing section has a 3/8" x 3/4" area and is 4" long. The mixing section exhausts into a plenum. A removable section at the entrance to the mixing section holds screens or grids which induce turbulence in the mixing section.

Samples of the mixed gases are obtained using a probe. This probe can be translated across the mixing region and measurements can be obtained at three axial positions. Gas samples extracted from the mixing region pass through a thermoconductivity cell. This cell is illustrated in Fig. 2. The cell contains four heated thin wire resistance elements. The sample gas passes over two of the wires. A reference gas (in these experiments argon from the argon plenum was used as the reference gas) passes over the two remaining wires. The four wires comprise a bridge circuit which measures the difference in voltage drop between a wire in the reference gas and a wire in the sample gas. This voltage difference is related to the thermal conductivities of the two gases by

$$\Delta V = C\left(\frac{1}{k_{ref}} - \frac{1}{k_{sample}}\right)$$

In order to evaluate the constant C, the probe is placed in pure helium outside the mixing region. With the sample ga helium and the reference gas argon, the two thermal conductivities are known, the ΔV is obtained and C is evaluated. Using this C (C is obtained for each run) the ΔV is obtained at several points within the mixing zone. The thermal conductivity as a function of the per cent of helium in the helium-

Test Chamber

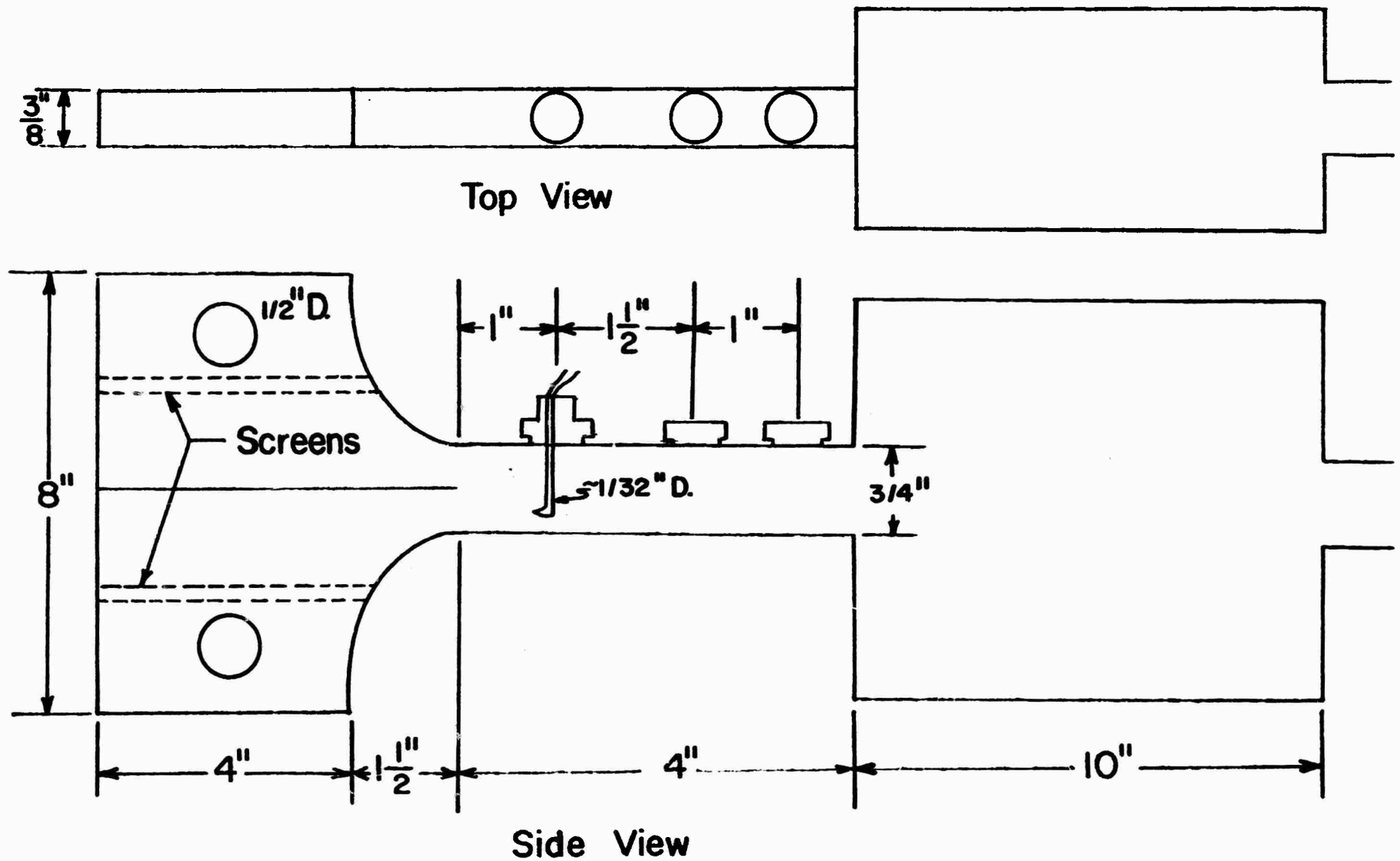

FIGURE 1

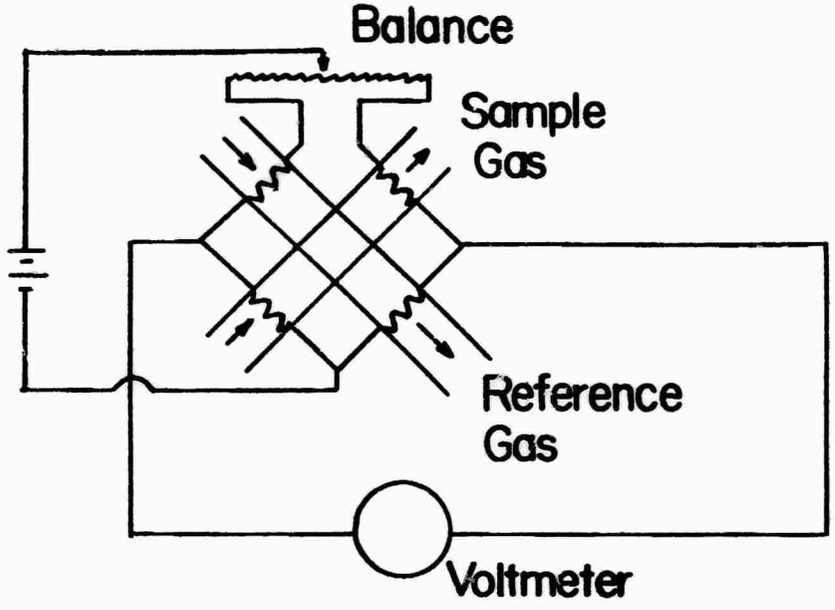

Thermoconductivity Cell Circuit

FIGURE 2

argon mixture is given in Ref. 1. The thermoconductivity cell is sensitive to concentrations of helium in argon as low as 1 part in 1000. A complete schematic diagram of the apparatus is shown in Fig. 3.

In order to calibrate the mixing tunnel the laminar mixing of helium and argon has been studied. Assuming a uniform velocity u, the molal concentration of helium C_{He} satisfies the equation

$$u \frac{\partial C_{He}}{\partial x} = D_{HeA} \frac{\partial^2 C_{He}}{\partial y^2} \tag{1}$$

where x is measured along the channel and y is measured across it. D_{HeA} is the binary diffusion coefficient for the mixing of helium and argon. Since mixing occurs across only a fraction of the channel, the appropriate boundary conditions for Eq. (1) are $C_{He} \to 0$ as $y \to -\infty$ and $C_{He} \to 1$ as $y \to +\infty$. The solution of Eq. (1) that satisfies these boundary conditions is

$$C_{He} = 0.5\left(1 + \text{erf}\left\{\frac{y}{2}\left[\frac{u}{D_{HeA}x}\right]^{1/2}\right\}\right) \tag{2}$$

Measurements of the laminar mixing profile for helium and argon have been carried out for a range of velocities and pressures with $X = 0.87"$. The results are given in Fig. 4. Good agreement between theory and experiment is obtained if the binary diffusion coefficient D_{HeA} (reduced to standard conditions, 300°K and 1 atm) is taken to be 0.18 cm^2/sec. This is a factor of four less than the value quoted in the literature (Ref. 1). Reasons for this discrepancy are being investigated.

In order to study the influence of turbulence induced by screens on the mixing process, concentration profiles were obtained for two different screens (with wire diameter of 0.012" and 0.018"). The results are given in Fig. 5 along with the profile for laminar diffusion (no screen).

For the finer screen the concentration in helium-rich mixtures was unaffected but a turbulent enhancement of mixing is noted for argon-rich mixtures. This difference can be explained by the different densities of argon and helium and the resultant differences in Reynolds number based on screen wire diameter. The Reynolds number for the screen in argon is a factor of ten larger than the Reynolds number for the screen in helium. For the coarser

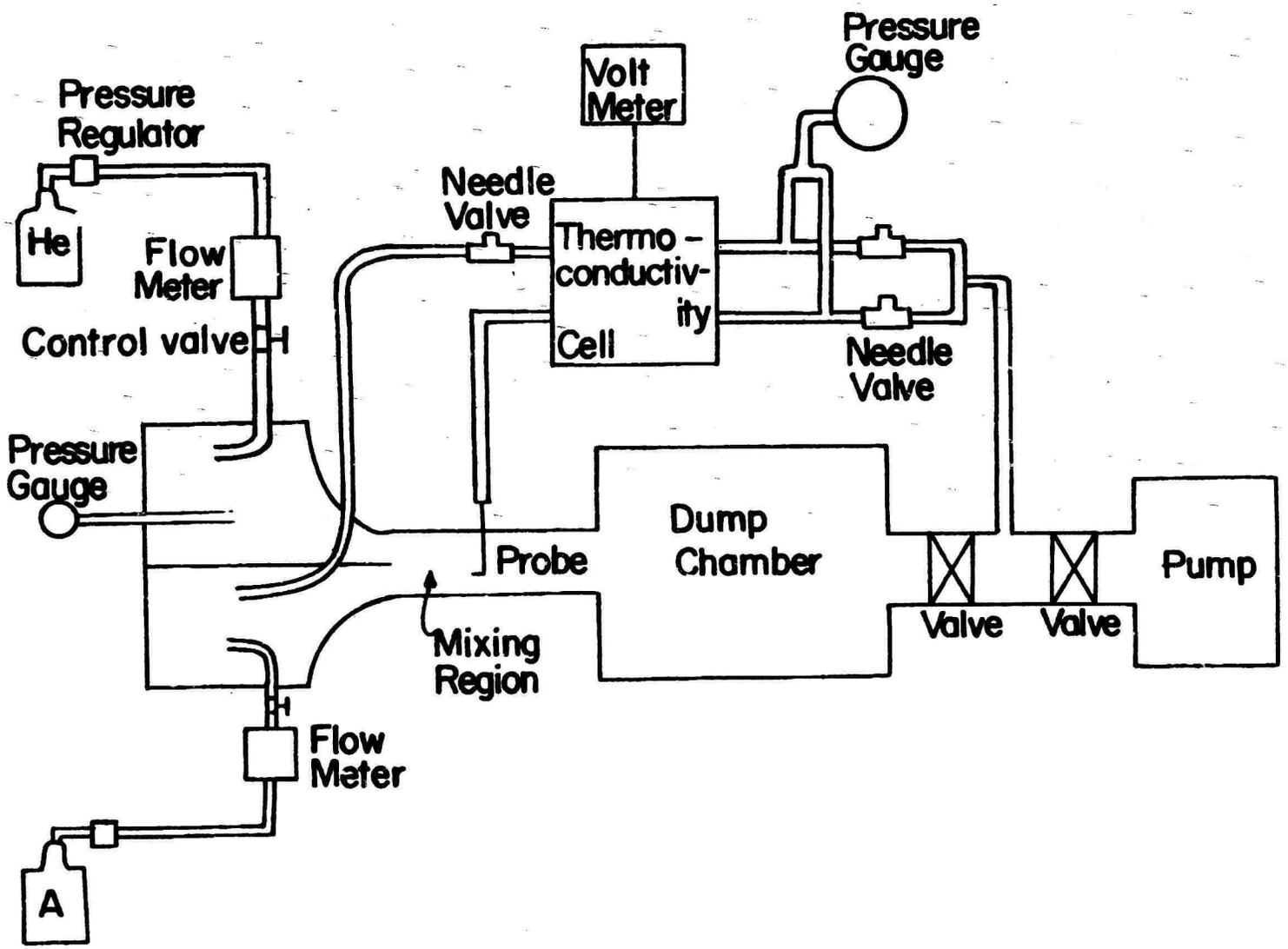
Pressure Regulator
He
Flow Meter
Control valve
Volt Meter
Pressure Gauge
Needle Valve
Thermo - conductiv- ity Cell
Needle Valve
Pressure Gauge
Probe
Dump Chamber
Pump
Valve
Valve
Mixing Region
Flow Meter
A

FIGURE 3

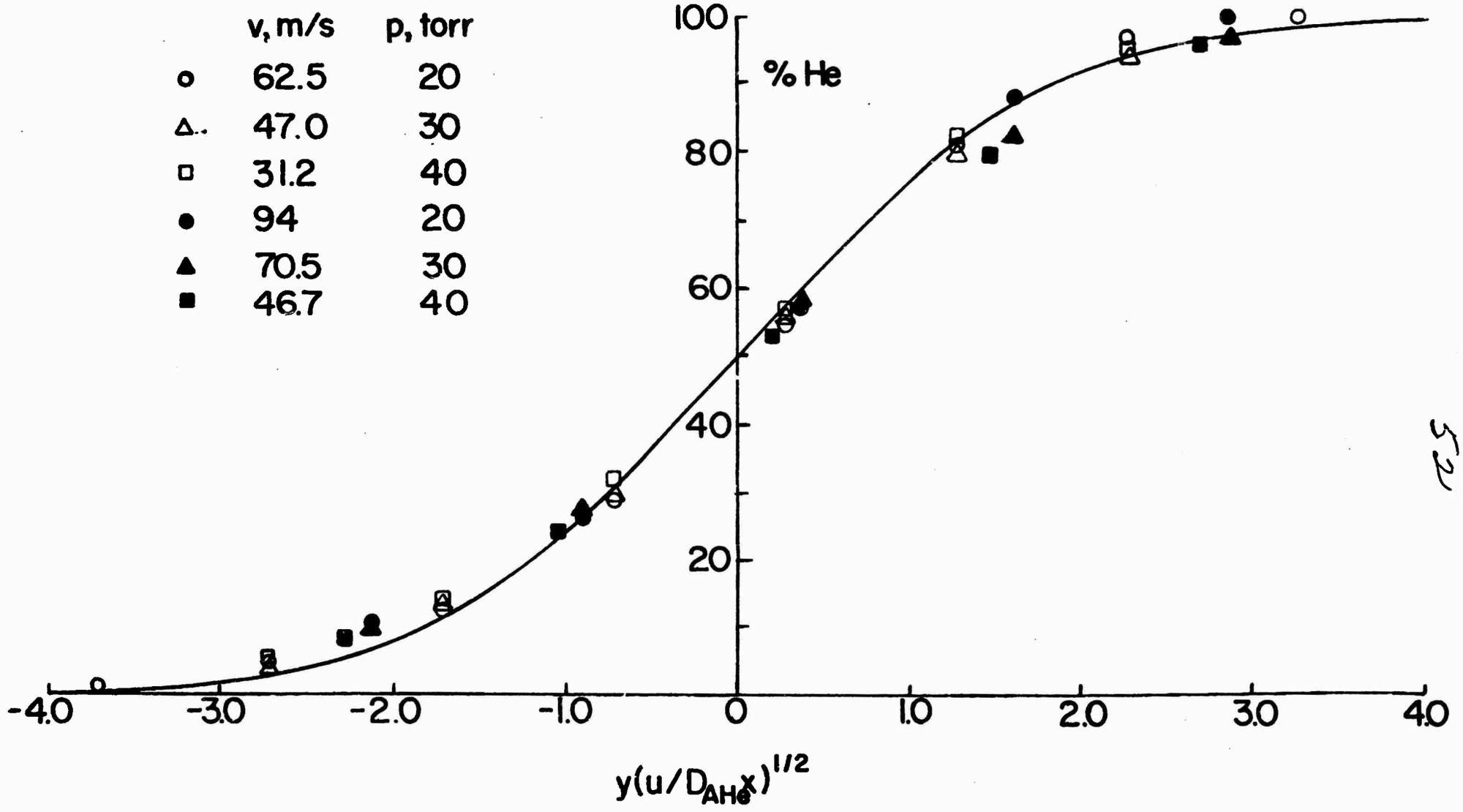
v, m/s
p, torr
62.5
20
47.0
30
31.2
40
94
20
70.5
30
46.7
40
100
80
60
40
20
% He
-4.0
-3.0
-2.0
-1.0
0
1.0
2.0
3.0
4.0
y(u/D_AHe x)^1/2

FIGURE 4

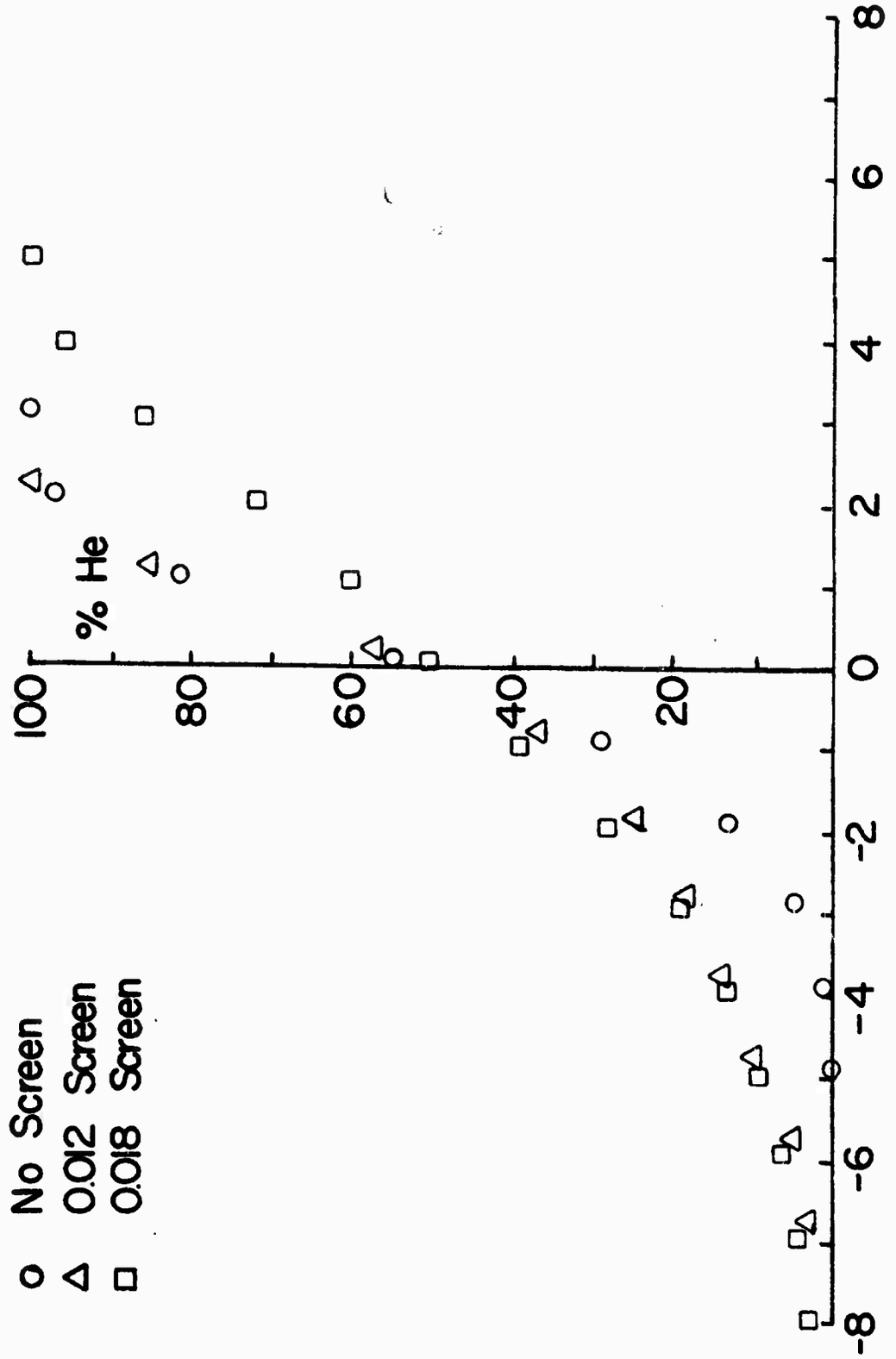
No Screen
0.012 Screen
0.018 Screen
% He
100
80
60
40
20
0
-2
-4
-6
-8
2
4
6
8
$y(u/D_{AHe}x)^{1/2}$

FIGURE 5

screen no additional mixing is observed in the argon but the mixing in the helium is now as effective as in the argon. Apparently the transition Reynolds number for the screen in helium has now been exceeded. Initial calculations indicate that screens are effective in generating turbulence at a Reynolds number (based on screen wire diameter) as low as 10. An understanding of this phenomenon at such low Reynolds numbers requires further study.

Initial studies have been carried out with a coarse grid (1/18" diameter wire) for generation of turbulence. Results indicate that substantial turbulence is induced and mixing is increased by up to an order of magnitude.

The results of a test of a typical chemical laser injector is shown in Fig. 6. The injector is a 1/8" diameter cylinder with 0.007" diameter holes spaced 3/16" apart. Injection takes place perpendicular to the flow. Helium was injected at sonic velocity into an argon flow with a speed of 150 ft/sec and a pressure of 30 torr. A concentration profile for the helium 2" downstream of the injector is shown in Fig. 6. Also included is the profile expected for purely laminar mixing. It is seen that the agreement between the measured profile and the profile expected for purely laminar mixing is quite good. This indicates that any turbulence induced by the injector has not been effective in speeding up the mixing. This is consistent with other results which indicate that single obstacles at the centerline of mixing are not effective in generating turbulence. Rather, a coarse grid of turbulence producing elements is required.

The apparatus is now available for measuring the mixing from any proposed injector for a wide range of pressures and subsonic velocities. Complete mixing profiles can be obtained 1", $2\frac{1}{2}$" and $3\frac{1}{2}$" downstream of the injector.

References:

1. S. Chapman and T. G. Cowling, The Mathematical Theory of Non-Uniform Gases, (Cambridge 1960).

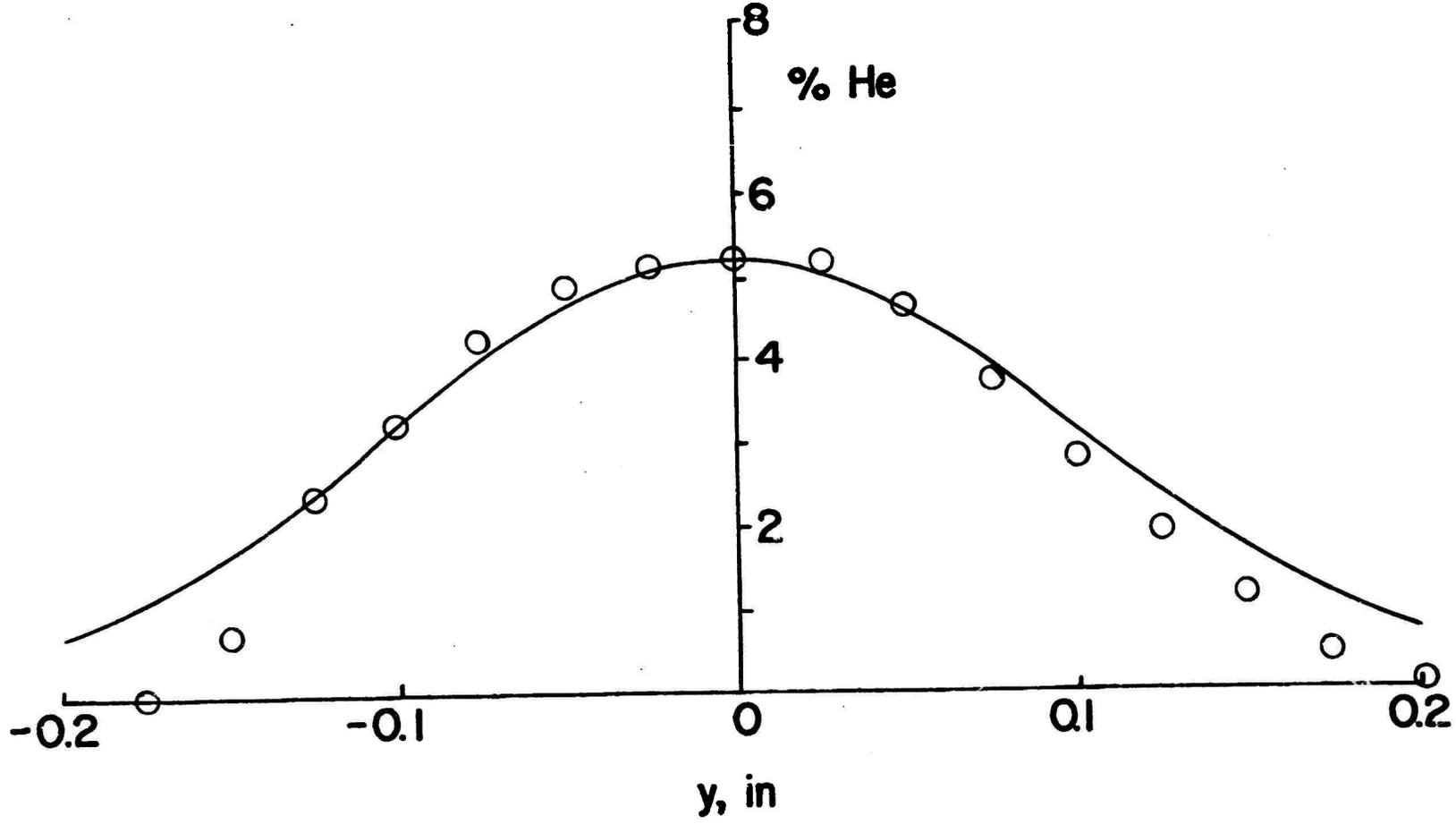

FIGURE 6

HIGH PRESSURE VIBRATIONAL RELAXATION

A. Introduction

A program of experimental determination of high pressure vibrational relaxation rates measured over a wide temperature range was initiated this past year. At the present time, such data does not exist since prior determinations (in CO_2 for example) using the spectrophone or ultrasonic dispersion measurements were not accurate and were taken only up to 1 atm. and over a very limited temperature range. Our plan is to measure vibrational relaxation from selected molecular levels in laser molecules (starting with $CO_2(00°1)$) in the pressure range 1-100 atm. and temperature range 77°K to greater than 600°K with a variety of molecular collision partners. The need for reliable experimental determination of high pressure vibrational relaxation times in molecular laser molecules stems, of course, from the desire to operate molecular lasers at high pressures. Already, CO_2 lasers operating at 1 atm. are commonplace in the laboratory and the operation of lasers at substantially higher pressures is being contemplated. The motivation for high pressure operation is, of course, to increase the stored energy density and permissible repetition rate in molecular laser devices.

B. Attempts to Operate a 4.3 μm CO_2 Laser

The method we have chosen to obtain vibrational relaxation data is the high pressure adaptation of the laser excited fluorescence technique that has been successfully applied to CO_2, N_2O, HF, etc., at pressures of one to ten Torr. The principal requirement for such experiments to be possible is to radiatively populate the molecular level whose vibrational relaxation is to be studied in a time short compared to the relaxation time. In the $CO_2(00°1)$ experiment a 10 n. sec. pulse at 4.3 μm and substantially resonant with $CO_2(00°0 - 00°1)$ vibration-rotation absorption is required. Our initial plan was to obtain the 4.3 μm laser from the 00°2 - 00°1 transition in CO_2 in accordance with a report by Javan et al[1]. In this

work the 00°2 - 00°1 inversion was supposedly obtained in a two step process: First, a pulsed discharge in a CO_2 laser mixture produced a high vibrational temperature in the (00°n) system of CO_2; second an intense pulse of 00°1 - 10°0 laser radiation (obtained from a Q switched CO_2 laser) was coupled through the medium to saturate the 00°1 - 10°0 transition thereby inverting 00°2 relative to 00°1. Our initial plan was to enhance operation of this 4.3 μm laser by using a TEA laser pulse of higher peak power to saturate the 00°1 - 10°0 transition in the medium to be inverted for 4.3 μm operation. Accordingly, we built a TEA, three electrode structure laser that provided 1-2 μ sec., 1/2 joule pulses of 00°1 - 10°0 radiation. With a 1 meter gain cell and suitable mirrors for 4.3 μm we were unable to detect any 4.3 μ lasing after a careful search over a broad range of operating conditions. That sufficient 00°1 - 10°0 saturating power was available was confirmed by lasing the gain tube at 10.6 μm and observing the termination of lasing upon coupling in the TEA pulse. Subsequent communication with Professor G. Flynn[2] revealed that the 4.3 μm oscillation was extremely weak, had been observed in a 3 m. gain tube, and was probably a weak transition in a combination band 10°2 - 10°1. This tentative assignment is discussed briefly in a later publication[3]. It is appropriate to mention that the 4.3 μm CO_2 source would not have given 10 n. sec. pulses and that we have designed and assembled all components of a GaAs electroptic shutter designed to pass an appropriate portion of the 4.3 μm pulse.

C. Operation of a 4.3 μm HBr Laser

In order to secure the required 4.3 μm laser source our attention turned to the HBr chemical laser for which 4.3 μm laser output had been observed by Deutsch[4]. Deutsch's observations indicated that several coincidences between HBr laser lines and CO_2 could be expected to within 0.1 cm^{-1}, and thus pressure broadening would not have to be relied upon to achieve appreciable absorption in CO_2(00°0 - 00°1). A 1 meter long, 1" ID, longitudinally pulsed, low pressure discharge in H_2+ Br_2 was made to lase on chemically produced, excited HBr. Lasing was achieved in both the free running (2 Au mirrors) and grating controlled modes. Free running, peak powers of 10 watts inside the cavity

were observed at a total operating pressure of about 5 torr. Pulse length was about 5 μ sec. The absorption of this radiation by CO_2 and N_2O was checked. Of the 17 lines made to lase in this system, 4 were abosrbed so heavily in N_2O that an α of 1/meter was observed at pressures of less than 5 torr. Later studies with the TEA HBr laser to be described revealed 2 or more lines in CO_2 with correspondingly good coincidences. The other lines required pressures of 100 to 500 torr to give α = 1/meter.

D. The High Pressure, Transverse Discharge HBr Laser

1. Experiments with a TEA, HBr Laser

The rather modest output power of the longitudinally pulsed HBr laser was not sufficient for purposes of the fluorescence experiment. Consequently, efforts were made to raise the output. Experiments at much higher pressures, 10 to 400 torr, resulted in factors of 100 improvement over the old design. The laser consisted of 1 meter long TEA pin laser using 1000 ohm resistors fed from a 0.1 μf capacator charged to 20 KV. This multi-pin geometry had to be reverted to because the gases used gave exceedingly poor performance in the 3-electrode pre-ionizing structure. The discharge contracted into one bright arc for any pressures in excess of about 40 torr.

A mixture of H_2 and Br_2 in this multi-pin laser gave powers on the order of 1 kw inside the cavity at pressures of 30 torr. The pulse length depended on the pressure, but was about 2 μ sec. under conditions of highest power. Both grating and 2 mirror operation was obtained (the powers quoted in both the TEA and the long tube experiments were measured with a 2 mirror cavity). It should be noted that more lines could be made to lase in the TEA than with the longitudinal discharge tube.

A series of quantitative tests were made to determine the effects of a variety of chemical species on the performance. These included the usual gases (N_2, He, O_2, etc.) as well as a series of brominated hydrocarbons in analogy to the use of hydrocarbons in the HF laser as sources of the F or H atoms, or both. In total, 19 species in addition to H_2 and Br_2 were introduced.

The testing scheme used on any given substance consisted of establishing lasing on a good coincidence line of HBr with N_2O in a H_2/Br_2 mixture at low pressure (about 5 torr) and then progressively introducing more of the substance until the power output changed appreciably. Up to approximately 5 to 10 times this amount was then introduced to see if the trend was monotonic.

and $Br + RH \rightarrow RBr + H$ --- (9)

or $Br + RH \rightarrow HBr + R$ --- (10)

As we are interested in short times, we have only shown above reactions involving reactants not products. The reverse of reactions (1) ... (10) above will be present but be proportional to [intermediate] [product] and thus be slow. Reactions involving reactants and products will be one of two forms.

$$AB + CD \rightarrow ABC + D \qquad (11)$$

or

$$AB + CD \rightarrow AC + BD \qquad (12)$$

Reaction (11), if ABC exists, will contribute to the number of free atoms present and will, in general, help matters. (12) is a our center exchange and can be expected to have a high activation energy and consequently to be slow at room temperature. For the same reason, reactions between the reactants e.g.,

$$RH + Br\,X \rightarrow RBr + HX \qquad (13)$$

$$RH + Br\,X \rightarrow R\,X + HBr \qquad (14)$$

will not be considered. This contention is supported by experimental evidence against $H_2 + Br_2 \rightarrow 2HBr$[5].

Deactivation of the HBr* produced in (1) by any of the other species present, particularly the Br X and the RH, will limit lasing, but is hard to estimate.

In general, we are looking for reactions that are easy to initiate with both chain propagating steps that are fast; with competing reactions that are slow, or if fast, feedback into the chain by (7) and (9), not by (8) and (10). If any of these steps is unusually exothermic, the possibility of V-V pumping from excited reactants is a hopeful possibility.

An analysis of the thermochemistry of reactions with various additions was made with the following results:

a. Reactions with hydrocarbons or brominated hydrocarbons result in highly endothermic chain propagation steps or less exothermic not than the direct reaction $H + Br_2 \rightarrow HBr + Br$. Thus hydrocarbons will not help in the performance of the HBr laser, either as

This was repeated starting with a high pressure (about 100 torr) of the H_2/Br_2 mix. If the substance contained Br, the opposite was done. For those substances which increased the output, various mixtures of these and H_2 and Br_2 were tried to optimize the peak power.

The results are summarized below. The symbols ++, +, 0, -, --, and t indicate a strong increase, a mild increase, no appreciable effect, a mild decrease, a strong decrease and termination of the lasing.

CH_4:-	Air: +
CH_3 Br:0	He:+ (High-press); - (low press)
CH_2 Br_2:-	Ar: ++
CH_2 BrCl:--	H_2O:-
CH Br_3:--	CO_2:t
C_2 H_6:--	N_2:+(high-press); -(low press)
C_2 H_5 Br:t	N_2O:t
	O:+(high press); ++ (low press)
	HBr: t
	HI:--

2. Chemistry of the HBr Laser

Chain prop steps:	H + Br X → HBr* + X	---	(1)
	X + RH → RX + H	---	(2)
Initiation	RH + m → R + H + m	---	(3)
	Br X + m → Br + X + m	---	(4)
Competing	H + Br X → HX + Br	---	(5)
	X + RH → HX + R	---	(6)
R + Br enter chain by	R + Br X → RBr + X	---	(7)
or	R + Br X → RX + Br	---	(8)

sources of H or Br atoms.

b. Use of the non-equilibrium abundance of atomic hydrogen present in some other chain reaction to feed into the hot $H + Br_2$ reaction is suggested. The addition of O_2 to the discharge should be beneficial if the $H_2 + O_2$ reaction can be used as a source of atomic hydrogen.

c. The brute force technique of using some hydride with very weak bonds was investigated as a useful additive. As an example, Silane (SiH_4) decomposes immediately in an electric discharge or at $T > 400°C$ and can be considered as a source of atomic hydrogen for the $H + Br_2 \rightarrow HB_r + Br$ reaction. In addition since the Si-X (X is a halogen) bonds are much stronger than the Si-H bonds, Silane might be effective as a hydrogen atom source via the chain reaction

$$H + Br_2 \rightarrow HBr + Br \quad , \quad \Delta H° = -41.4 \text{ Kcal}$$

$$Br + SiH_4 \rightarrow SiH_3Br + H \quad , \quad \Delta H° = +0.4 \pm 5 \text{ Kcal}$$

in which the second reaction is much more favorable than the corresponding reaction

$$Br + H_2 \rightarrow HBr + H \quad , \quad \Delta H° = +16.7 \text{ Kcal}$$

3. Correlation with Experimental Results

The addition of any of the hydrocarbons or brominated hydrocarbons tried did not increase the laser power or support lasing by serving either as a source of hydrogen atoms or of bromine atoms. The enrgetics are unfavorable. At best, they deactivate the HBr.

The addition of oxygen increased the peak power by a factor of 5 at low pressures and somewhat less as the pressure of the $H_2 + Br_2$ was increased. The pressure dependence is not understood at present, but the increase is most certainly due to a chemical reaction rather than intermolecular V-V pumping as in the case of $N_2 - CO_2$. The addition of N_2 increased the peak power by at most a factor of 2 at low H_2/Br_2 pressures. At higher pressures it decreased the peak power. N_2 vibrations are nearly resonant with HBr vibrations ($\Delta\nu < \sim 100$ cm^{-1}) and thus the increase at low pressures could be explained in terms of resonant pumping as in the case of CO_2. However, the vibration frequency of $O_2 \simeq 1550$ cm^{-1}. The mismatch with HBr is ~ 800 cm^{-1}.

Considering the size of kT this is hardly resonant. Since the masses and the Leonard-Jones parameters are roughly comparable for the two molecules, it is hard to attribute the increased power to anything but the chemistry of the $H_2/O_2/Br_2$ mixture.

The effects of the other gases added to the H_2/Br_2 mixture hold few surprises. The addition of CO_2 and N_2O terminated lasing due to their strong absorption at the frequency to which the laser was tuned (with the grating). He and Ar increased power. This was concurrent with the increased diffuseness of the discharge upon the addition of these gases and was probably due to the usual increased electron mobility in these gases (vs. electronegative gases). Cold HBr terminated lasing due to absorption or resonant transfer. Absorption is less likely since the lasing transition was either 4-3 or a 3-2. HBr introduced externally could not be made to lase. The exothermicity was needed. Monobromoethane terminated lasing, whereas ordinary ethane did not. This remains a mystery.

We are currently designing a larger TEA, HBr laser and setting up to experimentally study the effect of Silane addition to laser performance. With the addition of the beneficial additives discussed above the performance of our HBr laser is entirely sufficient to proceed with the vibrational relaxation experiments and further beneficial additives will simply improve an already satisfactory signal to noise ratio. We performed a crude vibrational relaxation experiment using CO_2 in a cell at 1 atm. and the simple, 1 meter, TEA pin HBr laser without additives described above. A 1mV fluorescent signal was observed with 100 watts of HBr laser excitation. Since we conservatively expect 1 Kwatt HBr output with additives we calculate that at 100 atm. CO_2 pressure we will have 10 mV of signal after signal averaging. This is a minimum figure also, since significant improvements can be expected in fluorescent collector efficiency with proper cell design.

4. Other Aspects of Experimental Design

We are currently completing drawings for the construction of the optical cell and the high pressure generating equipment. Vacuum and gas handling facilities have been installed. Optical and signal processing equipment are on hand. We expect final experimentation to begin within 60 days. In the interim time we shall optimize the final HBr laser, study its output spectrum and determine the degree of coincidence in all favorable cases with CO_2 and N_2O.

References

1. A. Javan, et al, Phys. Rev. Lett. 17, No. 5, 223 (1 Aug., 1966).
2. Professor G. Flynn, private communication.
3. A. Javan, et al, J. Molec. Spec. 25, 410 (1968).
4. Thomas F. Deutsch, App. Phys. Lett. 10, No. 8, 234 (15 April, 1967).
5. S. Benson, "The Foundations of Chemical Kinetics," p. 322.

64

THE REVIEW OF SCIENTIFIC INSTRUMENTS VOLUME 42, NUMBER 10 OCTOBER 1971

Continuous Wave Chemical Laser for Laser-Induced Fluorescence Studies*

RONALD R. STEPHENS† AND TERRILL A. COOL
Department of Thermal Engineering and Laboratory of Plasma Studies, Cornell University, Ithaca, New York 14850
(Received 21 May 1971)

Laser-induced vibrational fluorescence experiments have been accomplished with a newly developed cw chemical laser. The design and operating characteristics of this small-scale transverse flow chemical laser source are presented. The fluorescence measurement technique and apparatus provide several advantages over the use of pulsed chemical lasers for similar measurements. The present laser is also useful as a selectively tunable probe for single pass gain measurements in chemical lasers.

INTRODUCTION

MEASUREMENTS of the fluorescence from molecular vibrational bands selectively excited by the absorption of a modulated laser beam have provided a unique body of knowledge concerning vibrational energy transfer processes in gases.[1-4] At present, pending the development of continuously tunable laser sources of sufficiently narrow linewidth in the near infrared, fluorescence measurements are limited to vibrational energy transfer processes involving molecules possessing absorption bands matching existing laser wavelengths.

The exceptionally rapid vibrational energy transfer processes associated with the hydrogen and deuterium halides have heretofore been studied by monitoring the fluorescence decay following excitation by a pulse of radiation from HCl or HF chemical lasers.[4,5] Experimental difficulties associated with the use of such pulsed chemical lasers include a long pulse duration, an inherently low pulse repetition rate (only single pulses have been used to date), a large electrical noise associated with flash lamps or electrical discharges used to initiate laser action, and variability in pulse characteristics from shot to shot.

The recent development of small scale cw chemical lasers for laboratory research has made available convenient sources of laser radiation from HF, DF, HCl, and CO[6-9] (presumably HBr, DBr, DCl, and OH can be added to this list with some further investigation[10]). Such lasers typically provide multiline power outputs ranging from 0.1 to 2.0 W for conveniently small scale devices with moderate vacuum pumping requirements (25–150 liters/sec at pressures ~2–20 Torr). Selective single frequency operation at somewhat lower power output is possible with use of a dispersive resonator.[6]

We wish to discuss here the methods and apparatus we have recently developed for successful measurements of vibrational energy transfer rates of importance in the HF, DF, HF–CO_2, and DF–CO_2 chemical laser systems.[11] The use and construction of a small cw transverse flow chemical laser are described which provides an alternative, superior in many respects, to the use of pulsed chemical lasers for such studies.

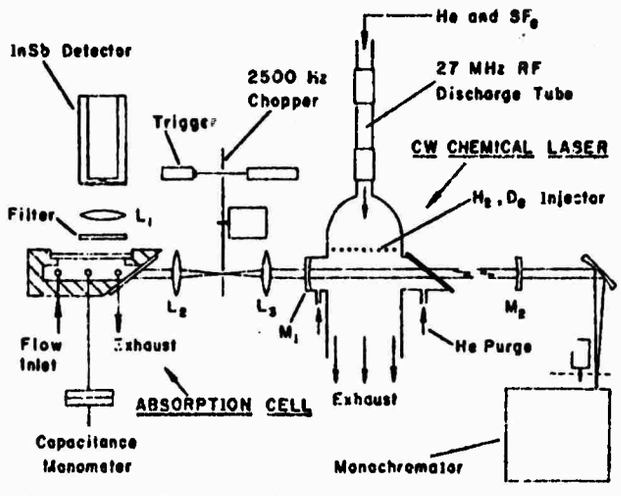

FIG. 1. Apparatus for laser-induced fluorescence measurements.

I. EXPERIMENTAL APPARATUS

Figure 1 shows a schematic diagram of the cw chemical laser, absorption cell, and associated apparatus used for the present measurements. The laser operated by means of the chemical reactions

$$F+H_2 \rightarrow HF(v=n)+H, \qquad (1)$$

where

$n=0$, 1, 2, or 3 for HF and $n=0$, 1, 2, 3, or 4 for DF.

An rf discharge was employed to produce requisite concentrations of F atoms by dissociation of SF_6 by electron impact. Design features of the laser test section included a subsonic flow and an optical axis transverse to the flow direction.

About 90% of the useful laser output was coupled from the optical cavity by the partially transmitting mirror M_1 and entered the absorption cell after being focused, modulated, and then recollimated by use of lenses L_2 and L_3 and the mechanical chopper. The additional 10% of the laser power output was coupled from the cavity by partially transmitting mirror M_2 to provide a determination of the laser spectral output characteristics with a McPherson model 216 monochromator–spectrograph. All external light paths were purged with dry nitrogen to prevent absorption by atmospheric gases. A helium purge

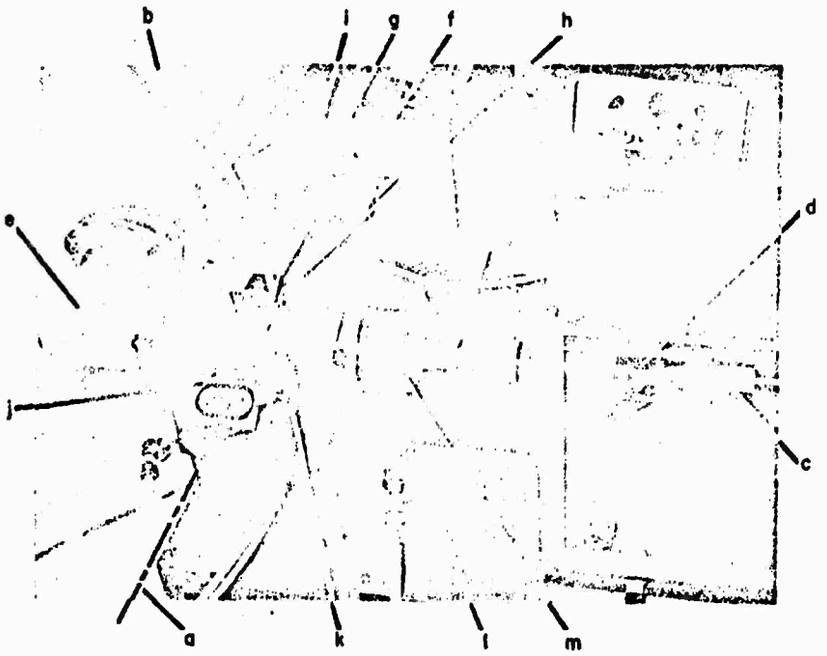

FIG. 2. Photograph of cw chemical laser. (a)—Optical axis; (b)—laser test section; (c)—rf discharge tube; (d)—downstream electrode; (e)—exhaust; (f)—purged light housing between mirror M_1 and the box (g) which contained the chopper and lenses L_2 and L_3; (h)—location of internally mounted mirror M_2; (i)—H_2 (or D_2) injection manifold; (j)—NaCl Brewster window; (k)—inlet for helium purge; (l)—pressure tap; (m)—5 cm i.d. plenum chamber.

was used in the laser test section to prevent absorption by ground state HF or DF in the space separating the inner optical surfaces from the main flow.

The desired fluorescence signal was provided by an InSb photovoltaic detector which was exposed to radiation sampled from the absorption cell through a narrow band interference filter by means of lens L_1.

The requisite gas mixtures for the absorption cell were carefully prepared and purified before being admitted to the cell. A continuous flow through the cell was provided to maintain sample purity despite inevitable surface reaction and contamination. Absorption cell pressures were measured with a capacitance manometer. Cell temperatures were monitored with a Chromel–Alumel thermocouple with an insulated stainless steel outer sheath.

The essential components of Fig. 1 are discussed in more detail in the remainder of this section.

A. Continuous Wave Chemical Laser

Figure 2 shows a photograph of the cw chemical laser employed for these studies. Identifiable in the photograph is the rf discharge tube used to accomplish initial F atom production by partial dissociation of SF_6 in a premixed flow of SF_6 and helium (see Fig. 1). The capacitively coupled discharge was maintained by means of a pair of aluminum foil strips of 5 cm width with a 5 cm space separating them, tightly wrapped around a 16 mm i.d. quartz tube. A one-half wavelength coaxial cable connected the discharge electrodes to the tank circuit of a 2500 W, 27.12 MHz rf oscillator–amplifier of our own construction. Under normal operating conditions the supply input power was maintained at 1400 W, of which perhaps about 600 W was delivered to the gas mixture. Forced air cooling of the discharge tube was provided from a fan which fed a Pyrex duct that enveloped the discharge tube.

Upon leaving the discharge and flowing 20 cm from the downstream electrode, the primary flow expanded into a plenum chamber of 5 cm inner diameter before entering the upstream end of the transverse flow chemical laser. The laser test section (see Fig. 3) was machined from a single piece of aluminum. A sonic throat of 3×4.5 cm cross section terminated a 3 cm length of constant area channel of 5×4.5 cm cross section to provide subsonic flow within the laser test section. The primary flow entered the test section through an inlet of 6.4×5 cm cross section and was rapidly mixed with a secondary flow of H_2(or D_2) injected by means of two opposing arrays of supersonic jets. The two rows of jets were aligned transverse to the primary flow with each row formed of 24 orifices of 0.033 mm diameter spaced 2 mm apart. The orifice rows were located in the top and bottom test section walls such that the jets intersected the primary flow at right angles with the top and bottom jet axes forming a staggered array (see Fig. 3).

The transverse optical axis was located 6 mm downstream from the injection orifices to allow for initial mixing and chemical reaction. The original design had provision to position the optical axis at various locations further downstream; however, Fig. 3 shows a fixed optical axis located to give maximum power output. Not shown in Fig. 3 are the H_2 injection manifold covers visible in the photograph of Fig. 2.

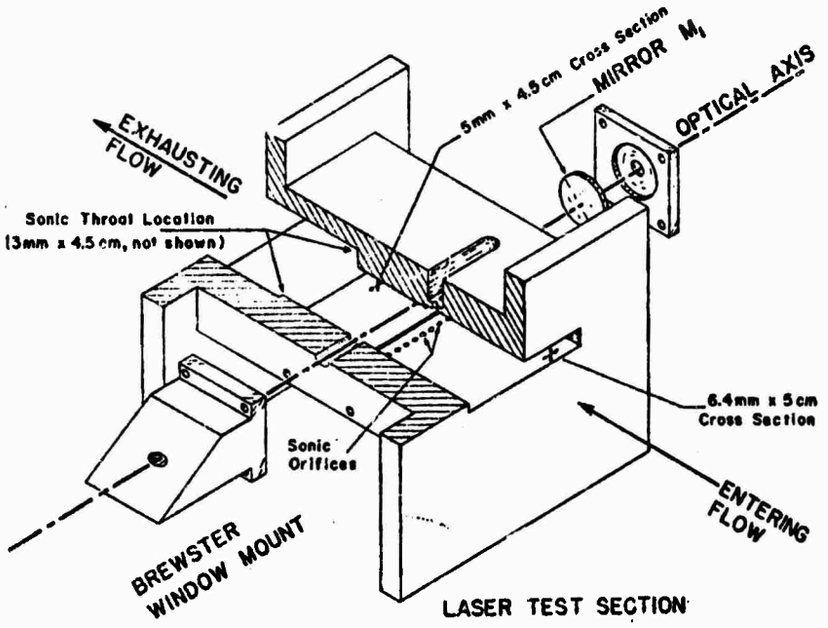

FIG. 3. Chemical laser test section.

It was found necessary to provide a small purge flow of helium to eliminate recirculation of ground state HF (or DF) molecules within the region separating the main flow from the inner surfaces of the Brewster window and mirror M_1 (see Fig. 3). Without the purge flow the power output of $1 \rightarrow 0$ band transitions was markedly reduced by absorption from the cold HF (or DF).

The partial flow rates found to provide a maximum power output for HF laser operation were: primary He, 25mM/sec; He purge flow, 0.4mM/sec; SF_6, 0.87mM/sec; H_2, 2.1mM/sec. The plenum pressure was 10.5 Torr; the pressure at the optical axis location was 9.8 Torr. The test section static temperature and mean flow velocity were about 515 K and 4.1×10^4 cm/sec at the optical axis.

For DF laser operation, optimum power output conditions were: primary He, 11mM/sec; He purge flow, 0.4mM/sec; SF_6, 0.26mM/sec; D_2, 1.4mM/sec. The plenum pressure was 5.1 Torr; the pressure at the optical axis was 4.65 Torr. The test section static temperature and mean flow velocity were about 480 K and 3.75×10^4 cm/sec at the optical axis.

The laser output spectrum for HF consisted of the $P(4)$, $P(5)$, and $P(6)$ $2 \rightarrow 1$ and $1 \rightarrow 0$ band transitions. The total output power from a 5% transmitting mirror M_1 was 1.5 W for all lines. The $1 \rightarrow 0$ band transitions made up about 50% of this power. For the HF laser case an additional approximately 1.5 W was lost because of mirror absorption.

For the DF laser case the laser output spectrum consisted of the $P(5)$, $P(6)$, and $P(7)$ transitions on the $3 \rightarrow 2$, $2 \rightarrow 1$, and $1 \rightarrow 0$ bands. The total output power from a 2% transmitting mirror M_1 was 0.5 W for all lines, of which about 25% was represented by $1 \rightarrow 0$ band transitions. The power loss because of mirror absorption was negligible.

It should be noted that both the HF and DF lasers were operated at somewhat higher power outputs than those reported here when F_2 was substituted for SF_6 as a source of F atoms, to enable initiation of the chain reaction between F_2 and H_2 or D_2. Because of the greater precautions necessary in the handling of F_2 it was, however, much more convenient to use SF_6.

The configuration of Fig. 3 required a vacuum pump capable of a minimum pumping rate of 180 liters/sec at a pump inlet pressure of about 2 Torr. Operation at smaller flow rates and correspondingly smaller power outputs could be accomplished by reducing the sonic throat height and/or transverse flow dimension from the values of Fig. 3.

B. Optical Cavity

The cavity mirrors of Fig. 1 were of 3 mm thick germanium with dielectric film coatings supplied by Laser Optics Incorporated to our specifications. The external mirror M_2 had a 4 m radius and a transmission of 0.5%. A sodium chloride Brewster window sealed with a Viton O-ring (see Fig. 2) was necessary to enable mirror M_2 to be positioned externally. Any of several mirrors (M_1) with transmissions of 2, 5, and 10% and of 10 m radius could be mounted internally (see Fig. 3). Mirror absorption could be neglected for the DF case, but the HF mirrors had absorption values approximately equal to their transmissions because of the presence of H_2O in the dielectric coating. A mirror separation of 95 cm was used to insure the presence of a longitudinal cavity mode near the peak of the unsaturated gain profile for a given laser transition.

The flow channel height of 5 mm was selected to insure a negligible loss from the TEM_{00} mode. In practice the laser tended to oscillate in either the TEM_{11} or TEM_{21} modes (x axis along flow direction) unless the beam was apertured slightly, which suggests a somewhat reduced flow channel height would be possible.

C. External Optical System

Lenses L_2 and L_3 had focal lengths of 5 cm; lens L_1 had a 2.5 cm focus. Lens L_1 was made of Irtran II; lenses L_2 and L_3 were of calcium fluoride. All external optical paths were purged with dry nitrogen to prevent atmospheric absorption.

The mechanical chopper was driven by a Globe synchronous motor model 75A1003-2 at 25 000 rpm with an audio oscillator and amplifier. The chopper wheel consisted of six slits of 0.25 mm width and 5 mm length aligned radially and equally spaced around the periphery of a 7 cm diam aluminum disk of 2 mm thickness. The slit edges were machined to a 0.3 mm thickness by milling away material in the vicinity of the slits on the surface of the wheel facing away from the incident beam. The recollimated light pulses produced with this chopper and lens arrangement were approximately Gaussian with an FWHM of 4 μsec, with peak powers equal to 78% of the cw laser output from mirror M_1. The standard deviation in pulse height was less than 5%. Narrower pulses would be difficult to achieve with the present arrangement because of the observed inability to focus the 3 mm diam laser beam to a spot much smaller than the 0.25 mm slit-widths employed. The approximately 400 μsec duration between pulses provided a convenient time interval during which to observe the fluorescence decay under appropriate absorption cell gas compositions and pressures.

A rotating mirror Q-switch arrangement was initially attempted, instead of the present arrangement, by rotating mirror M_2 (in this case flat and gold coated) at 150–200 cps. The pulse widths were shorter (about 1 μsec), and the peak pulse powers were about 2.5 times the cw power level. This very modest increase in peak Q-switched power over the cw power level reflects the small energy storage capacity of the HF system compared with other molecular lasers such as the N_2–CO_2 system. The slight advantages in peak power and pulse width were overcome by the disadvantages of pulse-to-pulse fluctuations and relatively low pulse repetition rate compared to the present chopping wheel arrangement.

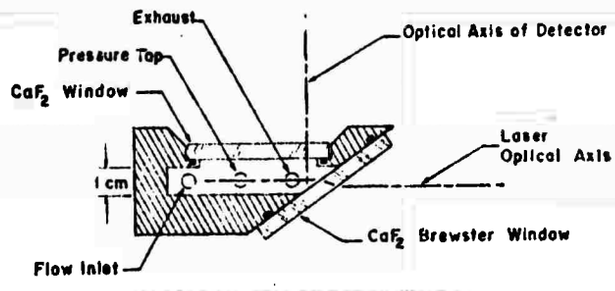

FIG. 4. Absorption cell configuration.

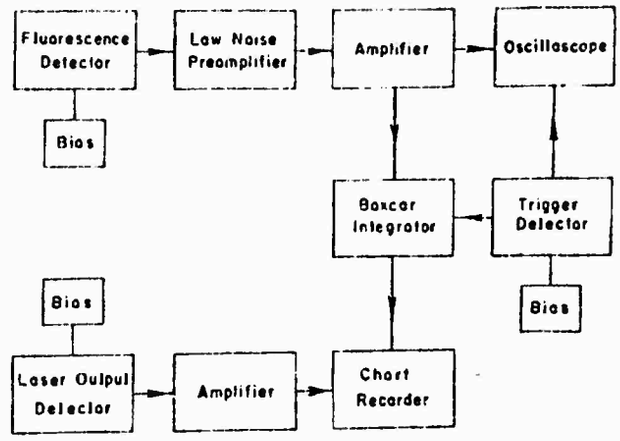

FIG. 5. Signal processing instrumentation.

Though not usually necessary, it was advantageous under conditions of very low fluorescence intensity to employ lens L_1 to focus fluorescence at the InSb detector element. The filters employed were manufactured by Optical Coating Laboratory, Inc. For HF fluorescence the filters W-02430-5 were used; the filters 3P31-551-045 and N-04410-9 were employed for the DF and CO_2 fluorescences, respectively. The HF and DF filters were specially designed to pass R-branch emission on the $1 \rightarrow 0$ bands, but rejected the scattered P-branch emission from the laser pulse. Usually two filters of a given type stacked in series (at a slight angular displacement to prevent multiple reflection between filters) were necessary to provide adequate rejection of the scattered HF or DF P-branch laser emissions.

D. Absorption Cell

Figure 4 shows the essential features of the absorption cell, machined from a single piece of aluminum. The cell operated at total pressures ~10 Torr and could be operated at temperatures from 300 to 450 K with a temperature regulated Nichrome heater. A typical total gas flow of 0.02mM/sec was maintained through the cell to minimize the effects of surface reactions in causing absorption or contamination of the HF or DF gas samples. Calcium fluoride windows sealed with Viton O-rings (see Fig. 4) successfully withstood intermittent operation extending over several months with no visible coating or deterioration caused by HF or DF. Because of the large absorption coefficient of HF, the detector was located as close as possible to the Brewster window (see Fig. 4).

The gas handling and purification procedures described by Airey and Fried[5] were followed to minimize contamina-

tion by H_2O. The total cell pressure and the partial pressure of each gaseous component within the cell were measured with an MKS model 144H-10SP Baratron capacitance manometer and the associated model 170M-5 electronics unit. Cell temperatures were monitored with an Omega model SCASS-020G-6 Chromel-Alumel insulated thermocouple before and after each run.

E. Instrumentation for Fluorescence Detection

A block diagram of the electronics instrumentation is shown in Fig. 5. The fluorescence signal was detected by a Philco-Ford ISC-301C InSb PV detector with a $D^*(500, 767, 1)$ of 1.45×10^{10} cm $(Hz)^{\frac{1}{2}}/W$. The element was 2.25 mm in diameter and was cooled to 77 K. The detector was back-biased to a zero voltage and operated with a 1000 Ω load resistor. The detector RC time constant with this load impedance was 1.2 μsec.

The voltage appearing across the load resistor was fed into a PAR model 113 low noise preamplifier which was used with a pass band from 0.03 Hz to 300 kHz and an amplification factor of 5000. The preamplifier output signal was further amplified 50 times by the internal circuits of a Tektronix type 532-S7 oscilloscope and type 53/54D plug-in unit which had a bandwidth of 2 MHz. The over-all time response of the detector, preamplifier, and oscilloscope amplifier was 2 μsec.

The vertical signal output of the oscilloscope was used to drive a PAR model CW-1 "boxcar" integrator. The scanning circuits of both the boxcar integrator and the oscilloscope were triggered by a phototransistor synchronized to the laser pulse. The phototransistor received a pulse of light from a light bulb located on the opposite side of the chopping wheel slot through which the focused laser beam passed.

The boxcar integrator output was recorded on one channel of a dual channel strip chart recorder. The second channel was used for display of a signal proportional to the total cw laser output provided by a thin film bolometer

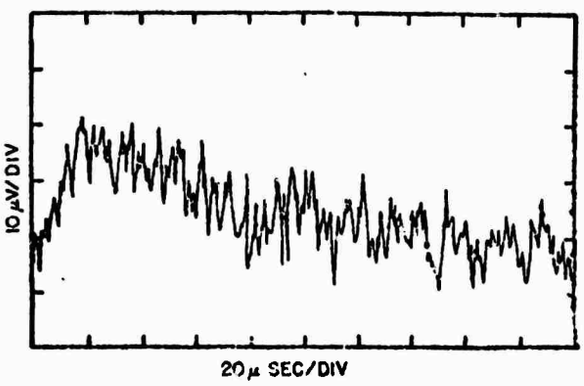

FIG. 6. Fluorescence of the $CO_2(00°1) \rightarrow CO_2(00°0)$ band following absorption of a single pulse of HF laser radiation in a mixture of HF and CO_2.

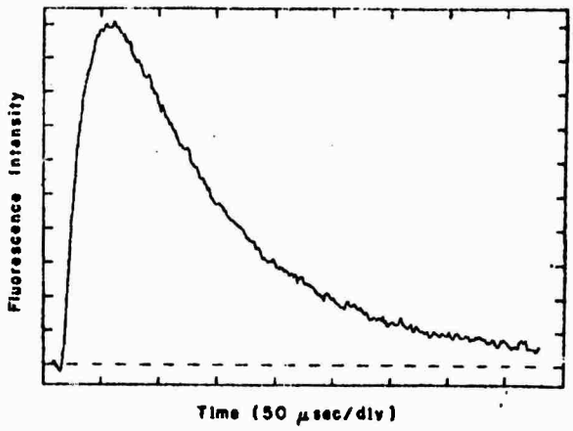

FIG. 7. Fluorescence of the $CO_2(00°1) \rightarrow CO_2(00°0)$ band after signal averaging for the conditions of Fig. 6.

and amplifier which detected a fraction of the laser output through mirror M_2. This provided a check on laser output stability while data were being recorded.

II. PERFORMANCE OF LASER-EXCITED FLUORESCENCE APPARATUS

Figures 6–8 demonstrate typical operation with the present apparatus. These data were taken at an absorption cell temperature of 295 K and cell partial pressures of CO_2, 0.27 Torr; HF, 0.18 Torr; and argon, 9.88 Torr (argon was present as an inert buffer to reduce the rate of diffusion to the tube walls). The fluorescence signal from either the $HF(v=1) \rightarrow HF(v=0)$ band or from the $CO_2(00°1) \rightarrow CO_2(00°0)$ band was monitored to examine vibrational energy transfer processes following the periodic production of HF molecules in the first vibrational level by the induced absorption of the $v=1 \rightarrow 0$ laser pulses.[11]

Figure 6 shows an oscilloscope trace of the fluorescence signal from the $CO_2(00°1) \rightarrow CO_2(00°0)$ band excited with a single laser pulse. It is evident that the fluorescence signal-to-noise ratio is no better than unity for a single pulse. This is markedly inferior to the performance one would expect with the usual pulsed chemical laser[4,5] which is capable of millijoule pulses in contrast to the microjoule pulses achievable with the present device. However, the high repetition rate and uniformity of the present pulses permit full utilization of modern signal averaging techniques to recover weak signals from background noise to provide quite good fluorescence traces as Figs. 7 and 8 demonstrate.

Figure 7 shows a chart recording of the output of the boxcar integrator (see Fig. 5) taken under the same conditions under which the single pulse of Fig. 6 was recorded. This trace was taken with a 3 μsec gatewidth, a 400 μsec time base, and a 1 msec time constant. The entire trace was recorded in a 2 min time interval. The exponential decay of Fig. 7 yielded a value of the rate constant for

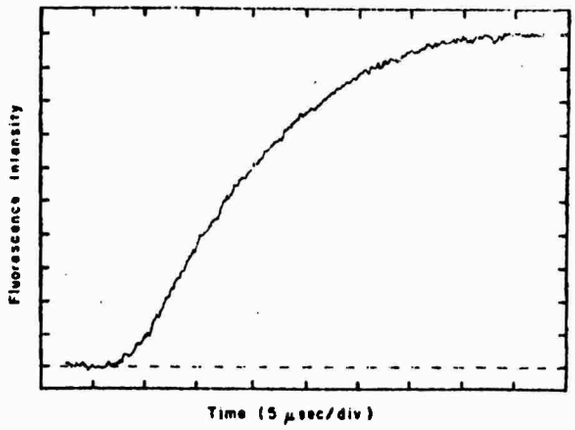

FIG. 8. The initial rise of the fluorescence signal of Fig. 7 obtained with an expanded time scale.

vibrational deactivation of $CO_2(00°1)$ by ground state HF.[11]

In order to examine the over-all process of vibrational energy transfer between HF($v=1$) and ground state CO_2, it was necessary to examine more closely the rise of fluorescence signals such as that shown in Fig. 7.[11] Figure 8 is a recording taken under identical conditions with a 1 μsec gate width, a 50 μsec time base, and 1 msec time constant in order to closely resolve the initial portion of the fluorescence signal. Again, the entire trace was accomplished in a 2 min time interval.

It is clear from these results that much weaker signals could be meaningfully examined without difficulty by increasing the signal averaging time. Our measurements of the HF ($v=1$) deactivation rate in pure HF obtained by monitoring the decay of HF($v=1$) → HF($v=0$) band fluorescence[11] agree well with the previous measurement of Airey and Fried[5] who employed the single-shot pulsed chemical laser technique.

III. A SELECTIVELY TUNABLE PROBE LASER

The present cw chemical laser has provided a convenient probe laser for single-pass gain measurements of HF and DF purely chemical lasers.[12] For this application, the mirror M_2 was replaced with a diffraction grating (Bausch & Lomb 35-63-05-730), blazed at 2.5 μ, of 300 lines/mm, which was Littrow mounted so that the first order diffracted beam sustained laser oscillation. Single frequency operation on any of the individual transitions discussed in Sec. II was possible with this arrangement. It was important to insure that the cavity resonance frequency for oscillation was stabilized near the center frequency of the unsaturated line profile to obtain meaningful gain measurements. For this purpose the grating was mounted upon a piezoelectric ceramic (Lansing model 21.817) stressed by a dc voltage controlled by a feedback network stabilized at maximum laser output power (Lansing model 80.210 lock-in stabilizer).

* Supported by the Advanced Research Projects Agency under ONR Contract N00014-67-A-0077-0006, by the Air Force Office of Scientific Research under Grant AFOSR-70-1952, and by the National Aeronautics and Space Administration under Grant NGL 33-010-064.

† NSF trainee.

[1] C. B. Moore, Acct. Chem. Research 2, 103 (1969).

[2] C. B. Moore, *Fluorescence*, edited by C. G. Guilbault (Marcel Dekker, New York, 1967), p. 133.

[3] W. A. Rosser, Jr., A. D. Wood, and E. T. Gerry, J. Chem. Phys. 50, 4996 (1969).

[4] H. L. Chen and C. B. Moore, J. Chem. Phys. 54, 4072 (1971).

[5] J. R. Airey and S. F. Fried, Chem. Phys. Lett. 8, 23, (1971).

[6] T. A. Cool, R. R. Stephens, and J. A. Shirley, J. Appl. Phys. 41, 4038 (1970).

[7] C. Wittig, J. C. Hassler, and P. D. Coleman, Nature 226, 845 (1970).

[8] J. J. Hinchen and C. M. Banas, Appl. Phys. Lett. 17, 386 (1970).

[9] J. A. Glaze, J. Finzi, and W. F. Krupke, Appl. Phys. Lett. 18, 173 (1971).

[10] Note that quite recently a pulsed OH chemical laser has been developed [A. B. Callear and H. E. Van Den Bergh, Chem. Phys. Lett. 8, 17 (1971)]; a cw device is perhaps feasible utilizing the reaction $H+O_3 \rightarrow OH^*+O_2$.

[11] R. R. Stephens and T. A. Cool, "Vibrational Energy Transfer and Deexcitation in the HF, DF, HF-CO_2, and DF-CO_2 Systems," J. Chem. Phys. (to be published).

[12] J. A. Shirley, R. N. Sileo, R. R. Stephens, and T. A. Cool, "Purely Chemical Laser Operation in the HF, DF, HF-CO_2, and DF-CO_2 Systems," AIAA 9th Aerospace Sciences Meeting, Jan. 1971, Paper 71-27.

Reprinted from:

JOURNAL OF APPLIED PHYSICS VOLUME 42, NUMBER 8 JULY 1971

Frequency Dependence of the Optical Saturation of Vibration-Rotation Transitions*†

N. Djeu‡ and G. J. Wolga
Cornell University, Ithaca, New York 14850
(Received 14 December 1970)

The optical saturation of a vibration-rotation transition in a molecular gas generally cannot be described by any of the saturation formulas obtained with the assumption of fixed pump rates. Its explicit form is derived here by treating rotational relaxation into each of the radiatively interacting levels as a variable pump rate dependent upon the degree of saturation. The formula exhibits a collision-induced power-broadening feature which is distinct from the well-known homogeneous power broadening in form as well as in physical origin. This effect has been observed indirectly in a CO_2 laser.

I. INTRODUCTION

The optical saturation of a pair of atomic levels with fixed pump rates has been considered in the homogeneously and inhomogeneously broadened limits by Gordon *et al.*[4] and in general by Close.[2] In the analysis of a vibration-rotation transition in a molecular gas, however, one cannot realistically assume the pump rates for the radiatively interacting rotational levels to be constant. It is more reasonable to assume fixed pump rates for the associated vibrational levels, since rotational relaxation is always much faster than vibrational relaxation. Consequently, the saturation formula given by Close is no longer applicable in the case of a vibration-rotation transition. One must modify the expression specifically to reflect the additional complication caused by the variable pump rates.

There have been several previous attempts at analyzing the saturation of a vibration-rotation transition,[3-5] but none of them succeeded in obtaining an analytical expression for the saturated incremental gain which is valid for any admixture of Doppler and collision broadening, as well as for arbitrary field intensities. Furthermore, these theories did not examine the frequency dependence of the saturated gain, which, as we shall see later, brings into evidence an entirely new kind of power broadening.

The method employed in arriving at the saturation formula consists of the simultaneous use of rate equations and the Lamb formalism for molecular interaction with an electromagnetic field.[6] The rate equations are written for the radiatively interacting rotational levels and their associated vibrational levels. An additional relation is obtained between the populations of these levels and the intensity of the saturating field, as well as its frequency. The simultaneous solution of these equations leads to an explicit saturation formula for a vibration-rotation transition in a molecular gas.

For sufficiently low pressures, our saturation formula reduces to that given by Close, with the rotational relaxation rate representing the level decay rate. At elevated pressures, the half-width of the saturated transition increases with increasing field intensity. This may occur even when the homogeneous width itself (as may be measured from the Lamb dip) is not significantly power broadened. To distinguish this phenomenon from the power broadening of the homogeneous width, we call it collision-induced power broadening.

II. DERIVATION OF SATURATION FORMULA

In a model of rotational relaxation which characterizes the coupling between one particular rotational level and all the remaining ones in the same vibrational level by a single rate constant, a total of four rate equations is needed for the discussion of the optical saturation of a vibration-rotation transition in a molecular gas. Denote the radiatively interacting rotational states in the upper and lower vibrational levels by a and b and the aggregates of the remaining rotational states in the corresponding vibrational levels by A and B and their respective population densities by N_a, N_b, N_A, and N_B. Molecules in individual rotational states can decay via rotational relaxation to other states in the same vibrational level, or by vibrational relaxation (either radiatively or collisionally) into a different vibrational level, or by diffusion to the wall and deactivation thereupon. Therefore, so long as the mean free path of the molecules is much smaller than the dimensions of the apparatus, we can write the following rate equations:

$$\frac{dN_a}{dt} = -\gamma_a N_a + \frac{\gamma_a}{n_a} N_A - R_a(N_a - N_a^e) + D_a \nabla^2 N_a + S,$$

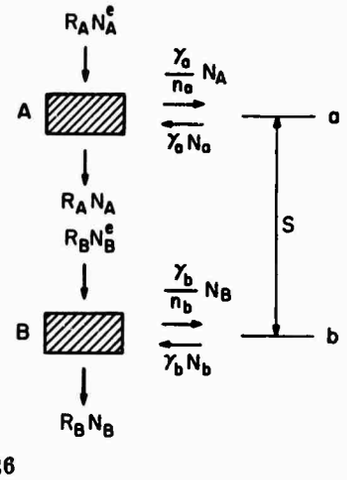

FIG. 1. Schematic of molecular processes on which the rate equations are based.

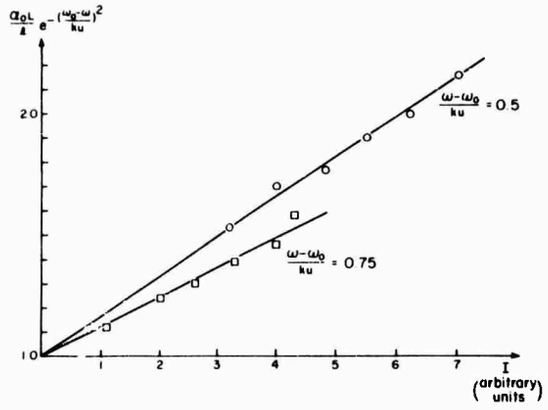

FIG. 2. Saturation of the CO_2 gain medium at two different frequencies of a 10.4-μ band transition.

$$\frac{dN_b}{dt} = -\gamma_b N_b + \frac{\gamma_b}{n_b} N_B - R_b(N_b - N_b^e) + D_b \nabla^2 N_b - S,$$

$$\frac{dN_A}{dt} = \gamma_a N_a - \frac{\gamma_a}{n_a} N_A - R_a(N_A - N_A^e) + D_A \nabla^2 N_A,$$

$$\frac{dN_B}{dt} = \gamma_b N_b - \frac{\gamma_b}{n_b} N_B - R_b(N_B - N_B^e) + D_B \nabla^2 N_B,$$

where γ_a and γ_b are the rotational relaxation rates, R_a and R_b are the vibrational relaxation rates, and $D_a \equiv D_A$ and $D_b \equiv D_B$ are the diffusion constants for the upper and lower levels, respectively. The interaction with radiation is represented by S and the superscript e denotes equilibrium populations (which are not thermal for a gain medium). The fractions $1/n_a$ and $1/n_b$ are equal to N_a^e/N_A^e and N_b^e/N_B^e, respectively.

For cylindrical geometry, the diffusion terms can be replaced by effective relaxation rates with radial dependence

$$\Gamma_\alpha(r) = -\frac{D_\alpha \nabla^2 N_\alpha(r)}{N_\alpha(r) - N_\alpha^e} \quad (\alpha = a,\ A,\ b,\ B).$$

Furthermore, under the assumption of large apparatus dimension, we always have $R_a, \Gamma_a \ll \gamma_a$ and $R_b, \Gamma_b \ll \gamma_b$. Defining $R_A(r) = \Gamma_A(r) + R_a$ and $R_B(r) = \Gamma_B(r) + R_b$ then, we simplify the above equations to obtain

$$\frac{dN_a}{dt} = -\gamma_a N_a + \frac{\gamma_a}{n_a} N_A + S, \tag{1}$$

$$\frac{dN_b}{dt} = -\gamma_b N_b + \frac{\gamma_b}{n_b} N_B - S, \tag{2}$$

$$\frac{dN_A}{dt} = \gamma_a N_a - \frac{\gamma_a}{n_a} N_A - R_A(r)(N_A - N_A^e), \tag{3}$$

$$\frac{dN_B}{dt} = \gamma_b N_b - \frac{\gamma_b}{n_b} N_B - R_B(r)(N_B - N_B^e), \tag{4}$$

which are illustrated schematically in Fig. 1.

It is clear now that $\gamma_a N_A/n_a$ and $\gamma_b N_B/n_b$ are the pump terms for the radiatively interacting levels a and b, respectively.

These pump terms will be shown to be variables dependent upon the intensity, as well as the frequency of the saturating field. This dependence is, in turn, reflected in the saturated gain for the transition connecting a and b.

In order to make use of the results in Ref. 2, we have to assume that a and b are nondegenerate, which admittedly is unrealistic for vibration-rotation transitions because of the existence of the magnetic sublevels. But for transitions where the mean deviation of the dipole moments of the degenerate sublevels from some average value is small, the approximation should be a good one. Such is the case for the P- and R-branch transitions,[7] to which we shall restrict our attention in what follows.

In this connection, it may be helpful to point out that for linearly polarized light, the number of active sublevels (those with nonzero matrix elements) in the upper rotational level is the same as in the lower whether $J_a = J_b - 1$ or $J_a = J_b + 1$. It is equal to the smaller of $g_a \equiv 2J_a + 1$ and $g_b \equiv 2J_b + 1$, and we shall label it g. It should be noted that N_a and N_b used in the rate equations above consist of only the active sublevels. That is, they are both g-fold degenerate.

With this understanding, then, we can use the basic results from Ref. 2. The saturated incremental gain for an electromagnetic wave traveling in the z direction with intensity I was given in rationalized mks units as

$$\frac{1}{I}\frac{dI}{dz} = \frac{\sqrt{\pi} p^2}{\epsilon_0 \hbar u}\left(\frac{N_A}{n_a} - \frac{N_B}{n_b}\right)\frac{\mathrm{Re}W(x+iy)}{(1+I/I_0)^{1/2}}, \tag{5}$$

with

$$W(x+iy) = \frac{2}{\sqrt{\pi}} e^{-(x+iy)^2} \int_{-i(x+iy)}^{\infty} e^{-t^2}\, dt,$$

where

$$u = (2kT/M)^{1/2},$$

$$x = (c/u\omega)(\omega_0 - \omega),$$

$$y = (c\gamma'/u\omega)(1 + I/I_0)^{1/2},$$

and

$$I_0 = (2\epsilon_0 c\hbar^2/p^2)\gamma_a\gamma_b\gamma'/(\gamma_a + \gamma_b).$$

Here ω is the angular frequency of the saturating light beam, ω_0 is the angular frequency of the absorbing transition at line center, γ' is the dephasing collision rate [not necessarily equal to $\frac{1}{2}(\gamma_a + \gamma_b)$], and, according to the discussion above, we have

$$p^2 = \frac{1}{g}\sum_{i=1}^{g}\sum_{j=1}^{g} |\langle a_i | P_x | b_j \rangle|^2,$$

where a_i and b_j are the magnetic sublevels of a and b, respectively. In the limit of $y \to 0$, $\mathrm{Re}W(x+iy)$ becomes the familiar Gaussian function.

We note in particular that N_A and N_B in (5) are vari-

ables. In order to write the saturation formula in terms of known parameters, we need an additional relation expressing the rotational disequilibrium within the vibrational levels. For that purpose, we rewrite Eq. (36) in Ref. 2 in terms of our own symbols as follows:

$$N_a(v) - N_b(v) = \left(\frac{N_A}{n_a} - \frac{N_B}{n_b}\right) U(v) \times \left(1 + \frac{\gamma' I}{2I_0}\left\{\left[\gamma' - i\left(\omega_0 - \omega + \frac{\omega}{c}v\right)\right]^{-1} + \text{c.c.}\right\}\right)^{-1}, \quad (6a)$$

where $N_a(v)$ and $N_b(v)$ are population densities of molecules with velocity v and $U(v)$ is the velocity distribution function

$$U(v) = (\sqrt{\pi}u)^{-1} \exp(-v^2/u^2).$$

Integrating (6a) over velocity, we find

$$N_a - N_b = \left(\frac{N_A}{n_a} - \frac{N_B}{n_b}\right)\left[1 - \frac{\gamma'\sqrt{\pi}c}{u}\frac{I}{I_0}\frac{\mathrm{Re}W(x+iy)}{(1+I/I_0)^{1/2}}\right]. \quad (6b)$$

Equation (6b) shows precisely how rotational equilibrium is disturbed by the saturating optical field. The simultaneous solution of Eqs. (1) – (4) in steady state and (6b) yields

$$\frac{N_A}{n_a} - \frac{N_B}{n_b} = \left(\frac{N_A^e}{n_a} - \frac{N_B^e}{n_b}\right)\left(1 + \frac{\sqrt{\pi}\gamma\gamma'}{ku\bar{\gamma}}\frac{I}{I_0}\frac{\mathrm{Re}W(x+iy)}{(1+I/I_0)^{1/2}}\right)^{-1},$$

where

$$\gamma = 2(1/\gamma_a + 1/\gamma_b)^{-1}$$

and

$$\bar{\gamma} = 2(1/n_a R_A + 1/n_b R_B)^{-1}.$$

We thus arrive at the following explicit saturation formula for vibration-rotation transitions:

$$\frac{1}{I}\frac{dI}{dz} = \frac{\sqrt{\pi}p^2}{\epsilon_0 \hbar u}\left(\frac{N_A^e}{n_a} - \frac{N_B^e}{n_b}\right)\frac{\mathrm{Re}W(x+iy)}{(1+I/I_0)^{1/2} + K(I/I_0)\mathrm{Re}W(x+iy)}, \quad (7)$$

where

$$K = \sqrt{\pi}\gamma\gamma'/ku\bar{\gamma}.$$

We first investigate the low-pressure behavior of this formula. The rates γ and γ' are directly proportional to pressure, whereas a diffusion-dominated $\bar{\gamma}$ (below ~0.1 Torr) is inversely proportional to pressure. Therefore, the parameter K approaches zero with a cubic dependence on pressure. However, it must be remembered that Eq. (7) was derived with the assumption that the rotational relaxation rate is much faster than the diffusion rate ($\Gamma_a, \Gamma_b \ll \gamma_a, \gamma_a$). This condition implies pressures in excess of 10^{-2} Torr for typical molecules. But it is still possible to have $K \ll 1$ for pressures greater than this lower limit, because the numbers N_a and N_b are generally quite large. In this case ($K \ll 1$) the saturation formula reduces to

$$\frac{1}{I}\frac{dI}{dz} = \frac{\sqrt{\pi}p^2}{\epsilon_0 \hbar u}\left(\frac{N_A^e}{n_a} - \frac{N_B^e}{n_b}\right)\frac{\mathrm{Re}W(x+iy)}{(1+I/I_0)^{1/2}}. \quad (8)$$

Interpreting the rotational relaxation rate in I_0 as the level decay rate, we see that Eq. (8) is identical to the formula given by Close for atomic levels with constant pump rates. This is to be expected, since in the pressure regime for which Eq. (8) is valid the levels a and b are coupled mainly to A and B, while the latter are coupled mainly to the region outside of the saturating beam. Consequently, the vibrational populations will remain in equilibrium regardless of the intensity of the saturating field. It is not surprising, then, that we obtain the result corresponding to constant pump rates in this limit.

For K on the order of unity, a comparison of Eqs. (7) and (8) show that saturation sets in for a smaller I/I_0 for the former at all frequencies. Furthermore, due to the presence of the $\mathrm{Re}W(x+iy)$ term in the denominator of Eq. (7), the transition is less readily saturated away from line center. This kind of frequency dependence gives rise to the phenomenon of collision-induced power broadening, which we now discuss.

III. COLLISION - INDUCED POWER BROADENING

For pressures above 10^{-1} Torr or so, $\bar{\gamma}$ becomes dominated by volume quenching, and K begins to have a linear dependence on pressure. For $K \gg 1$, the saturation formula becomes

$$\frac{1}{I}\frac{dI}{dz} = \frac{\sqrt{\pi}p^2}{\epsilon_0 \hbar u}\left(\frac{N_A^e}{n_a} - \frac{N_B^e}{n_b}\right)\frac{\mathrm{Re}W(x+iy)}{1 + (I/I_0)K\mathrm{Re}W(x+iy)}. \quad (9)$$

For the purpose of comparison, we write down the frequency and intensity dependence of the saturated linear absorption coefficient for a collision broadened transition[6]:

$$\frac{1}{I}\frac{dI}{dz} \sim \frac{\gamma^2[\gamma^2 + (\omega - \omega_0)^2]^{-1}}{1 + (I/I_s)\gamma^2[\gamma^2 + (\omega - \omega_0)^2]^{-1}}, \quad (10)$$

where

$$I_s = \epsilon_0 c(\gamma^2 \hbar^2/p^2).$$

The power broadening of such a homogeneously broadened line is well known. For the same field intensity, saturation sets in more slowly as the frequency of the field moves away from line center simply because the small-signal absorption coefficient decreases away from line center. In other words, the saturating field becomes less effective in distorting the level populations from equilibrium as its frequency moves towards the wings of the Lorentzian line shape.

Superficially, Eq. (9) is just Eq. (10) with a Gaussian-like function replacing the Lorentzian function. But in physical origin, the power broadening exhibited by Eq. (9) is quite different. According to Eq. (9), power broadening can take place even for a Doppler-broadened transition. This substantially modifies the customary notion that power broadening is to be associated with a homogene-

ously broadened line. For vibration-rotation transitions, power broadening (in the high-pressure regime) results from the varying degrees of deviation of the vibrational level populations (and hence the pump rates) from equilibrium as the frequency of a fixed-intensity saturating field changes. for the same power density, the pump rates for the radiatively interacting rotational levels are altered the most for a saturating wave with its frequency equal to that at molecular line center. Because of the obvious connection between rotational relaxation and this phenomenon, we refer to it as collision-induced power broadening.

In order to make the distinction between collision-induced power broadening and the usual power broadening of a homogeneous transition absolutely clear, let us examine the power dependence of the width of the hole burned in the Doppler-like profile. It can be shown[9] that the hole width is given by

$$\gamma_h = \gamma'(1+I/I_0)^{1/2}.$$

Therefore, the homogeneous component, which is represented by the hole, begins to broaden for I comparable to I_0. On the other hand, from Eq. (9), we see that collision-induced power broadening would occur for I of the order of I_0/K. Since $K \gg 1$, it is possible to have power broadening of the overall molecular line shape while γ_h remains close to γ'. This analysis shows clearly that collision-induced power broadening is not a manifestation of the power broadening of the homogeneous components.

IV. EXPERIMENT IN A CO_2 LASER

A simple experiment was performed using a CO_2 laser to demonstrate the collision-induced power-broadening effect. Consider a symmetrically constructed laser operating on a single mode. The holes burned in the gain profile in such a laser are symmetric about line center. If the overlap of these holes is small, they can be assumed to saturate the transition independently. If I is the intensity of the wave traveling in either direction inside the cavity, it can be shown[9] that Eq. (7) would apply now with $2K$ replacing K. Thus, for $I \ll I_0$ and $\gamma' \ll ku$, we have

$$\frac{1}{I}\frac{dI}{dz} = \frac{\alpha_0 \exp[-(\omega-\omega_0)^2/(ku)^2]}{1+2K(I/I_0)\exp[-(\omega-\omega_0)^2/(ku)^2]},$$

where

$$\alpha_0 = \frac{\sqrt{\pi}p^2}{\epsilon_0 \hbar u}\left(\frac{N_A^e}{n_a} - \frac{N_B^e}{n_b}\right).$$

The output of the laser from either end mirror is the intensity of one of the traveling waves inside the cavity multiplied by the transmittivity of the mirror. Therefore, the field intensity inside the cavity can be determined from the detected output power density. Since the gain inside the cavity at the frequency of oscillation is saturated down to the loss level, we can write, for small $\alpha_0 L$

$$\frac{\alpha_0 L \exp[-(\omega-\omega_0)^2/(ku)^2]}{1+2K(I/I_0)\exp[-(\omega-\omega_0)^2/(ku)^2]} = l,$$

where L is the length of the active medium and l is the cavity loss per transit. Rearranging, we obtain

$$(\alpha_0 L/l)\exp[-(\omega-\omega_0)^2/(ku)^2] = 1+2K(I/I_0)\exp[-(\omega-\omega_0)^2/(ku)^2]. \quad (11)$$

For a given ω, then, the plot of $(\alpha_0 L/l)\exp[-(\omega-\omega_0)^2/(ku)^2]$ vs I is a straight line intercepting the ordinate at unity. The slope of the straight line should have the Doppler dependence on ω as required by Eq. (11). The ratio $\alpha_0 L/l$ itself is easily calculated from

$$\alpha_0 L/l = \exp[(\tfrac{1}{2}\Delta\omega)^2/(ku)^2],$$

where $\Delta\omega$ is the single-mode oscillation width.

The experiment employed a 1.45-m-long cavity with a 1-m water-cooled CO_2 gain tube. The resonator was formed by a 98% reflecting curved mirror (with a 5.7-m radius of curvature) and a 150-line/mm grating operated in Littrow (with 96% efficiency). Only CO_2 and N_2 were used in the gain tube, with a total pressure of 0.58 Torr (thus ensuring $\gamma' \ll ku$). Gain was varied by adjusting the discharge current, and it was assumed that the procedure leaves all the other parameters unchanged. With increasing current, the tuning curves, which all exhibited the Lamb dip, showed progressively larger oscillation widths. But the condition $I \ll I_0$ was fulfilled even for the highest gain used.

Analysis was made of the saturation behavior at $(\omega-\omega_0)/(ku) = 0.5$ and 0.75, for which the overlapping of the homogeneous holes is indeed insignificant. The results are shown in Fig. 2, where the power intensity axis is approximately scaled to W cm^{-2}. When the slopes of the straight lines are computed, we find this ratio to be 1.3, in good agreement with the predicted ratio of 1.37 obtained from (11). Thus, the experiment suggests strongly that the effect of collision-induced power broadening does exist for vibration-rotation transitions in molecular gases.

*Work supported by the Advanced Research Projects Agency of the Department of Defense and was monitored by CNR, under Contract No. N00014-67-A-0077-0006.

†This paper is based on a thesis submitted by N. Djeu to Cornell University in partial fulfillment of the requirements of the Ph.D. degree.

‡Present address: Naval Research Laboratory, Washington, D.C. 20390.

[1] E. I. Gordon, A. D. White, and J. D. Rigden, in *Proceedings of the Symposium on Optical Masers at the Polytechnic Institute of Brooklyn*, 1963 (Polytechnic Press, Brooklyn, New York, 1963).

[2] D. H. Close, Phys. Rev. 153, 360 (1967).

[3]I. Burak, J.I. Steinfeld, and D.G. Sutton, J. Quant. Spectry. Radiative Transfer 9, 959 (1969).
[4]O. R. Wood, II, P. L. Gordon, and S. E. Schwarz, IEEE J. Quantum Electron. Q.E.-5, 302 (1969).
[5]C. P. Christensen, C. Freed, and H. A. Haus, IEEE J. Quantum Electron. QE-5, 276 (1969).
[6]W. E. Lamb, Jr., Phys. Rev. 134, A1429 (1964).
[7]H. C. Allen, Jr. and P. C. Cross, *Molecular Vib-Rotors* (Wiley, New York, 1963).
[8]R. Karplus and J. Schwinger, Phys. Rev. 73, 1020 (1948).
[9]N. Djeu, Ph. D. thesis (Cornell University, Ithaca, N.Y., 1970) (unpublished).

IEEE JOURNAL OF QUANTUM ELECTRONICS, VOL. QE-7, NO. 6, JUNE 1971

Repetitive Passive Q Switching of Single-Frequency Lasers

HOWARD T. POWELL AND GEORGE J. WOLGA

Abstract—A simple model describing repetitive passive Q switching of a single-frequency laser with an intracavity saturable absorber is presented. Three coupled nonlinear rate equations are postulated to describe the inversion density of the amplifier, the inversion density of the absorber, and the photon density in the laser cavity. Each of the three variables is assumed to exhibit a simple exponential relaxation. By considering the linear equations describing small deviations about the expected equilibrium point, a condition on the various parameters is found that describes when repetitive pulsing will occur. Digital computer solutions are shown to verify this condition. Experiments with a CO_2 laser with an internal CO_2 absorber provide qualitative agreement with the model.

I. Introduction

SATURABLE absorbers within a CO_2 laser cavity can produce spontaneous repetitive pulsing of the laser intensity. The gases SF_6, C_3H_6 (propylene), heated CO_2, BCl_3 plus a small amount of NH_3, and others have been used to provide saturable absorption [1]–[5]. This mode of operation was labeled repetitive passive Q switching by its first observers, Wood and Schwarz [1]. They have suggested that the operating intensity of the laser must produce significant saturation of the absorber for such pulsing. A simple model that yields a more detailed condition on the laser parameters delineating when repetitive pulsing will occur is presented here. An approximate formula for the pulsation frequency is also given, but the analysis does not predict the pulse height or width.

A clear distinction must be made between repetitive passive Q switching and pulsation in mode-locked lasers. It was observed that passive Q switching can occur in a single-mode single-frequency CO_2 laser. Hence such Q switching does not depend on the interaction of numerous cavity modes. Multimode lasers with an internal saturable absorber can exhibit passive Q switching and mode locking concurrently [6]. Mode interactions are neglected and thus this treatment applies best to single-mode lasers.

The phenomenon of output spikes in solid-state lasers has been widely discussed. Theoretical considerations of a mathematical system of two rate equations governing the field intensity and inverted population density have predicted that only damped relaxation oscillations should occur [7]. The present treatment uses an independent third rate equation to describe the absorber. This additional degree of freedom will be shown to allow the possibility of repetitive pulsation. Shimoda has shown theoretically that a supposed cavity loss, whose saturation follows the instantaneous value of the field, can produce undamped relaxation oscillations [8]. A more general model is used for better examination of the system dynamics.

Intracavity absorbers are commonly used in the pulsed ruby laser to act as a saturable switch that has the effect of compressing the optical energy into a single giant pulse. Theoretical treatments of such giant pulses [9], [10] use equations resembling those applied here. However, since such studies presumed a pulsed pumping source, the need to consider repetitive pulsing did not arise.

II. Rate Equations and Approximations

In the simplest use of phenomenological rate equations one neglects any spatial dependence and deals only with inversion and photon densities. In this model all gain and loss parameters are considered to be uniformly distributed throughout the optical cavity. This approximation is only valid if the photon transit time is short compared to the time scale of population or laser intensity changes. For a 3-m cavity the use of such rate equations to describe changes on the microsecond scale is well justified. It is also assumed that the entire level population interacts with the radiation field, i.e., homogeneous broadening. Since this assumption is not satisfied for Doppler-broadened gaseous absorbers, the model must be applied with some discretion.

A two-level approximation for both the amplification medium and the absorption medium is assumed. For application to a CO_2 amplifier the levels correspond to specific rotational states of the 00^01 and 10^00 vibrational states. Treating the CO_2 laser as a two-level system despite the presence of strongly coupled rotational levels is certainly an approximation and is discussed in Section VI.

The relaxation of a population difference to an equilibrium that produces either an amplification or absorption can often be described by a single exponential decay. For many continuously lasing media the lower level exhibits a much faster relaxation (either radiative or collisional) than the upper. For moderately saturating intensities the upper state population is sizably depressed while the lower state population is virtually unchanged. The time dependence of the population inversion is then described by a single relaxation rate, which is the

Manuscript received August 25, 1970; revised January 4, 1971. This work was supported by the Advanced Research Projects Agency of the Department of Defense and monitored by ONR under Contract N00014-67-A-0077-0006.

The authors are with Cornell University, Ithaca, N. Y. 14850.

relatively slow rate of the upper level. Assume that the population differences describing amplification and absorption in a Q-switching system are each governed by a single relaxation rate. These assumptions lead to a set of three rate equations:

$$\frac{dn_1}{dt} = -\alpha n_1 S - \gamma_1(n_1 - n_1^0) \tag{1a}$$

$$\frac{dn_2}{dt} = -\beta n_2 S - \gamma_2(n_2 - n_2^0) \tag{1b}$$

$$\frac{dS}{dt} = (\alpha n_1 - \beta n_2)S - \gamma_c S \tag{1c}$$

where

- n_1 equivalent inversion density of the gain medium if distributed over the cavity length;
- n_2 negative inversion density of the absorption medium also distributed;
- S photon number density;
- α, β field interaction coefficients; $c\lambda^2/(8\pi t_{spon})g(\nu)$ [$g(\nu)$ is a normalized line shape factor and t_{spon} is the radiative lifetime between the upper and lower levels];
- γ_1, γ_2 relaxation rates for the gain and loss media;
- γ_c cavity loss rate;
- n_1^0, n_2^0 inversion densities in the absence of a laser field but with the presence of pumping sources.

Notice that the usual pumping terms have been incorporated into n_1^0 and n_2^0; hence the relaxation returns the population difference to the equilibrium value equally for either positive or negative deviations. A more general model with rate equations for both the upper and lower levels of each medium could be postulated giving a more complex system of five equations.

By digital computer solution it is shown that the set of nonlinear equations (1a)–(1c) does exhibit a periodic pulsing mode for some sets of parameters. Such a solution is visualized as a closed trajectory or limit cycle in the n_1, n_2, S space. Before discussing what choices of parameters lead to a limit cycle first consider the expected steady state where all the time derivatives of (1) are equal to zero.

III. Equilibrium Solution of Rate Equations

Denote the expected steady-state values by $\bar{n}_1$, $\bar{n}_2$, and $\bar{S}$. Setting the time derivatives in (1) equal to zero, we obtain

$$\bar{n}_1 = \frac{n_1^0}{1 + \alpha\bar{S}/\gamma_1} \tag{2a}$$

$$\bar{n}_2 = \frac{n_2^0}{1 + \alpha\bar{S}/\gamma_2} \tag{2b}$$

$$\gamma_c\bar{S} = \frac{\alpha n_1^0\bar{S}}{1 + \alpha\bar{S}/\gamma_1} - \frac{\beta n_2^0\bar{S}}{1 + \beta\bar{S}/\gamma_2}. \tag{2c}$$

Equation (2c) determines the value of $\bar{S}$ for which the total saturated gain is equal to the cavity loss. A graphical solution of (2c) provides considerable insight and is

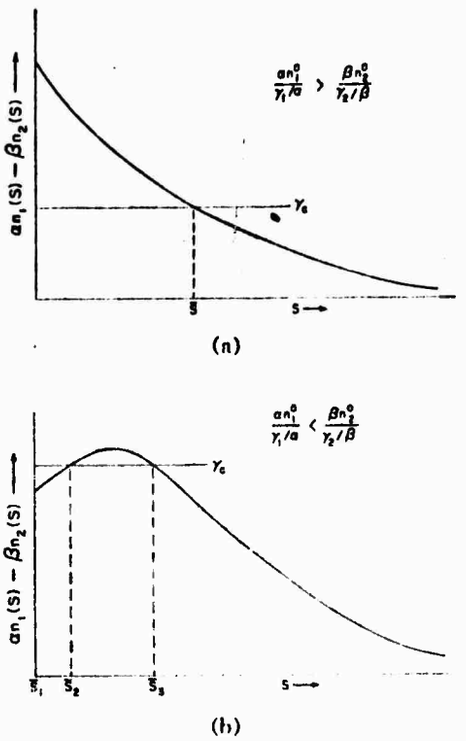

Fig. 1. Saturated amplifier gain minus saturated absorber loss is shown as a function of CW laser intensity. Possible steady-state photon densities are found when this effective saturated gain rate equals the cavity loss rate.

shown in Fig. 1. Fig. 1(a) shows a monotonic decrease of the effective gain with the steady-state field. Fig. 1(b) shows an initial increase in the effective gain due to the saturation of the absorption for small fields. This initial increase can occur when the absorption rate βn_2^0 divided by its saturation parameter γ_2/β is greater than the corresponding ratio for the amplifier. This condition is easily found by examining the sign of the linear term in $\bar{S}$ in the expansion of the effective gain (2c) for small fields.

In Fig. 1(b), $\bar{S}_1 = 0$ is a stable solution of (2c) since the total unsaturated gain is less than the cavity loss. We expect $\bar{S}_3$ to be a stable solution while $\bar{S}_2$ is obviously not. From (1c) notice that small deviations from $\bar{S}_2$ cause the photon density to move from that point to either the stable point $\bar{S}_1$ or $\bar{S}_3$. This argument is essentially that detailed in [11]. Kazantsev *et al.* [11] argue that the presence of two stable solutions ($\bar{S}_1$ and $\bar{S}_3$) can cause hysteresis behavior and sudden transitions from one solution to the other as laser parameters are slowly changed. A simple example of this is seen by changing the cavity loss rate γ_c. For Fig. 1(b) there is a region of intensities bordering zero that are not allowed. If the loss is decreased from a large value, the zero intensity solution is preferred until the intensity must jump to a finite value. However, if the loss is increased from a small value, intensity solutions like $\bar{S}_3$ are chosen until the field must drop suddenly to zero. Such intensity jumping and hysteresis have been observed experimentally [12].

In the next section it is shown that supposedly stable solutions considered here, may give pulsing behavior.

IV. Stability Requirements

The set of nonlinear equations (1a)–(1c) is not amenable to analytic solution. However, it can be determined if a presumed equilibrium point gives stable operation. An equilibrium point is stable if and only if the linear system of equations describing small deviations about that equilibrium point, exhibits fundamental modes that are all damped [13]. It will be shown that near a presumed equilibrium point, small deviations may sometimes grow in an oscillatory fashion. The condition for this happening is identified with that of repetitive passive Q switching.

Strictly speaking an oscillatory instability need not lead to a limit cycle, but our computer solutions have shown that the identification is valid at least for cases where there are no stable equilibrium points. For very special cases where there is one stable equilibrium point at $\bar{S} = 0$ and two other unstable ones, simply studying small deviations is not adequate. From the linear equations the condition for a pulsing intensity to occur may be correctly identified, but no information is obtained about the amplitude of the expected pulsation or its precise time dependence. Our numerical solutions show that the frequency of the nonlinear oscillation is approximately given by the frequency found in the linear region.

Following the general prescription, the supposed equilibrium is expanded to first order in the deviations,

$$\begin{aligned} n_1(t) &= \bar{n}_1 + x(t) \\ n_2(t) &= \bar{n}_2 + y(t) \\ S(t) &= \bar{S} + s(t) \end{aligned} \tag{3}$$

$$\frac{dx}{dt} = -\alpha\bar{S}x - \alpha\bar{n}_1 s - \gamma_1 x$$

$$\frac{dy}{dt} = -\beta\bar{S}y - \beta\bar{n}_2 s - \gamma_2 y$$

$$\frac{ds}{dt} = (\alpha x - \beta y)\bar{S} + (\alpha\bar{n}_1 - \beta\bar{n}_2 - \gamma_c)s. \tag{4}$$

Temporarily assume that the equilibrium condition corresponds to nonzero $\bar{S}$ so that through saturation $\alpha\bar{n}_1 - \beta\bar{n}_2 - \gamma_c$ is zero. Assuming a solution vector (x, y, s) proportional to $e^{\lambda t}$, one obtains the usual determinant condition that yields a cubic equation for λ,

$$\begin{aligned} \lambda^3 + \left[\frac{\gamma_1 n_1^0}{\bar{n}_1} + \frac{\gamma_2 n_2^0}{\bar{n}_2}\right]\lambda^2 \\ + \left[\left(\frac{\gamma_1 n_1^0}{\bar{n}_1}\right)\left(\frac{\gamma_2 n_2^0}{\bar{n}_2}\right) + \bar{S}(\alpha^2\bar{n}_1 - \beta^2\bar{n}_2)\right]\lambda \\ + \bar{S}\left[\alpha^2\bar{n}_1\frac{\gamma_2 n_2^0}{\bar{n}_2} - \beta^2\bar{n}_2\frac{\gamma_1 n_1^0}{\bar{n}_1}\right] = 0. \end{aligned} \tag{5}$$

Equations (2a) and (2b) have been used to reexpress such terms as $\alpha\bar{S} + \gamma_1$. The case $\bar{S} = 0$ is always a possible equilibrium solution of (1). In this instance one must retain all the terms in (4) and the expected values of $\lambda = -\gamma_1$, $\lambda = -\gamma_2$, and $\lambda = \alpha n_1^0 - \beta n_2^0 - \gamma_c$ can be easily found. For amplifier gain minus absorber loss greater than the cavity loss, $\bar{S} = 0$ is not a stable equilibrium as expected.

The bracketed coefficients in (5) are all functions of $\bar{S}$, which is easily varied through the cavity loss. Presume that the cavity loss is decreased just to the point where it equals the total effective gain. The system roots for λ are then $-\gamma_1$, $-\gamma_2$, and 0. As $\bar{S}$ is increased from zero by decreasing γ_c, the three roots must move smoothly in the complex λ plane. If any of the roots enters the positive half-plane, the system point is ruled unstable.

A special case of the Hurwitz algorithm [14] is applicable. All three roots of the cubic polynomial $\lambda^3 + a_1\lambda^2 + a_2\lambda + a_3$ (a_1, a_2, and a_3 real) exhibit negative real parts if and only if the following conditions are satisfied: $a_1 > 0$, $a_3 > 0$ and $a_1 a_2 > a_3$. For polynomial (5) the first condition is trivially satisfied. The second condition requires for stability that

$$\alpha^2\bar{n}_1\frac{\gamma_2 n_2^0}{\bar{n}_2} - \beta^2\bar{n}_2\frac{\gamma_1 n_1^0}{\bar{n}_1} > 0. \tag{6}$$

The fact that certain solutions approaching $\bar{S} = 0$ are not stable corresponds to the root at the origin for $\bar{S} = 0$ moving into the positive half-plane along the real axis as γ_c is decreased. Indeed these unstable solutions can be shown to be like $\bar{S}_2$ in Fig. 1(b). An alternative condition for this type of instability is

$$\frac{d}{d\bar{S}}(\alpha\bar{n}_1 - \beta\bar{n}_2)\,|_{s=0} > 0. \tag{7}$$

One may easily show that this implies the stability condition (6) and provides a nice cross check of the present formalism.

For stability the third condition requires

$$\left(\frac{\gamma_1 n_1^0}{\bar{n}_1} + \frac{\gamma_2 n_2^0}{\bar{n}_2}\right)\left(\frac{\gamma_1 n_1^0}{\bar{n}_1}\right)\left(\frac{\gamma_2 n_2^0}{\bar{n}_2}\right) + \bar{S}(\alpha^2\gamma_1 n_1^0 - \beta^2\gamma_2 n_2^0) > 0. \tag{8}$$

It is asserted that passive Q switching results when (8) is not satisfied. This third condition corresponds to one real negative root and two complex conjugate roots whose real part is crossing zero. This can be proved by assuming such roots and expanding to find the corresponding polynomial. One also finds that the square of the oscillation frequency is given by a_2 if the real part of the complex roots is zero. Thus condition (8) gives a sinusoidally growing deviation of approximate frequency

$$\omega^2 \simeq \left(\frac{\gamma_1 n_1^0}{\bar{n}_1}\right)\left(\frac{\gamma_2 n_2^0}{\bar{n}_2}\right) + \bar{S}(\alpha^2\bar{n}_1 - \beta^2\bar{n}_2). \tag{9}$$

Equation (9) is exact only when (8) is satisfied as an equality.

Some simple predictions can be made from (8). A necessary requirement for pulsed operation is

$$(\beta n_2^0)\beta\gamma_2 > (\alpha n_1^0)\alpha\gamma_1. \tag{10}$$

78

The unsaturated amplification and absorption rates have been enclosed by parentheses. We see from (8) that CW operation should always be achieved for $\bar{S}$ sufficiently close to zero. Since the first term of (8) contains powers up to $\bar{S}^3$, there is also a maximum $\bar{S}$ that allows pulsation.

To illustrate the typical magnitude of the terms in (8), consider a gaseous molecular medium for both the amplifier and absorber. The effective relaxation rates are likely to be between 10^3 and 10^6 s^{-1}. With, for example, a 3-m cavity and an average coupling loss of 10 percent, γ_c is 10^7 s^{-1}. For reasonable amplification and absorption the rates αn_1^0 and βn_2^0 must be comparable to γ_c. Furthermore, with moderate gain saturation the stimulated emission rate $\alpha\bar{S}$ is comparable to the relaxation rate γ_1. First assume that the inequality (10) is substantially satisfied, for instance by a factor of 2. At typical intensities the second term in (8) is one to four orders of magnitude greater than the first with the fastest to slowest relaxation rates mentioned. Hence the upper and lower limits for $\bar{S}$ bounding the pulsation region may be extremely large and small, respectively, compared to usual laboratory intensities. When (10) is barely satisfied observable transitions between pulsed and CW operation can occur by varying $\bar{S}$. One can check from (8) that if the relaxation rate of either media is comparable to γ_c, pulsing is difficult to achieve.

Under most conditions, (10) determines when pulsing will occur. Condition (10) agrees with the experimental observation of Karlov *et al.*, [4] that passive Q switching is promoted by increasing the relaxation rate of the saturable absorber. Distinct features of the absorber favor pulsation. For rapid absorber bleaching, which allows a pulse to rise in a Q-switched manner, the absorber should interact more strongly with the field than the amplifier. Then as the intensity starts to fall the absorber should repump its population more rapidly than the amplifier to quench that pulse. Eventually the system relaxes to a point where the pulse action repeats. Equation (10) describes the balance between these features.

By applying the saturated gain condition (2c) to (9), it is observed that the oscillation frequency of small deviations increases with S provided β/α is less than unity. From (9) ω^2 is given at very low intensities by $\gamma_1\gamma_2$. For intensities giving moderate saturation of the gain medium and with α comparable to β, ω^2 is approximately given by $\gamma_1\gamma_c$. A similar range of nonlinear pulsation frequencies is expected.

V. Digital Computer Solutions

To verify the general conclusions digital computer solutions of the nonlinear system (1) were obtained for a few special cases. Dimensionless variables n_1/n_1^0, n_2/n_2^0, and $\alpha S/\gamma_1$ were used. Complete numerical specification of (1) is then given by the rates αn_1^0, βn_2^0, γ_1, γ_2, and γ_c and the ratio β/α, which was fixed at unity. Primarily for illustration γ_1 was fixed at 5×10^4 s^{-1}, γ_2 at 1×10^6 s^{-1}, αn_1^0 at 20×10^6 s^{-1} (corresponding to 20 percent gain/pass for a 3-m cavity), and γ_c at 5×10^6 s^{-1}. For βn_2^0 greater than 10×10^6 s^{-1} (8) predicts pulsation for nearly all $\bar{S}$.

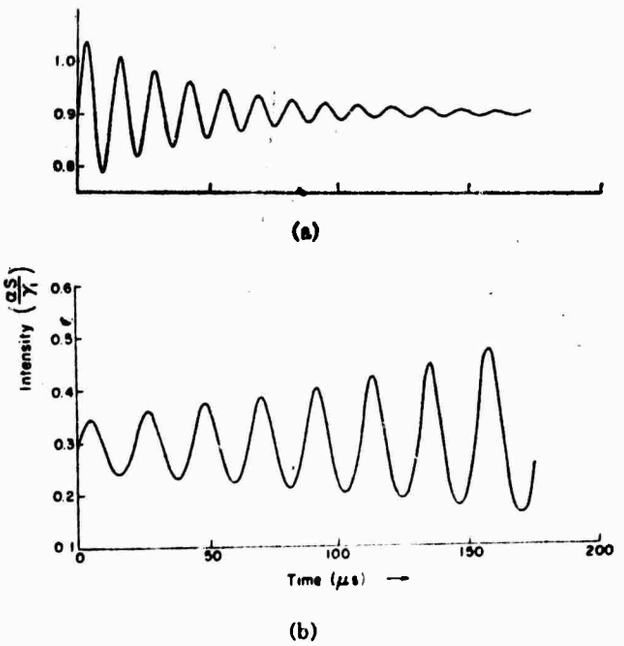

Fig. 2. (a) Computer solution for the decay of an initial deviation to a stable-equilibrium photon density. (b) Growth of an initial deviation away from an unstable-equilibrium photon density.

The initial values used were the equilibrium values $\bar{n}_1/n_1^0$, $\bar{n}_2/n_2^0$, and $\alpha\bar{S}/\gamma_1$, which were computed to two significant figures. This procedure left a significant deviation from the exact equilibrium to test for stability. In Fig. 2(a) βn_2^0 was chosen to be 8×10^6 s^{-1}, and thus the system is predicted stable by (8). A damped sinusoid was found. In Fig. 2(b) βn_2^0 was chosen to be 12×10^6 s^{-1} and the expected exponentially growing sinusoid was initially generated. Integrating the equations to times beyond 1 ms the stable limit cycle shown in Fig. 3 was eventually reached. Notice that the pulses generated look very much like reported experimental pulses [2], [3]. The computer-generated pulse amplitudes are about 10 times the expected CW level for our choice of parameters. One should also note that the actual pulse spacing is about 50 percent greater than the oscillation period found in the linear region.

From these solutions it is concluded that pulses rather like those observed experimentally can be obtained from (1) using reasonable parameter values. The assumption that an oscillatory instability leads to a limit cycle is also confirmed. A digital computer study of the effects of various parameters on the pulsation was viewed as impractical due to the lengthy computation required to reach the steady state.

VI. Approximations for CO_2

In these experiments a heated CO_2 absorber at pressures less than 5 torr was employed. Since Doppler broadening applies for CO_2 at these pressures [15], the assumption

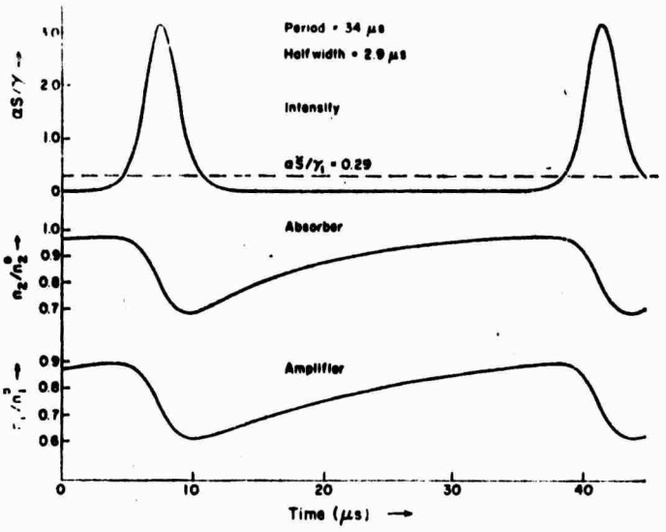

Fig. 3. Computer solution for the stable pulsing corresponding to the final state reached from Fig. 2 (b) after about 1 ms.

of homogeneous broadening in our rate-equation model must be reconsidered. Experiments with a CO_2 laser have shown that even when the Lorentz width is significantly less than the Doppler width, the inversion density versus longitudinal velocity profile in the presence of a strong CW laser field saturates essentially uniformly with only a relatively small hole [16]. This type of homogeneous saturation results from the hole filling due to elastic collisions [16]. For a line saturating in this uniform manner, (1) is still valid provided a normalized Doppler shape is used for $g(\nu)$. Despite these comments at least a small hole is burnt in the CO_2 inversion at pressures less than 1 torr. A relatively shallow Lamb dip has been observed with the CO_2 laser [17], [18] and in the next section we report the observation of a central tuning peak (inverted Lamb dip) [19] due to a low-pressure CO_2 absorber.

The relaxation of a CO_2 laser level exhibits at least two rates, a rapid rotational relaxation rate and a slower vibrational relaxation rate. The rotational relaxation rate is about 10^7 s^{-1} $torr^{-1}$ at room temperature [20]. For a typical high-gain CO_2 amplifier at a pressure of several torr the vibrational relaxation rate is between 10^3 and 10^4 s^{-1} depending on the component pressures and the discharge conditions [21]. Moreover the vibrational relaxation of the gain is not exactly described by a single exponential [21]. For a thermal-equilibrium CO_2 absorber at pressures less than 1 torr, diffusion of molecules out of the laser beam dominates the vibrational response [22], [23].

In agreement with [2] pulse rise times of about 1 μs were observed. This is considerably longer than the time required for a vibrational band of the amplifier to adjust to the field. The exact deviation of the set of rotational levels from equilibrium depends somewhat on the rate of transfer by inelastic collision between pairs of rotational states. If we assume that rotational thermalization is maintained, (1a) is modified only slightly.

Rotational thermalization requires the population of a rotational level to be some constant fraction χ, determined by the rotational temperature, of the total population in that vibrational state. If in (1a) the density n_1 refers to the total population in all rotational levels, $-(\chi n_1)\alpha S$ must be used for the field interaction term. Multiplying this modified equation by χ, it is found that the presence of strongly coupled rotational levels merely modifies the rate equation of a single rotational level by reducing its coupling to the field by the factor χ. Thus the measured saturation parameter should be χ^{-1} larger than that expected from the measured vibrational relaxation rate and interaction coefficient as other authors have remarked [22], [24].

It was just shown that for tightly coupled levels the saturation caused by a laser field is reduced by simply sharing the population deviation. The calculation of Section IV can be easily redone with population-sharing factors χ_1 and χ_2 inserted into (1a) and (1b). Equation (8) is changed only in the second term; factors of χ_1 and χ_2 enter the respective products of amplifier and absorber parameters. Thus pulsing is enhanced if the absorber is tightly coupled to fewer levels than the amplifier.

Complete rotational thermalization of a CO_2 absorber is unlikely at typical pressures with pulsed operation (0.2–1.0 torr). Hanst *et al.* [2] have suggested that only a single rotational line of the absorber is bleached during a pulse. Lack of rotational thermalization of the absorber augments the possibility of pulsation in two ways. First, a single absorber line is more easily saturated by the pulse and second, a rapid rotational component is added to its relaxation. This conclusion is substantially the same as reached in the previous paragraph by letting the absorber be thermalized with fewer levels than the amplifier.

If α equals β as is applicable in these experimental studies, (10) requires γ_2 to be greater than γ_1 for repetitive pulsing to occur. In this work the absorber was often at a pressure one-tenth that of the amplifier. Even accounting for an increase in the vibrational relaxation due to heating the absorption cell and an increase from diffusion at the lower absorber pressures, it is unlikely that the vibrational relaxation rate of the absorber exceeded that of the amplifier. Lack of rotational thermalization in the absorber is than mandatory for the present model to explain the pulsing.

VII. Experimental Observations

The repetitive passive Q switching of a CO_2 laser caused by a heated CO_2 absorber inside the laser cavity was studied using a 0.5-m gain cell and a 1.5-m absorption cell separately terminated with NaCl Brewster windows. A 2.75-m optical cavity was formed by a 150-lines/mm grating and a 98 percent reflectivity, 4-m-radius-of-curvature Ge-output mirror. A flowing mixture of equal parts CO_2 and N_2 was excited by a dc voltage to provide

gain. Several torr of He were often added for increased amplification. The absorption cell could be heated to 400°C by a nichrome wire heater coil. The laser output was monitored by the dc output of a Cu:Ge detector, displayed on an oscilloscope. A load resistance of 1 kΩ was used when a detector response time of less than 1 μs was desired. The output mirror was mounted to a piezoelectric translator so that the cavity length could be swept about 12 μ with a maximum repetition rate of ten times per second. With proper adjustment to a single mode and single rotational line, distinctive arch-shaped tuning curves separated by regions of zero intensity were produced as the cavity length was swept.

Pulsed operation on numerous P and R lines could be obtained for absorber pressures between 0.2 and 1.0 torr and temperatures above 200°C. The laser pulses resembled those pictured by Hanst *et al.* [2] and were generally separated by regions of zero intensity. By slowing opening an aperture (at fixed cavity length) a pulse spacing of about 500 μs near threshold was continuously reduced to as small as 15 μs as the average laser intensity was increased. The pulse heights and pulsewidths (1–5 μs) were relatively constant during this variation. At the highest absorber temperatures combined with the lowest absorber pressures, pulsing was restricted to a region of intensities bordering zero. By increasing the intensity further the pulses came together to a minimum spacing, diminished in amplitude, and CW oscillation began. At the lowest absorber temperatures along with the lowest absorber pressures, pulsation was found at intermediate intensities with CW operation occurring at both higher and lower intensities. For less marginal conditions pulsation occurred for all intensities achieved.

The dependence on the average intensity of both the pulse spacing and the transitions between pulsed and CW operation, agree with the qualitative predictions of our model. The observed range of pulsation frequencies can be used together with the approximate values ($\gamma_1\gamma_2 \leq \omega^2 \leq \gamma_1\gamma_c$) computed in Section V to estimate the phenomenological relaxation rates γ_1 and γ_2. With an estimated 5 percent cavity loss per pass, relaxation rates of 10^4–10^6 s^{-1} are predicted. The uncertainty arises from the approximate relation between ω and the actual pulsation frequency. These computed rates are somewhat faster than vibrational relaxation, probably indicating the presence of a rapid rotational component.

The dependence of the pulsation on the average intensity was roughly the same if the cavity length rather than the cavity loss was changed to produce the intensity variation. The cavity-length tuning curve in Fig. 4 shows transitions between pulsed and CW operation as well as a tuning peak [19] in the CW region. The frequency width of the peak is the homogeneous width of the CO_2 absorber. This peak was only observed during CW operation over a very limited range of absorber temperatures and pressures. Generally, pulsing occurred

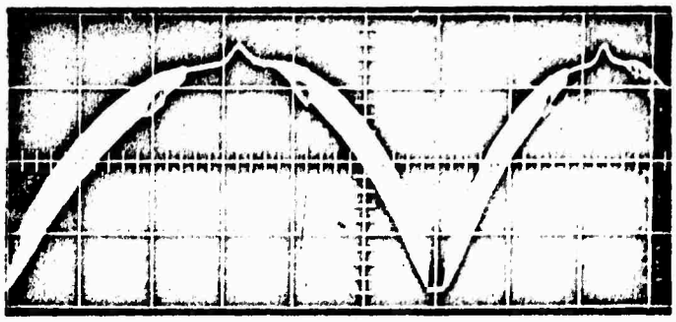

← Time (10 ms/div).

Fig. 4. Output intensity versus cavity length showing a central peak with CW operation. The intensity band is produced by passive Q switching on a much shorter time scale. The pulse heights are RC limited by the detector load resistance and some nonlinearity of the frequency sweep is evident (P_{abs} = 0.3 torr, T_{abs} = 300°C).

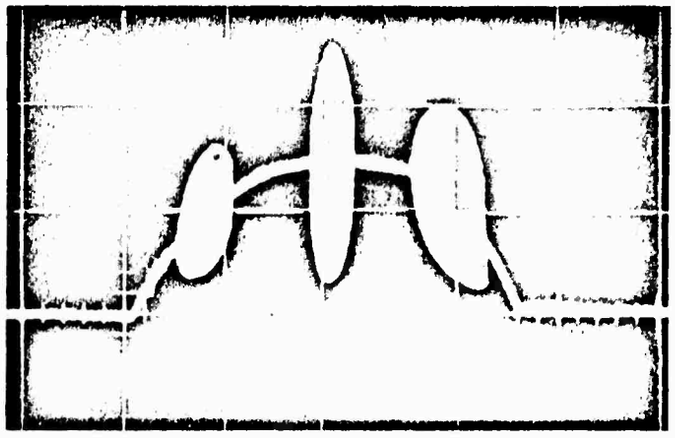

← Time (10 ms/div).

Fig. 5. Intensity versus cavity-length tuning curve showing regions of repetitive passive Q switching that are well separated by regions of CW operation. The model presented gives a qualitative explanation of pulsing domains (P_{abs} = 0.4 torr, T_{abs} = 200°C).

throughout the central tuning region and was accompanied by some peaking of the pulse heights about line center. The pressure dependence of the half-maximum width of the peaking of the pulse heights had a slope of about 6 MHz/torr and a zero pressure intercept of about 2 MHz. A tuning peak produced by a CO_2 absorber in a pulsed CO_2 laser has been previously reported [25].

A cavity-length tuning curve displaying marginal pulsing is shown in Fig. 5. This picture, taken near the lowest absorber temperature for passive Q switching, shows regions of pulsing at intermediate intensities with CW operation occurring for both higher and lower intensities. The central band of pulsing comes where a tuning peak might otherwise have occurred. The saturation of the absorber is heightened for frequencies within the homogeneous width of its line center, this effect leading to the tuning peak [19]. The preference for pulsing in the central region is qualitatively explained by the increased absorption saturation.

For CO_2 absorber pressures above 2 torr and temperatures below 200°C sudden jumps between zero and

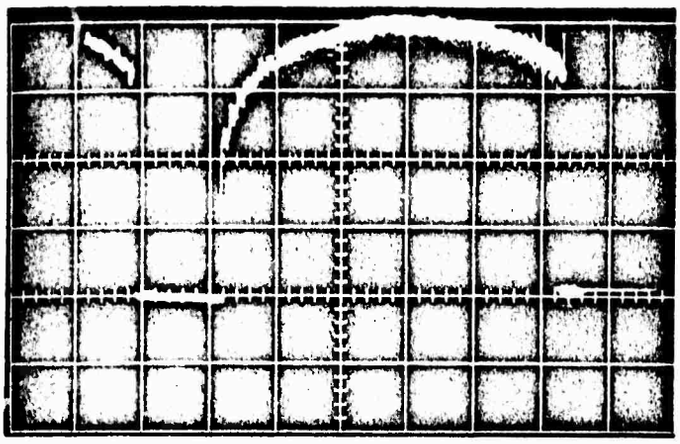

← Time (0.5 s/div).

Fig. 6. Intensity versus cavity-length tuning profile showing a region of unallowed CW intensities bordering zero. The jump distance going from zero to a finite intensity differs from the distance going from a finite value to zero intensity (P_{abs} = 5.5 torr, T_{abs} = 50°C).

finite intensities were observed by slowly varying the cavity loss. This indicates that the absorber loss was saturating more rapidly with intensity than the gain (Section III). Such intensity jumps were also found by sweeping the cavity length (Fig. 6). Intensity jumping and pulsing did not occur together. This agrees with (6) and (8) that imply that γ_2 must be less than γ_1 for intensity jumps but greater than γ_1 for pulsing (provided α equals β).

The addition of buffer gases to either the amplifier or absorber produced interesting effects. Adding larger amounts of He to the amplifier than needed to produce the best gain, enhanced the onset of pulsing. However, by adding about 0.5 torr of either He, N_2, or H_2O to the absorber, pulsation was stopped. Both observations are consistent with the view that these gases aid rotational thermalization. In the amplifier, rotational thermalization augments pulsation but in the absorber it hinders pulsation (Section VI).

A new domain of passive Q switching using a CO_2 absorber was observed. At an absorber pressure of 5 torr and an absorber temperature of about 50°C, the addition of 0.3 torr H_2O vapor caused the laser to pulse regularly. Pulsing was limited to a narrow region of intensities near threshold operation. The pulses were about 500 μs wide, separated by approximately 2 ms, and about 5 times higher than the expected CW intensity. We speculate that the addition of H_2O vapor barely caused the vibrational relaxation rate of the absorption to exceed that of the gain, thus allowing weak pulsing.

VIII. Summary

A model has been given that explains some aspects of repetitive passive Q switching. Equations (8) and (10) could be useful in the selection of saturable absorbers to produce pulsing of CO_2 and other lasers. It is likely that repetitive passive Q switching can be based on media with varied relaxation mechanisms.

Acknowledgment

The authors are grateful to Prof. C. L. Tang for constructive suggestions and also to the Materials Science Center of Cornell University, Ithaca, N. Y., for the use of their facilities.

References

[1] O. R. Wood and S. E. Schwarz, "Passive Q-switching of a CO_2 laser," *Appl. Phys. Lett.*, vol. 11, 1967, pp. 88–89.
[2] P. L. Hanst, J. A. Morreal, and W. J. Hanson, "Repetitive pulsing of the CO_2 laser by means of CO_2 gas and other absorbers," *Appl. Phys. Lett.*, vol. 12, 1968, pp. 58–61.
[3] J. T. Yardley, "Passive Q-switching of the CO_2 laser by vinyl chloride," *Appl. Phys. Lett.*, vol. 12, 1968, pp. 120–122.
[4] N. V. Karlov, G. P. Kuz'min, Yu. N. Petrov, and A. M. Prokhorov, "Q-switching of a CO_2 laser with a saturating filter based on boron trichloride," *JETP Lett.*, vol. 7, 1968, pp. 134–136.
[5] T. Y. Chang, C. H. Wang, and P. K. Cheo, "Passive Q-switching of the CO_2 laser by CH_3F and PF_5 gases," *Appl. Phys. Lett.*, vol. 15, 1969, pp. 157–159.
[6] O. R. Wood and S. E. Schwarz, "Passive mode locking of a CO_2 laser," *Appl. Phys. Lett.*, vol. 12, 1968, pp. 263–265.
[7] H. Statz and G. DeMars, "Transients and oscillation pulses in masers," in *Quantum Electronics*, C. H. Townes, Ed. New York: Columbia University Press, 1960, pp. 530–537.
[8] K. Shimoda, "Amplitude and frequency variations in ruby optical masers," *Proc. Symp. Optical Masers*. New York: Polytechnic Press, 1963, pp. 95–108.
[9] W. G. Wagner and B. A. Langyel, "Evolution of the giant pulse in a laser," *J. Appl. Phys.*, vol. 34, 1963, pp. 2040–2046.
[10] A. Szabo and R. A. Stein, "Theory of laser giant pulsing by a saturable absorber," *J. Appl. Phys.*, vol. 36, 1965, pp. 1062–1066.
[11] A. P. Kazantsev, S. G. Rautian, and G. I. Surdutovich, "Theory of a gas laser with nonlinear absorption," *Sov. Phys.—JETP*, vol. 27, 1968, pp. 756–762.
[12] V. N. Lisitsyn and V. P. Chebotayev, "Hysteresis and 'hard' excitation of a gas laser," *JETP Lett.*, vol. 7, 1968, pp. 1–3.
[13] See for example, J. LaSalle and S. Lefschetz, *Stability by Liapunov's Direct Method with Applications*. New York: Academic Press, 1961, ch. 2.
[14] See for example, R. Schwarz and B. Friedland, *Linear Systems*. New York: McGraw-Hill, 1965, ch. 12.
[15] E. T. Gerry and D. E. Leonard, "Measurement of the 10.6 μ laser transition probability and optical broadening cross-sections," *Appl. Phys. Lett.*, vol. 8, 1966, pp. 227–229.
[16] T. Kan and G. J. Wolga, "The influence of collisions on radiative saturation and Lamb dip formation in CO_2 molecular lasers," *IEEE J. Quantum Electron.*, vol. QE-7, Apr. 1971, pp. 141–150.
[17] C. Bordé and L. Henry, "Study of the Lamb dip and of rotational competition in a carbon dioxide laser," *IEEE J. Quantum Electron.*, vol. QE-4, Nov. 1968, pp. 874–880.
[18] T. Kan, H. T. Powell, and G. J. Wolga, "Observation of the central tuning dip in N_2O and CO_2 molecular lasers," *IEEE J. Quantum Electron.* (Corresp.), vol. QE-5, May 1969, pp. 297–300.
[19] P. H. Lee and M. Skolnik, *Appl. Phys. Lett.*, vol. 10, 1967, pp. 303–304.
[20] a. P. K. Cheo and R. L. Abrams, "Rotational relaxation of CO_2 laser levels," *Appl. Phys. Lett.*, vol. 14, pp. 47–49, 1969;
b. R. L. Abrams and P. K. Cheo, "Collisional relaxation of CO_2 rotational levels by N_2 and He," *Appl. Phys. Lett.*, vol. 15, 1969, pp. 177, 178.
[21] C. B. Moore, R. E. Wood, B. Hu, and J. T. Yardley, "Vibrational energy transfer in CO_2 lasers," *J. Chem. Phys.*, vol. 46, 1967, pp. 4222–4231.
[22] C. P. Christensen, C. Freed, and H. A. Haus, "Gain saturation and diffusion in CO_2 lasers," *IEEE J. Quantum Electron.*, vol. QE-5, May 1969, pp. 276–283.
[23] D. C. Smith and J. H. McCoy, "Effects of diffusion on the saturation intensity of a CO_2 laser," *Appl. Phys. Lett.*, vol. 15, 1969, pp. 282–284.
[24] D. F. Hotz and J. N. Ferrer, "Intrinsic flux limits for continuous and Q-pulse gain of the 10.6 μ line of CO_2," *J. Appl. Phys.*, vol. 39, 1968, pp. 1797–1800.
[25] Yu. V. Brshayovsky, V. P. Chebotayev, and L. S. Vasilenko, "Collision effect on the saturation character of the vibration-rotation transitions for 00^01–10^00 band of CO_2," *IEEE J. Quantum Electron.*, vol. QE-5, Mar. 1969, pp. 146–151.

82

Reprinted from:

THE JOURNAL OF CHEMICAL PHYSICS VOLUME 54, NUMBER 2 15 JANUARY 1971

Optical Saturation of a Single Vibration–Rotation Transition in the ν_3 Fundamental of SF_6*,†

N. DJEU‡ AND G. J. WOLGA
Cornell University, Ithaca, New York 14850
(Received 22 April 1970)

A well-resolved vibration–rotation transition in the ν_3 infrared fundamental of SF_6 has been revealed at 200°K by using the tuned laser spectroscopy technique. The frequency-dependent saturation behavior of that transition has been studied at low pressures, and the results fitted to theoretically predicted curves. From the pressure dependence of the saturation parameter, the quantity $(\gamma'/\gamma)A_{ab}$, which is the product of the Einstein A_{ab} coefficient and the ratio of the dephasing collision rate and the rotational relaxation rate, was determined to be 53 sec^{-1}. This is considered as a good upper bound for the Einstein A_{ab} coefficient itself.

INTRODUCTION

In the past two years, a large number of experiments have been performed on SF_6 in connection with its absorption at the 10.6-μ wavelength of the CO_2 laser. They range from the observations of self-induced transparency,[1] of photon echo,[2,3] and of transient nutation[4,5] to investigations of the inverted Lamb dip[6,7] and studies of steady-state saturation.[8,9] But in spite of the extensive literature, our knowledge of the physical properties of that molecule is far from being complete. As a case in point, the figures reported for the Einstein A_{ab} coefficient for the ν_3 band, which is responsible for the absorption of radiation near 10.6 μ, vary by as much as two orders of magnitude. Further experiments on that gas were therefore deemed desirable.

Quite apart from the above-mentioned developments, we have derived elsewhere[10] a saturation formula for molecular gases which predicts that in a limited pressure region the optical saturation of a vibration–rotation transition should be identical to that of a two-level atomic transition. Optical saturation measurements carried out in that pressure region ought to yield directly the product $(\gamma'/\gamma)A_{ab}$, where γ' is the dephasing collision rate and γ the rotational relaxation rate. Since γ' is expected to be only slightly greater than γ, one can obtain a good upper bound for A_{ab} from such saturation studies.

Tuned laser spectroscopy revealed[10] that at 200°K and for sufficiently low pressures there lies within the Doppler width of the $P(18)$ transition of the CO_2 10.4-μ band a well-resolved SF_6 vibration–rotation transition belonging to the ν_3 fundamental. It was thus possible to test the validity of the saturation formula in SF_6 over a restricted pressure range. Furthermore, the saturation parameter measured as a function of pressure determined $(\gamma'/\gamma)A_{ab}$ unambiguously.

The saturation studies reported here differ from the earlier ones[8,9] in that we operated under temperature and pressure conditions which insured single-line absorption in SF_6 and that the CO_2 laser radiation employed was frequency tuned. This procedure permitted the saturation formula to be tested in detail.

EXPERIMENTAL ARRANGEMENT

A schematic of the apparatus used for making small signal and saturated absorption measurements is shown in Fig. 1. The 1-m water-cooled active laser discharge column operated on a flowing mixture of 12.5% CO_2, 25% N_2, and 62.5% He at a total pressure of 3 torr. The discharge current could be adjusted to give a

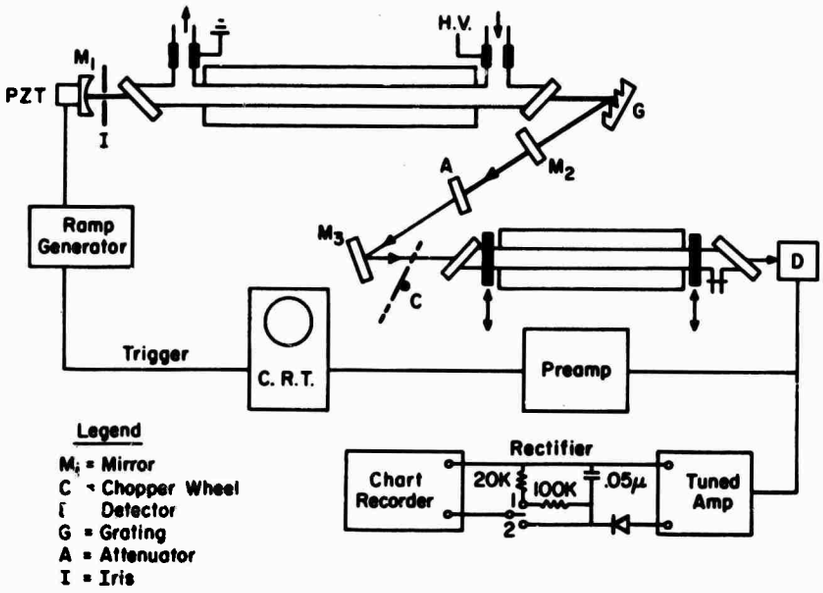

FIG. 1. Experimental arrangement for absorption measurements.

variable power output. The cavity was formed by a curved mirror M_1 (5.7-m radius of curvature, 98% reflecting), a grating G (150-lines/mm gold replica blazed for 8 μ) which permitted selective oscillation on any one particular vibration–rotation transition, and a flat mirror M_2 (40% transmitting). The total cavity length was 1.60 m, and fine tuning was accomplished by mounting M_1 on a piezoelectric element driven by a voltage ramp generator capable of sweeping with various ramp slopes. The angle formed by M_1, G, and M_2 was so chosen that when oscillation took place on any of the 9.4- or 10.4-μ band transitions with M_1 and M_2 as end mirrors (the grating was not used in Littrow), M_1 and G alone did not form a high Q cavity for any of the laser transitions. With the use of an iris near M_1, it was possible to limit oscillation to only the fundamental transverse mode. The output beam, after going through an attenuator A, was deflected by a flat gold mirror M_3, modulated by a chopper wheel C, and detected by a gold-doped germanium detector D cooled to liquid-nitrogen temperature. The output of the detector, after being amplified 100 times, was displayed on an oscilloscope for absolute measurements. It was also sent into a tuned amplifier, whose output, after rectification, was fed into a chart recorder.

A 1-in. i.d. Pyrex pipe of 82 cm over-all length with NaCl Brewster windows served as the absorption cell. An open jacket around the cell could be filled with dry ice to cool the entire cell, except for 4 cm on each end, to 200°K. The power detected with the empty cell in and out of the path of the laser beam agreed to within 2% or 3%. Integrated loss was deduced by comparing the unattenuated signal with the transmitted signal when the cell, filled to a given pressure, was intercepting the beam.

SMALL SIGNAL ABSORPTION

The full width between $1/e$ points for a Doppler broadened vibration–rotation line in SF_6 near 10.6 μ at 200°K is 29.4 MHz. On the other band, the single-frequency tuning range for the CO_2 laser used was 94 MHz. Therefore, SF_6 transitions whose line centers are only a few tens of MHz from CO_2 laser line centers could be studied in detail by the tuned laser spectroscopy technique. The unattenuated single-frequency tuned laser output was compared with the transmitted signal after the beam traversed the absorption cell. Provided the power level of the incident radiation was much lower than that needed for saturation, taking the logarithm of the ratio of the two signals at various frequencies yielded directly the line shape of the absorbing SF_6 transition.

The upper curve in Fig. 2 is the incident intensity at the minimum noise-free level (about 1 mW/cm²) as a function of frequency of the CO_2 laser operating on the $P(18)$ transition of the 10.4-μ band. The asymmetric lower curve is the transmitted signal after passage through the absorption cell containing a mixture of 0.007 torr of SF_6 and 0.11 torr of He at 200°K. The partial pressure of He, while not high enough to cause any appreciable collision broadening, was sufficient to insure unsaturated absorption.[10] The vertical lines are drawn in to match frequency points on the incident power curve to corresponding ones on the transmitted signal. They are evenly spaced by 3.75 MHz but have no fixed reference. The SF_6 line center is seen to be displaced from the CO_2 line center by about 10 MHz, in agreement with the Lamb dip spectroscopy result.[7]

When the logarithm of the ratio of the incident signal over the absorbed signal for different points along the

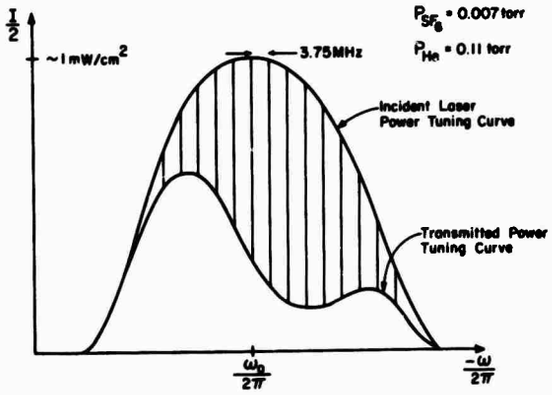

FIG. 2. Small signal incident and transmitted power curves as functions of frequency.

frequency axis is taken, we obtain the data displayed in Fig. 3. This can be fitted very closely to a Gaussian curve of 30-MHz full width between $1/e$ points if the base line for that curve is taken slightly above the zero level of the actual absorption data. The displacement is interpreted as an uniform background absorption attributable to the wings of adjacent lines. It is about 8% of the total absorption at line center under the experimental conditions given above. The single line absorption coefficient α_0 was found to be 3.6 cm^{-1}·torr^{-1} for SF_6 at 200°K.

A similar fit for data taken with the same mixture but at room temperature revealed the background to be

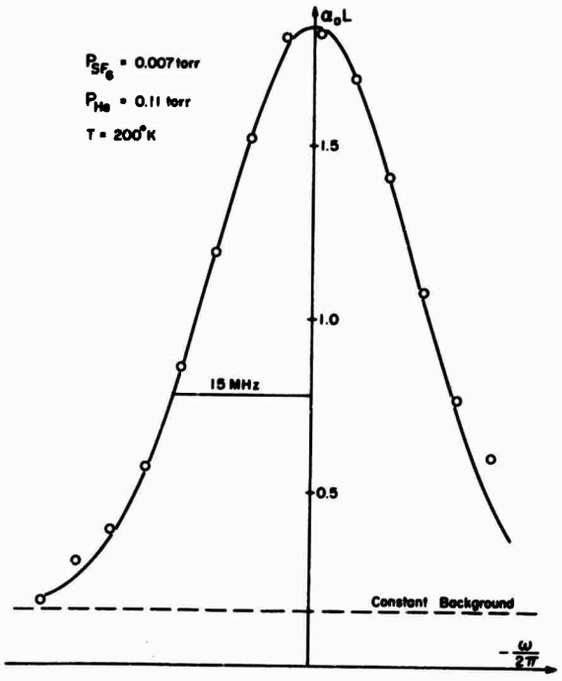

FIG. 3. Experimental line shape fitted to a Gaussian curve.

35%. The additional overlapping is attributed to the rising importance of hot band absorption at room temperature. Furthermore, when the He partial pressure was increased to 1 torr, the single-line feature was almost totally obscured. These effects are compatible with the finding of Rabinowitz *et al.*[7] that the typical separation between vibration–rotation transitions near 10.6 μ is of the order of the Doppler linewidth.

SATURATION RESULTS

We have shown elsewhere[10] that the saturated incremental loss for a traveling wave interacting with a vibration–rotation transition in a molecular gas can be

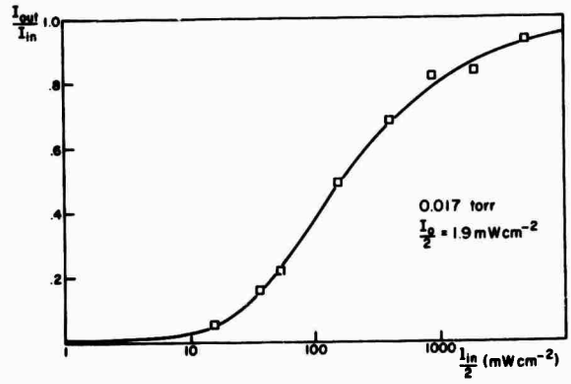

FIG. 4. Integrated loss at line center vs input intensity compared to computer generated theoretical curve (P=0.017 torr, T=200°K).

written in Gaussian units as

$$\frac{1}{I}\frac{dI}{dz} = \frac{\alpha_0 \,\mathrm{Re}W(x+iy)}{(1+I/I_0)^{1/2}+K(I/I_0)\,\mathrm{Re}W(x+iy)}$$

with

$$W(x+iy)=2\pi^{-1/2}\exp[-(x+iy)^2] \times \int_{-i(x+iy)}^{\infty}\exp(-t^2)dt,$$

where

$$x=(Mc^2/2kT)^{1/2}[(\omega_0-\omega)/\omega],$$

$$y=(Mc^2/2kT)^{1/2}[1+(I/I_0)]^{1/2}\gamma'/\omega,$$

$$I_0=c\gamma\gamma'\hbar^2/4\pi p^2,$$

$$K=(\pi Mc^2/2kT)^{1/2}[\gamma\gamma'(\Gamma_a+\Gamma_b)/2n\omega\Gamma_a\Gamma_b].$$

Here I is the field intensity, I_0 the saturation parameter, z the direction of the traveling light beam, ω its angular frequency, α_0 the unsaturated (small signal) incremental loss, ω_0 the angular frequency of the absorbing transition at line center, Γ_a and Γ_b the relaxation rates of the upper and lower vibrational levels, respectively,

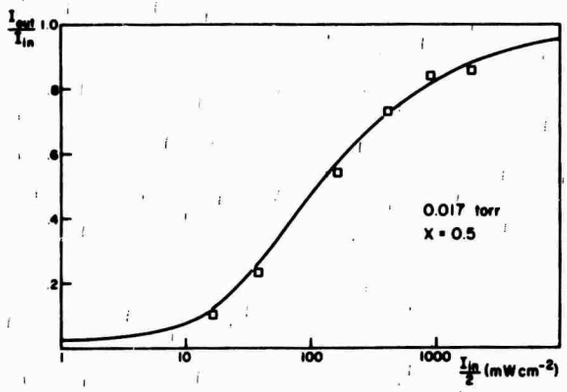

FIG. 5. Integrated loss at $x=0.5$ vs input intensity compared to computer generated theoretical curve ($P=0.017$ torr, $T=200°K$).

and $1/n$ the ratio of the absorbing rotational population to the associated vibrational population at thermal equilibrium. The average dipole moment squared is given by

$$p^2=g_b^{-1}\sum_{i=1}^{g_a}\sum_{j=1}^{g_b}|\langle a_i|P_z|b_j\rangle|^2,$$

where a_i and b_j are magnetic sublevels of the upper and lower absorbing rotational states, and g_a and g_b their respective degeneracies. The degenerate levels to be summed over are those with different M and K quantum numbers but the same J. If Coriolis and other interactions remove the K degeneracy partially, then the summation is over those sublevels which remain unsplit.

The saturation formula given above is a modified version of the one derived by Close.[11] The modification becomes necessary for vibration–rotation transitions because rotational relaxation effectively constitute variable pump rates for the particular rotational levels which are interacting with the radiation. In the low-

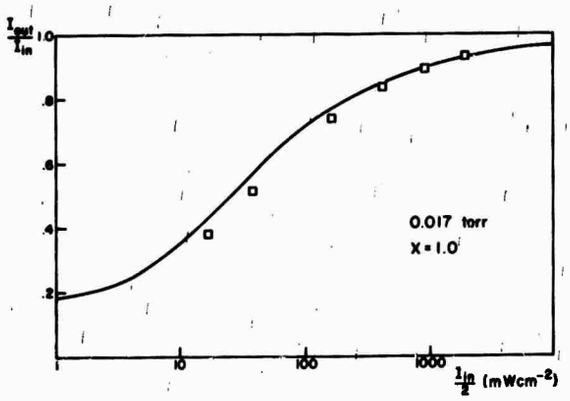

FIG. 6. Integrated loss at $x=1.0$ vs input intensity compared to computer generated theoretical curve ($P=0.017$ torr, $T=200°K$).

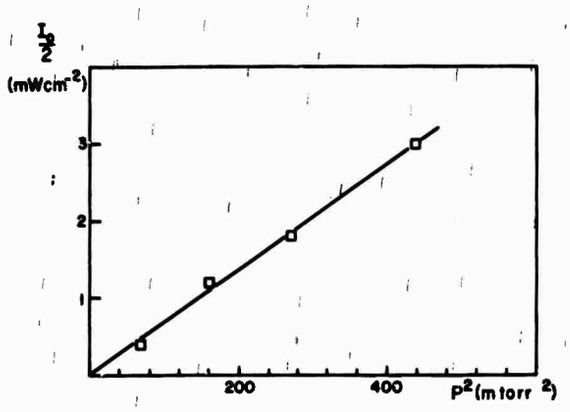

FIG. 7. Saturation parameter as a function of pressure squared.

pressure limit (less than 0.1 torr for SF_6 at 200°K), $k\ll1$ and the saturation formula reduces to[12]

$$\frac{1}{I}\frac{dI}{dz}=\frac{\alpha_0\,\mathrm{Re}W(x+iy)}{[1+(I/I_0)]^{1/2}}.$$

Since we know α_0 from our own measurements and γ' from Ref. 2, the quantity

$$(\gamma'/\gamma)A_{ab}=(64\pi^4\gamma'/h\lambda^3\gamma)p^2$$

can be deduced from the experimentally determined integrated loss as a function of incident laser intensity.

Saturation measurements were made in pure SF_6 at 200°K for pressures of 0.009, 0.013, 0.017, and 0.022 torr. Input and output power curves similar to those shown in Fig. 2 were obtained. The integrated loss at line center as well as at other frequencies was readily found by plotting the ratio of the two curves at various points along the abscissa. Also, for each given pressure, a computer was used to generate the integrated loss at line center as a function of incident power intensity in units of I_0. A fit of the experimental data to the theoretical curve then ascribed a unique value to I_0 at each pressure. Such a fit for 0.017 torr of SF_6 is exhibited in Fig. 4.

Using the I_0 determined in this fashion, saturation curves were also generated (now as a function of intensity in units of milliwatts per square centimeters) for $x=0.5$ and 1.0 at 0.017 torr. They are shown in Figs. 5 and 6, together with the experimental results cor-

TABLE I. The Einstein A_{ab} coefficient as given (or implied) by various authors.

A_{ab}	Ref.
67 sec^{-1}	a
40	c
24	8
0.83	5
0.7	1

[a] C. K. Rhodes and A. Szoke, Phys. Rev. 184, 25 (1969).

rected for background absorption. The agreement suggests the correctness of the reduced saturation formula in its frequency dependence.

When the parameter I_0 is plotted as a function of pressure squared in Fig. 7, the points fall on a straight line passing through the origin. This is to be expected, because both γ and γ' are proportional to the pressure. From the slope of the line, we calculate $(\gamma'/\gamma)A_{ab}$ to be 53 sec^{-1}. Since nearly all phase-interrupting collisions involve a change in the rotational quantum number in a molecular gas, the ratio γ'/γ should be greater than but very close to unity. Therefore, the rate given above is regarded as a good upper bound for A_{ab}.

Previous appraisals of the transition moment lead to the values for the Einstein A_{ab} coefficient given in Table I. The first was estimated from pulse transmission, while the second and third were obtained from integrated band intensity. The fourth figure came from the transient nutation effect and the last from the self-induced transparency experiment. The large discrepancies between these last two and our own upper bound require some comments.

The inverse Lamb-dip experiment,[7] as well as a recent high-resolution spectroscopic study of SF_6 using a tunable diode laser,[13] shows quite conclusively that the K degeneracy is indeed removed by the Coriolis interaction. With this assumption and the knowledge of the statistical weights of the rotational sublevels derived from symmetry considerations, one readily calculates the population densities of these sublevels. The results show that if the absorption of the $P(18)$ CO_2 line is due to one of the sublevels with the largest populations, the measured small signal absorption coefficient would lead to an A_{ab} coefficient in agreement with that deduced from our saturation experiment. Thus, the small signal absorption coefficient alone sets a lower bound on A_{ab} which is about two orders of magnitude larger than those given by the self-induced transparency and the transient nutation experiments. We therefore hold the last two numbers in Table I to be highly suspect.

CONCLUSION

We conclude by mentioning some deficiencies as well as merits of studying molecular systems by means of saturation measurements. The two major drawbacks are that one must know the dephasing collision rate before an analysis of the data can be made and that the procedure yields not one single physical constant, but the product $(\gamma'/\gamma)A_{ab}$. This restriction, however, also proves to be an asset in that it introduces a degree of flexibility. The knowledge of either γ or A_{ab} enables a calculation of the other. In general, A_{ab} is more accessible, and we see our technique as an accurate way of determining the rotational relaxation rate in complicated molecular systems. Furthermore, $(\gamma'/\gamma)\,A_{ab}$ is a very good upper bound for A_{ab} itself.

* This work was supported by the Advanced Research Projects Agency of the Department of Defense and was monitored by ONR under Contract No. N00014-67-A-0077-0006.

† This paper is based on a thesis submitted by N. Djeu to Cornell University in partial fulfillment of the requirements for the Ph.D. degree.

‡ Present address: Naval Research Laboratory, Washington, D.C.

[1] C. K. N. Patel and R. E. Slusher, Phys. Rev. Letters 19, 1019 (1967).

[2] C. K. N. Patel and R. E. Slusher, Phys. Rev. Letters 20, 1087 (1968).

[3] J. P. Gordon, C. H Wang, C. K. N. Patel, R. E. Slusher, and W. J. Tomlinson, Phys. Rev. 179, 294 (1969).

[4] G. B. Hocker and C. L. Tang, Phys. Rev. Letters 21, 591 (1968).

[5] G. B. Hocker and C. L. Tang, Phys. Rev. 184, 356 (1969).

[6] F. Shimizu, Appl. Phys. Letters 14, 378 (1969).

[7] P. Rabinowitz, R. Keller, and J. T. LaTourrette, Appl. Phys. Letters 14, 376 (1969).

[8] I. Burak, J. I. Steinfield, and D. G. Sutton, J. Quant. Spectry. Radiative Transfer 9, 959 (1969).

[9] O. R. Wood II, P. L. Gordon, and S. E. Schwarz, IEEE J. Quantum Electron. 5, 502 (1969).

[10] N. Djeu, Ph.D. thesis, Cornell University, Ithaca, N.Y. 1970.

[11] D. H. Close, Phys. Rev. 153, 360 (1967).

[12] This is identical to the formula given by Close for atomic levels with constant pump rates. One can understand this since at low pressures molecular diffusion to the wall becomes extremely fast and the populations of the vibrational states to which the radiatively interacting rotational levels belong remain in thermal equilibrium regardless of the degree of saturation.

[13] E. D. Hinkley, Appl. Phys. Letters 16, 351 (1970).

IEEE JOURNAL OF QUANTUM ELECTRONICS, VOL. QE-7, NO. 4, APRIL 1971

Influence of Collisions on Radiative Saturation and Lamb Dip Formation in CO_2 Molecular Lasers

TEHMAU KAN AND GEORGE J. WOLGA

Abstract—Saturated gain profile measurements in CO_2 at pressures where a Lamb dip appears in the laser intensity reveal that individual rotation–vibration transitions saturate with a strong Doppler component in addition to the Lorentzian holes expected for a Doppler broadened line. This mixed inhomogeneous–homogeneous behavior represents cross-relaxation effects induced by collisions that change the molecule's velocity. A rate equation formulation of collision effects elucidates the role of elastic and rotational thermalizing collisions on saturation and Lamb dip formation in molecular lasers.

Introduction

In the absence of collisions a Doppler broadened transition that is subjected to a resonant monochromatic field will saturate by the mechanism of spectral hole burning [1]. This saturation behavior results in the appearance of the Lamb dip [2] in the intensity of a standing wave laser as its frequency is tuned through the line center frequency. Since the dip width is the radiative interaction width of individual molecules exclusive of Doppler broadening, information on collision effects can be obtained by investigating the pressure dependent behaviour of the dip.

Collision broadening studies in atomic Ne utilizing the Lamb dip technique have been based upon phenomenological modifications of Lamb's collisionless equation for the laser intensity. The simple procedure of introducing a density dependence into the radiative line width parameter γ' (total phase interruption rate) was used by Smith [3] to study the $3s_2 \rightarrow 2p_4$ transition in Ne at $\lambda = 0.6328\ \mu$. In a different approach, Szöke and Javan [4] used two collision parameters, the hard and soft line widths, to characterize the Lamb dip in the $2s_2 \rightarrow 2p_4$ transition in Ne at $\lambda = 1.15\ \mu$.

The Lamb dip has also been observed in rotation–vibration transitions of the H_2O [5] and CO_2 [6] molecular laser systems. Attempts to derive collisional information for these molecules from the Lamb dip have involved the use of both the one and two parameter expressions for the laser intensity developed for atomic transitions mentioned above. Despite the outward similarity of the Lamb dip phenomena in atomic and molecular lasers, the collision processes that affect saturation are not the same for atoms and molecules and furthermore, the extent to which collisions influence the saturation behavior in atomic and molecular transitions are different due to large differences in level lifetimes. The description of collisions in molecular systems by the use of atomic formulas in [5] and [6] is therefore not *a priori* justifiable.

We present in this paper a study of the CO_2 laser that elucidates the role of collisions in saturation and Lamb dip formation in molecular lasers. The experimental study focuses attention on the changes induced in the velocity distribution of the levels undergoing saturation. This information is obtained by measuring the frequency profile of the saturated gain [7] on individual transitions by the simultaneous use of two monochromatic fields. An intense fixed-frequency field saturates the transition while a weak frequency-tunable field measures the change in the profile of the optical gain. A rate equation theory is developed to describe the collision effects.

Saturation of Molecular Transitions

The fact that Doppler broadened transitions can saturate in a manner that is different from the simple hole burning process is demonstrated by the results, to be presented shortly, of the experiment shown in Fig. 1 where the saturation-induced change in the frequency profile of the gain in laser L_s is measured by a single pass gain probe of the lasing medium.

Both lasers were single frequency oscillators operated in the TEM_{00q} mode. The $CO_2 + N_2$ mixture in L_s was set at pressures below 1 torr where the Lamb dip is observable [8], while the gas mixture in L_p was set at pressures above 1 torr to produce a smooth tuning curve. The probe beam was injected into L_s by reflection off an intracavity NaCl Brewster angle plate and its return back into L_p was prevented by operating the two lasers in orthogonal polarizations in conjunction with a pair of Ge Brewster plates within the L_s optical cavity. A second pair of Ge Brewster plates placed before the detector served to reject the small amount of L_s radiation scattered from the internal plates. The differential gain (DG), defined as the unsaturated gain minus the saturated gain, was obtained directly by periodic interruption of the L_s lasing, and phase sensitively demodulating the amplified probe signal. The saturating frequency ω_s can be held at any desired point on the transition by the L_s PZT ceramic. The probe frequency is tuned across the transition by a linear ramp voltage applied to the L_p ceramic.

While the simple hole-burning picture seems to adequately describe the saturation behaviour in the $2p_4$ level

Manuscript received April 15, 1970; revised October 28, 1970. This research was supported by the Advanced Research Projects Agency of the Department of Defense and monitored by the Office of Naval Research under Contract N00014-67-A-0077-0006 and by the Materials Science Center through its central facilities.

T. Kan is with the Naval Research Laboratory, Washington, D. C.

G. J. Wolga is with Cornell University, Ithaca, N. Y.

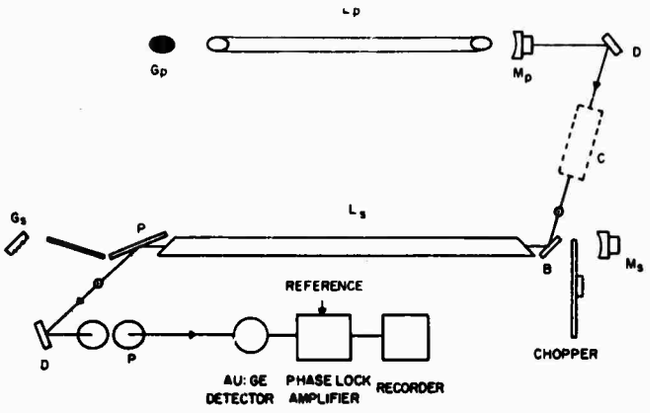

Fig. 1. Apparatus for probe of saturated gain. *B*—NaCl beam splitter, *C*—collimation optics, *D*—deflecting mirrors, *G*—diffraction grating, *M*—spherical mirror, *P*—Ge Brewster angle plates.

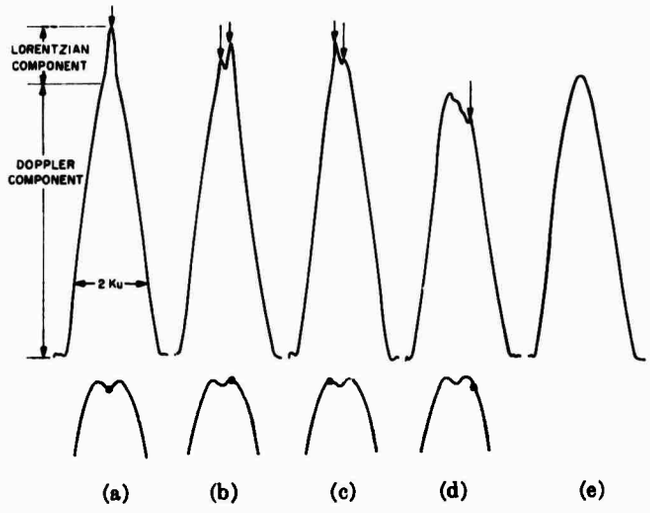

Fig. 2. (a)–(d) Frequency dependence of the DG in L_s at 0.4 torr pressure (top tracings) with both lasers oscillating on the $P(18)$ (00°1)–(10°0) transition. Bottom tracings show the position of the fixed L_s frequency relative to its tuning curve for which the corresponding DG tracings were made. Vertical arrows locate the Lorentzian holes whose asymmetric strength is due to loss anisotropies. (e) DG on the $P(20)$ (00°1)–(10°0) transition with L_s oscillating on the $P(18)$ transition.

of Ne [7], the saturated gain in CO_2 on the $P(18)$ (00°1)–(10°0) transition at a pressure of 0.4 torr reveals a different behavior. See Fig. 2(a)–(e). In addition to the Lorentzian holes expected of an inhomogeneously broadened line, a Doppler saturation in the form of a much broader and stronger component that displays the Doppler width of the transition occurs. Whereas an inhomogeneously broadened line responds to a monochromatic field over a frequency width that is small compared to the spectral line width and a homogeneously broadened line responds to a resonant field over the entire spectral width, the CO_2 transitions (Fig. 3) behave in a mixed inhomogeneous–homogeneous manner despite the fact that the radiative interaction width γ' is small compared to the Doppler width. The condition $\gamma' \ll$ Doppler width is therefore not a sufficient condition for the spectral line to saturate inhomogeneously [9]. A little thought will show that the additional Doppler saturation is the result of spectral cross-relaxation processes induced by collisions that change the molecular velocity. These collisions cause diffusion within the Doppler distribution and act to maintain the equilibrium line shape against radiative distortions.

This can be understood in the following way. In the absence of velocity diffusion, only those molecules whose Doppler shifted emissions fall within a width $2\gamma'$ about the frequency ω_s can interact appreciably with a field at frequency ω_s. The DG of such a nondiffusing distribution will therefore consist of Lorentzian holes. When velocity diffusion occurs, molecules located further than a width γ' from ω_s now possess a probability of increasing their interaction with the field through collisions, which move them closer to ω_s. The probability that a molecule will augment its interaction with the field in this manner can be seen to be an increasing function of the ratio between the diffusion rate (inverse velocity diffusion time) across the distribution to the rate at which molecules leave the distribution (inverse level lifetime). If the level lifetime is short compared to the diffusion time then a molecule will have a low probability of reaching the neighborhood of ω_s before leaving the level. In this case the distribution of Lorentzians comprising the Doppler broadened line can be considered almost static. This behavior is characteristic of transitions between short lived atomic levels. If, however, the level lifetime is long compared to the velocity diffusion time, then the molecule will suffer several velocity-changing collisions within its lifetime and the probability of reaching the neighborhood of ω_s and interacting with the field is enhanced. This behavior is representative of transitions between long-lived rotation–vibration transitions. Velocity-changing collisions therefore induce saturation across the entire velocity distribution and qualitatively explain the presence of the Doppler saturation component. The appearance of Doppler saturation in the CO_2 levels and its apparent absence in the Ne $2p_4$ level[1], reflects the fact that the collisionally induced cross-relaxation rate is much faster than the slow vibrational decay rate for the low lying levels of CO_2 while the collisionally induced cross-relaxation rate is slower than the decay rates for the pertinent levels of Ne.

Collisions that change only the velocity are but a partial specification of the total cross-relaxation process. In molecular systems with rotational fine structure, a molecule with velocity v_1 in rotational level j can migrate to a different velocity v_2 within the same level j via two collisions, the first of which carries the molecule into any of the other rotational levels j', and the second one carrying the molecule back into level j. Spectral cross-

[1] The upper $3s_2$ level, which was not probed in [7], may contain a nonnegligible Doppler component due to its longer lifetime.

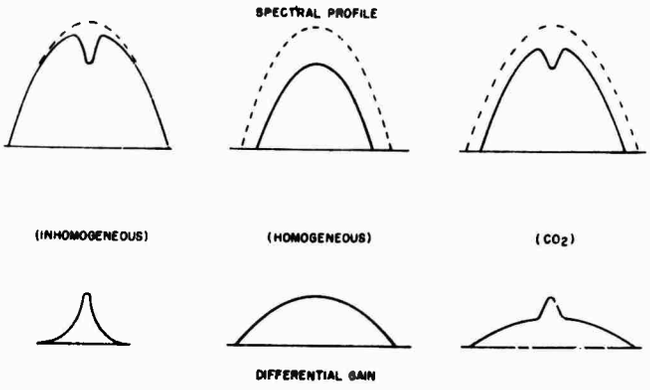

Fig. 3. Saturation behavior of spectral lines with different broadening properties. Dotted curve is the unsaturated spectral profile. Solid curve is the saturated profile for a monochromatic wave at line center.

relaxation effects in rotation–vibration levels must therefore include both the elastic velocity-changing and inelastic rotational level-changing collision processes.

A probe of the adjacent $P(20)$ transition with L_s oscillating on the $P(18)$ transition [Fig. 2(e)] shows that collisional coupling causes the entire rotational distribution to saturate when one pair of levels is being saturated. The Doppler saturation within the pair of levels being stimulated and the saturation of the rotational distribution are thus quite similar phenomena. Both are cross-relaxation or equivalently cross-saturation effects brought about by collisions. In the former case the cross saturation occurs between different portions of the same spectral line while in the latter case cross saturation occurs between different portions of the rotational distribution.

The pressure dependence of the mixed saturation behavior in CO_2 was measured using traveling wave saturation in an oscillator amplifier experiment shown in Fig. 4. Here, lasers L_s and L_p supply the saturating field and the probing field, respectively, for the amplifier L_A. A flowing premixed ratio of 50 percent CO_2 and 50 percent N_2 gases dc excited along the 1.3-m-discharge length constituted the amplifying medium. The three-mirror configuration for both lasers was chosen to avoid the strongly divergent beam from the curved mirror member of a two-element grating resonator.

A sample of the DG data for the $P(18)$ (00°1)–(10°0) transition is shown in Fig. 5. Figs. 6 and 7 plot the pressure dependence of the hole width (half-width at half-maximum) in the DG and of the ratio s between the line center amplitude of the hole component to the amplitude of the Doppler component in the DG under the following conditions: I_s = 1 W/cm², I_p = 20 mW/cm², and amplifier current of 30 mA. The nonzero intercept of the hole width plot at zero pressure is consistent with the observed frequency stability of the two oscillators[2] and it is clear

[2] Observation of the beat frequency signal between the two lasers generated in a Ge:Au detector showed a short-term jitter of approximately 1 MHz.

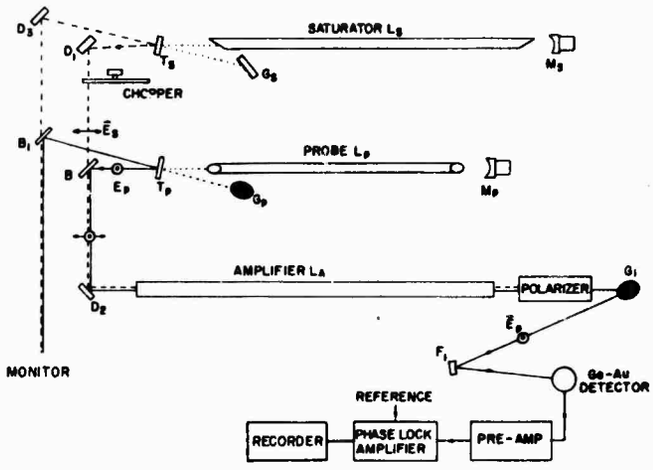

Fig. 4. Traveling wave probe of saturated gain. B—beamsplitter, D—deflecting mirror, F—focusing mirror, G—grating, M—spherical mirror, T—partially transmitting flat mirror.

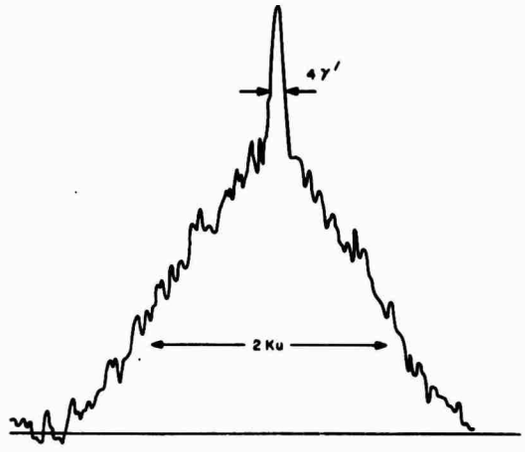

Fig. 5. DG on the $P(18)$ (00°1)–(10°0) transition at 0.2-torr pressure. L_s and L_p oscillating on common transition.

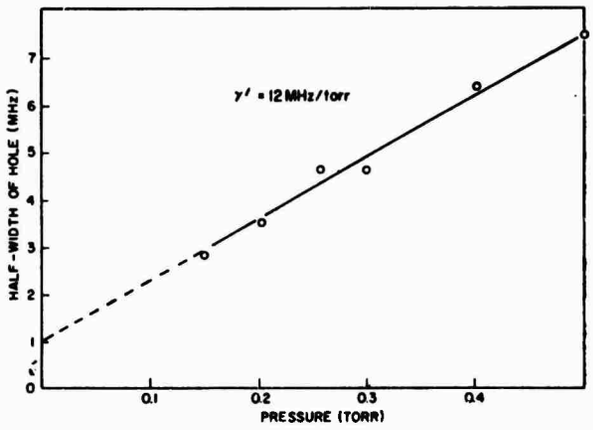

Fig. 6. Half-width at half-maximum of hole in DG.

from Fig. 7 that individual rotation–vibration transitions assume greater inhomogeneous character with decreasing pressure.

We will now present a rate equation formulation of

collision effects in molecular rotation–vibration transitions. Our goal is to obtain an expression for the optically induced change in the frequency profile of the inversion. The theory will predict the observed pressure dependence of the saturation behavior and will elucidate the effect of collisions towards Lamb dip formation in molecular lasers.

Rate Equations

An exact treatment of the collision problem for CO_2 requires the inclusion of both rotational and vibrational energy exchange collisions. To simplify the analysis we will only treat the more rapid and therefore more important rotational coupling process explicitly. This is done by assuming a single rotation–vibration manifold of levels for the upper and lower states. A straightforward extrapolation of the results of the simple model will account for the effects of the slower coupling to other vibrational levels.

The dynamic processes that will affect the saturation response of a single transition within the rotation–vibration spectrum are shown in Fig. 8. Denote the vibration and rotation indices by the pair (a, j_a) where $a = 2$ for the upper vibrational level and $a = 1$ for the lower vibrational level. For a single linearly polarized field we can write the following equations for the population distribution of the level pair being stimulated.

$$\frac{d}{dt}[n_{aj_a}(v)] = w_{aj_a}(v) - \gamma n_{aj_a}(v) \pm R(\omega, v) \cdot \left[n_{2j_a}(v) - \frac{g_2}{g_1} n_{1j_1}(v)\right] - \left[\int_{-\infty}^{\infty} dv'\, S_{ae}(v, v') n_{aj_a}(v) - \int_{-\infty}^{\infty} dv'\, S_{ae}(v', v) n_{aj_a}(v')\right] - \sum_{j_a' \neq j_a} \left[\int_{-\infty}^{\infty} dv'\, S_{ar}(j_a v, j_a' v') n_{aj_a}(v) - \int_{-\infty}^{\infty} dv'\, S_{ar}(j_a' v', j_a v) n_{aj_a'}(v')\right]. \quad (1)$$

For clarity the equations have been written so that collision processes are expressed in terms of their respective rates. In (1), v is the velocity component along the field propagation direction, unprimed rotational indices represent the two levels connected by the field, and primed rotational indices represent all other levels. The pump rates $w_{aj_a}(v)$ are assumed to equal $w_{aj_a} f(v)$ where $f(v) = (\sqrt{\pi}\, u)^{-1} \exp -(v/u)^2$ and $\frac{1}{2}mu^2 = kT$. Equations for rotational levels not connected by the field are obtained from (1) by setting $R(\omega, v)$ to zero.

The stimulated emission rate $R(\omega, v)$ can be obtained from the rate equation approximation of the density matrix equations modified to include molecular motion. For a traveling wave field

$$E_{\pm}(r, t) = \text{Re}\,\{eE \exp i(\pm K \cdot r - \omega t)\}$$

$R(\omega, v)$ is given by the expression

$$R(\omega, v) = \frac{\gamma'}{2}\left(\frac{p}{\hbar}\right)^2 E^2 L_{\pm}(\omega - \omega_0 \mp Kv). \quad (2a)$$

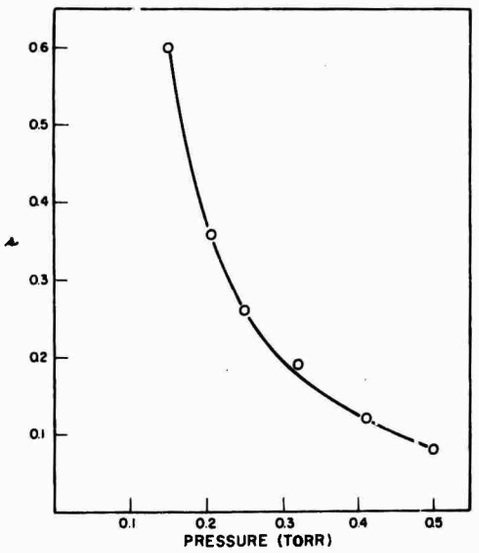

Fig. 7. Ratio of the line center amplitude of the hole component to the Doppler component in the DG.

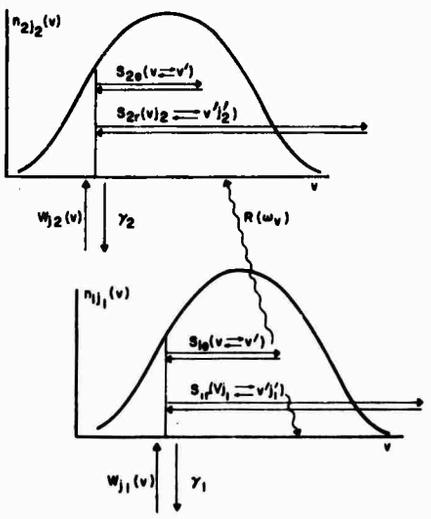

Fig. 8. Processes affecting saturation. Only the two rotational levels connected by the field are shown. *1*—lower vibrational quantum number, *2*—upper vibrational quantum number, *j*—rotational quantum number, *w*—pump rate, γ—vibrational decay rate, *Se*—elastic velocity-changing scattering rate, *Sr*—rotational level-changing scattering rate, *R*—radiative transition rate.

For a standing wave field

$$E(r, t) = E_+(r, t) + E_-(r, t),$$

$R(\omega, v)$ becomes

$$R(\omega, v) = \frac{\gamma'}{2}\left(\frac{p}{\hbar}\right)^2 E^2 [L_+(\omega - \omega_0 - Kv) + L_-(\omega - \omega_0 + Kv)]. \quad (2b)$$

In (2) $p^2 = (2j_2 + 1)^{-1} |\langle 1j_1 |\mathbf{p}\cdot\mathbf{e}| 2j_2\rangle|^2$, ω_0 is the line center frequency. $L_{\pm}(x) = [x^2 + (\gamma')]^{-1}$, and γ' is the total phase interruption rate whose component contributions we will not separate. Two physical processes have not been included in (1) and (2). First, spatial diffusion of

excited states through the finite extent of a laser beam at low pressures competes with other vibrational relaxation processes [10]. The rate equations with the diffusion terms included, however, are not analytically soluble. For our purposes it is adequate to realize that the effect of diffusion is to decrease the available time for interaction with the field and can therefore be treated in an approximate manner by augmenting the vibrational decay rate γ. Second, it is known that collisions can cause shifts and asymmetries in the molecule-field interaction while $R(\omega, v)$ is devoid of such properties. Since our primary interest does not encompass such effects, which are expected to be small anyway, they will be neglected in the following analysis.

We assume the following elastic and rotational collision models

$$S_e(v, v') = S_e f(v) \tag{3}$$

$$S_r(jv, j'v') = x_i S_r f(v). \tag{4}$$

x_i is the rotational Boltzmann factor given by

$$g_i \exp -[E(j)/kT] / \sum_j g_j \exp -[E(j)/kT].$$

The elastic model requires the molecule to scatter into a Boltzmann distribution of final velocities regardless of its initial velocity while the rotational scattering model in addition ignores Δj selection rules. The latter assumption is consistent with the results of rotational relaxation measurements in the pertinent levels of CO_2 [11]. For the above models the elastic and rotational scattering terms in the rate equations, denoted by $n_i(v)|_e$ and $n_i(v)|_r$, respectively, become

$$\frac{d}{dt} n_i(v)|_e = -S_e \left[n_i(v) - f(v) \int_{-\infty}^{\infty} dv'\, n_i(v') \right] \tag{5a}$$

$$\frac{d}{dt} n_i(v)|_r = -S_r \left[(1 - x_i) n_i(v) - x_i f(v) \cdot \sum_{j' \neq j} \int_{-\infty}^{\infty} dv'\, n_{j'}(v') \right]. \tag{5b}$$

To obtain an explicit equation for the inversion $\Delta n(v) = n_{2j_2}(v) - n_{1j_1}(v)$, we make the following simplifying assumptions: $S_{1e} = S_{2e}$, $S_{1r} = S_{2r}$, and $\gamma_1 = \gamma_2$. These approximations are conveniences that do not affect the manner in which collisions influence saturation but do simplify the manipulation of the equations. An additional simplification can be obtained by noticing that under typical CO_2 laser plasma conditions ($T = 400°K$) the ratio g_2/g_1 is near unity for transitions near the peak of the distribution ($g_2/g_1 = 0.95$ for a $P(18)$ transition). We therefore set the ratio to unity.

Using the above approximations and the following definitions

$$N_J(v) = \Delta n(v)$$

$$w_J(v) = w_{2j_2}(v) - w_{1j_1}(v)$$

in which J represents the pair of rotational quantum numbers $(j_1, j_2) \rightarrow (j_1, j_1 \pm 1)$, (3) and (5) combine to give the following equation for the inversion density $N_J(v)$:

$$N_J(v) = w_J(v) - \gamma N_J(v) - 2R(\omega, v) N_J(v) - S_e \left[N_J(v) - f(v) \int_{-\infty}^{\infty} dv'\, N_J(v') \right] - S_r \left[(1 - x_J) N_J(v) - x_J f(v) \cdot \sum_{J' \neq J} \int_{-\infty}^{\infty} dv'\, N_{J'}(v') \right]. \tag{6}$$

To obtain the steady-state solution $N_J(v)$, we must evaluate the sum in (6) over all levels not directly coupled to the field. This is done in Appendix I. The result is

$$N_J(v) = \frac{A\left(\frac{\gamma}{\gamma_t}\right) N_J^0 f(v) + \left(\frac{\gamma_{er}}{\gamma_t}\right) f(v) \int_{-\infty}^{\infty} dv'\, N_J(v')}{1 + \left(\frac{2}{\gamma_t}\right) R(\omega, v)}. \tag{7}$$

The quantities γ_{er}, γ_t, and A are defined by the following relations

$$\gamma_{er} = S_e + \frac{1 - x_J}{1 + \frac{\gamma}{x_J S_r}} S_r \tag{8}$$

$$\gamma_t = \gamma + S_e + (1 - x_J) S_r \tag{9}$$

$$A = 1 + \frac{1}{x_J} \cdot \frac{1 - x_J}{1 + \frac{\gamma}{x_J S_r}} \tag{10}$$

$$\gamma_t - \gamma_{er} = A\gamma. \tag{11}$$

γ_{er} is the collisional cross-relaxation rate.

Before we proceed to a detailed consideration of (7), a very important influence of rotational coupling on the saturation process can be seen by disregarding molecular motion. Setting $v = 0$, $\int_{-\infty}^{\infty} dv'\, N_J(v') = N_J$ and using the line center value of $R(\omega)$ in (7), we obtain

$$N_J = \frac{N_J^0}{1 + \frac{E^2}{AE_0^2}} \tag{12}$$

The quantity $E_0^2 = \gamma\gamma'(\hbar/p)^2$ is the saturation parameter for the J transition calculated assuming two isolated levels. The A-fold increase in the saturation parameter over the value for an isolated transition results from the fact that collisional coupling among the rotational levels funnels the available inversion in adjacent rotational levels into the pair being stimulated [12]. In the limit $\gamma/x_J S_r \ll 1$ the factor A approaches $(1/x_J)$, which is 15.5 for a $P(18)$ transition at $T = 400°K$.

Returning to (7) we can obtain an exact solution for $N_J(v)$ by integrating the equation to extract the total inversion density $\int_{-\infty}^{\infty} dv'\, N_J(v')$. This solution, however, involves the function $\int_{-\infty}^{\infty} dv\, f(v)[1 + (2/\gamma_t)R(\omega, v)]^{-1}$, which cannot be analytically evaluated. To obtain analytically tractable expressions, we confine our attention to the regime of strong Doppler broadening ($\gamma'/Ku \ll 1$) and weak saturation ($2/\gamma_t)R(\omega, v) \ll 1$. Equation (7) is evaluated in Appendix II in the above limits. We find that

the differential inversion (DI) (unsaturated inversion-saturated inversion) naturally separates into two terms with different velocity dependences

$$\delta N_J(v, \omega) = \delta N_L(v, \omega) + \delta N_D(v, \omega). \tag{13}$$

The predominently Lorentzian term

$$\delta N_L(v, \omega) \simeq \left(\frac{\gamma'}{\gamma_t}\right)\left(\frac{p}{\hbar}\right)^2 E^2 N_J^0 f(v) \cdot \begin{Bmatrix} L_\pm \\ L_+ + L_- \end{Bmatrix}, \tag{14}$$

which represents saturation of the velocity distribution over a velocity width $2\gamma'/K$ and is small compared to the full distribution width $2u$, is the well known Lorentzian hole expected for a Doppler broadened line. The additional Doppler component

$$\delta N_D(v, \omega) \simeq \frac{\sqrt{\pi}}{Ku} \exp\left[-\left(\frac{\omega - \omega_0}{Ku}\right)^2\right]\left(\frac{\gamma_{er}}{A\gamma\gamma_t}\right) \cdot \left(\frac{p}{\hbar}\right)^2 E^2 N_J^0(v) \cdot \begin{Bmatrix} 1 \\ 2 \end{Bmatrix}, \tag{15}$$

which indicates saturation across the entire velocity distribution, is the result of collisions that change the molecular velocity. The upper and lower cases in braces of (14) and (15) correspond to traveling wave and standing wave fields, respectively.

The degree of mixed saturation behavior is best characterized[3] by the ratio r defined by

$$r = \frac{\delta N_L(0, \omega_0)}{\delta N_D(0, \omega_0)}. \tag{16}$$

From (14) and (15) we have

$$r = \frac{Ku}{\sqrt{\pi}} \frac{A\gamma}{\gamma' \gamma_{er}}. \tag{17}$$

The ratio r is thus independent of field in the weak saturation limit. In the limit $\gamma/\gamma_{er} = \infty$ the DI assumes the pure Lorentzian form. In the opposite limit $\gamma/\gamma_{er} = 0$ the DI assumes a pure Doppler form. Collisions can therefore restore homogeneity to a line with strong Doppler broadening.

To appreciate the physical significance of (17) it is helpful to derive the quantity r by an alternative, intuitive method for pure elastic scattering in the following way. The ratio r is approximately equal to the ratio P_1/P_2 where P_1 is the field interaction probability for a molecule whose Doppler shifted emission frequency coincides with that of the field ($|(\omega - \omega_0) \mp Kv| < \gamma'$) and P_2 is the interaction probability for a molecule whose Doppler shifted emission lies far from the field frequency ($|(\omega - \omega_0) \mp Kv| > \gamma'$). P_1 evaluated at $\omega = \omega_0$ and $v = 0$ is approximately $R(\omega_0, 0)/[\gamma_t + R(\omega_0, 0)]$. P_2, however, consists of an infinite sum of terms, $P_2 = \sum_{n=1}^{\infty} p_n$, in which p_n is the probability that a molecule of velocity v will migrate to the neighborhood $|(\omega - \omega_0) \mp Kv| < \gamma'$ of the field and interact with it after undergoing n velocity-changing collisions,[3]

$$p_n \simeq \left[\frac{1}{\gamma_t}\int_{-\infty}^{\infty} dv'\, S_e(v, v')\right]^{n-1}\left[\frac{1}{\gamma_t}\left(\frac{\gamma'}{\sqrt{\pi}\, Ku}\right)S_e\right]P_1. \tag{18}$$

P_2 and r become

$$P_2 \simeq \frac{\gamma'}{\sqrt{\pi}\, Ku}\left(\frac{S_e}{\gamma_t}\right)\sum_{n=0}^{\infty}\left(\frac{S_e}{\gamma_t}\right)^n P_1 = \frac{\gamma'}{\sqrt{\pi}\, Ku}\left(\frac{S_e}{\gamma}\right)P_1 \tag{19}$$

$$r = \frac{P_1}{P_2} \simeq \sqrt{\pi}\left(\frac{Ku}{\gamma'}\right)\left(\frac{\gamma}{S_e}\right).$$

Except for a numerical factor of π, the above result is identical to the elastic limit of (17). We can now interpret r as follows. γ'/Ku is the probability that a molecule will scatter into the interaction region of width $2\gamma'/K$ in velocity space out of the total available width $2u$ of the velocity distribution while S_e/γ represents the effective number of ways that the above scattering process can occur due to all possible collision routes.

The presence of a set of closely spaced rotational levels adds additional features to this picture. The cross-relaxation rate must now be generalized to include rotational collisions since population can now be exchanged among different portions of the velocity distribution via rapid exchanges with other rotational levels. The form (8) of the rotational contribution to γ_{er} is a consequence of the fact that a velocity shift in a given rotational level induced by rotational scattering requires a minimum of two collisions ($vj \rightarrow v'j' \rightarrow v''j$). This assertion is easily demonstrated by considering the elastic example again. If we impose the condition that a minimum of two collisions be required to transport a molecule into the vicinity of the field, then the summation in (19) must be replaced by

$$\left(\frac{S_e}{\gamma_t}\right)\sum_{n=1}^{\infty}\left(\frac{S_e}{\gamma_t}\right)^n = \frac{1}{\gamma}\,\frac{S_e}{1 + \frac{\gamma}{S_e}}. \tag{20}$$

The cross-relaxation rate is therefore reduced from S_e by a factor in the denominator which is analogous to the rotational coupling factor $(1 + \gamma/x_J S_r)^{-1}$ appearing in the rotational term of (8). Because this factor is essentially unity in the pressure range of a few tenths of a torr, and since rotational thermalization is rapid in CO_2, the rotational scattering process constitutes an important contribution to the spectral cross-relaxation or spectral hole-filling process.

More important than its contribution to the cross-

[3] The probability that a molecule will not scatter into the vicinity of the field in a collision is given by $(1/\gamma_t)\int dv' S_e(v, v')$ where the proper limits of integration exclude the field interaction region. In the strong Doppler limit, however, inclusion of the narrow interaction region is of little consequence.

relaxation process, which restores homogeneity to the line, however, is the opposite tendency for rotational scattering to augment the inhomogeneity of the line by the factor A. This effect results from an A-fold increase in the vibrational decay rate γ and is explained by the fact that the effective decay rate in the presence of rotational coupling is neither the vibrational decay rate γ, nor the total rotational scattering rate $(1 - x_J)S_r$, but is the net rate out γ_t minus the net rate in γ_{cr}, which is just $A\gamma$ from (11). Since the rotational contribution to γ_{cr} is generally smaller than the elastic contribution, the net effect of strong rotational coupling is to augment the inhomogeneity of the rotation–vibration transition. The extent to which rotational collision effects actually influence saturation is determined by the rotational coupling factor $(1 + \gamma/x_J S_r)^{-1}$ (8) and (10). The tight coupled and decoupled limits are given by $\gamma/x_J S_r = 0$ and $\gamma/x_J S_r = \infty$, respectively.

It is now obvious what the effects of collisional coupling among the various vibrational levels will be. First the factor A will be multiplied by the effective number of vibrational levels coupled to the upper and lower laser levels and second a term whose magnitude depends on the ratio between the rates for vibration–vibration transfer and vibrational decay must be added to γ_{cr}.

Lamb Dip

The laser intensity can be calculated by requiring that the saturated gain $\alpha(\omega, \omega_s)$ be equal to a cavity distributed loss parameter β. The gain $\alpha(\omega, \omega_s)$ for a Doppler broadened line is $\alpha(\omega, \omega_s) = \int_{-\infty}^{\infty} dv\, N_J(v, \omega_s)\, \sigma(\omega - Kv)$. The field independent quantity $\sigma(\omega - Kv) = (\hbar\omega/I)R(\omega, v)$ is the stimulated emission cross section per molecule.

$$\sigma(\omega - Kv) = \sigma_0 \cdot \left\{ \frac{L_\pm}{L_+ + L_-} \right\}$$

with $\sigma_0 = \gamma'(\hbar\omega/c\epsilon_0)(p/\hbar)^2$. Using (14) and (15) for a standing wave field we find

$$\alpha(\omega, \omega_s) \simeq \alpha_0(\omega) - \alpha_0(\omega)\left(\frac{2}{\gamma\gamma_t}\right)\left(\frac{p}{\hbar}\right)^2 E^2 \cdot \left\{1 + \frac{r}{4}\left[1 + (\gamma')^2 L(\omega - \omega_0)\right]\right\}. \quad (22)$$

If t is the mirror transmittance, the laser intensity $I(\omega - \omega_0) = (\frac{1}{2})c(\epsilon_0/2)E^2 t$ becomes

$$I(\omega - \omega_0) = \tfrac{1}{2}c\epsilon_0 t\gamma'\gamma_t y\left(\frac{\hbar}{p}\right)^2 \frac{1 - \beta/\alpha_0(\omega)}{1 + yL'(\omega - \omega_0)} \quad (23)$$

where

$$y = \frac{1}{1 + \frac{4}{r}} \quad (24)$$

$$L'(\omega - \omega_0) = (\gamma')^2 L(\omega - \omega_0). \quad (25)$$

The strength of the Lamb dip is controlled by the parameter y. We see that the dip depth reflects the degree of mixed broadening in the line. This is perfectly clear since the Lamb dip is a manifestation of the Lorentzian holes burned into the inversion. When cross relaxation is weak ($r \gg 1$), the DI assumes strong Lorentzian character and the depth parameter y approaches 1. This is the limit most favorable for Lamb dip formation and is closely approached in atomic gas lasers where the short level lifetimes ($\gamma^{-1} \simeq 10^{-8}$ s) render the effects of velocity-changing collisions less important. As cross-relaxation effects become more prominent ($r \ll 1$) due to longer level lifetimes, the DI assumes a stronger homogeneous character and the Lamb dip weakens. In contrast to atomic levels, the relatively long vibrational lifetimes ($\gamma^{-1} \simeq 10^{-3}$ s) of molecular levels allow collisional processes to dominate the saturation behaviour. Formation of the Lamb dip in the CO_2 laser at pressures between 0.1 torr and 1.0 torr where it has been observed is made possible through the influence of strong rotational coupling, which effectively increases the inhomogeneous character of the transition.

Collisional effects in saturation of atomic transitions have also been treated theoretically by density matrix approaches [13] and [14]. Our formulation and that of [13] and [14] share the common feature of identical elastic collision models. Although the saturated inversion is not calculated in the self-consistent field approach [13], the dependence of the Lamb dip factor on the atomic collision parameter[4] given by [13, eq. (125), [128)], in the limit of equal upper and lower state lifetimes, agrees exactly with the dependence predicted by (24) in the limit of no rotational coupling, $S_r = 0$. A calculation of the second order polarization using the formalism of [13] also shows exact agreement with the elastic limit of (14) and (15). The method adopted in [14] allows an exact solution of the density matrix equations for a traveling wave perturbation. The phenomenon of Doppler saturation again appears.

Comparison of Experimental Result With Theory

While the quantity r describing the saturation behavior was calculated by assuming interaction of the molecules with a single field, a probe of the saturated gain involves the simultaneous interaction of two resonant fields. The relationship between r and the measured gain quantity $s = \delta\alpha_L(\omega_0, \omega_0)/\delta\alpha_D(\omega_0, \omega_0)$ will therefore be determined by the details of the nonlinear coupling between the two fields.

Dienes [15] has shown that in the absence of collisions both the magnitude and the frequency behavior of the coupling is dependent upon the level degeneracies. Using the theory of [15] for a $P(18)$ ($J = 18 \rightarrow J = 19$) transition and orthogonal fields we have found that the frequency

[4] The -1 exponent in the expression for θ appearing in [13, eq. 128b] should be absent.

dependence of the coupling is not changed appreciably from the classical Lorentzian result but the amplitude of the coupling is reduced from the classical value. In terms of the inversion quantity $\delta N_L(v, \omega_s)$, the coupling can be expressed approximately as

$$\delta\alpha_L(\omega_p, \omega_s) \simeq c_1 \int_{-\infty}^{\infty} dv\ \delta N_L(v, \omega_s)\sigma(\omega_p - Kv)$$

where $c_1 \simeq 0.07$. Using (14) we have

$$\delta\alpha_L(\omega_p, \omega_s) \simeq c_1\left(\frac{\pi}{\gamma_t K}\right)\left(\frac{p}{\hbar}\right)^2 \sigma_0 N_J^0 E^2 f\left(\frac{\omega_p - \omega_0}{K}\right) \cdot \frac{2}{(\omega_p - \omega_s)^2 + (2\gamma')^2}. \quad (26)$$

Notice that the hole in the DG is twice the width of the hole in the DI because the probe beam, which interacts with molecules in a frequency width $2\gamma'$ about ω_p, interacts with the hole of width $2\gamma'$ over a region of width $4\gamma'$. This result and the slope of Fig. 6 gives a value for the phase interruption rate of $\gamma' = 12$ MHz/torr, which agrees with values obtained from measurements of the Lamb dip width [6].

Collisions, which result in a change of the DI from the form $\delta N_L(v, \omega)$ to $\delta N_L(v, \omega) + \delta N_D(v, \omega)$, introduce complications. The form of the coupling in this case is difficult to predict because a two-field theory including degeneracy and collision effects is not available. We can speculate, however, that the relation between r and s would fall within the rather large interval bounded by the limits in which the magnitude of the coupling C_2 for the Doppler component is either the same as for the Lorentzian component or is equal to 1 (no coupling).

$$\delta\alpha_D(\omega_p, \omega_s) \simeq c_2 \int_{-\infty}^{\infty} dv\ \delta N_D(v, \omega_s)\sigma(\omega_p - Kv).$$

From (15)

$$\delta\alpha_D(\omega_p, \omega_s) \simeq c_2\left(\frac{\pi}{\gamma' K}\right)\left(\frac{\sqrt{\pi}}{Ku}\right)\frac{\gamma_{cr}}{A\gamma\gamma_t}\left(\frac{p}{\hbar}\right)^2 \cdot \exp\left[-\left(\frac{\omega_s - \omega_0}{Ku}\right)\right]\sigma_0 N_J^0 E^2 f\left(\frac{\omega_p - \omega_0}{K}\right). \quad (27)$$

We therefore might expect $2s \lesssim r \lesssim 2as$.

To compare with experimental results, we can deduce the quantity y from the data of Fig. 7 assuming $r = 2s$. This result is compared in Fig. 9 with values of y obtained by measuring the depth of the Lamb dip in a separate experiment using a flow laser with a 50/50 mix of CO_2 and N_2 gases.[5] There is good qualitative agreement between these two independent determinations of y. The other limit $r = 2as$ produce values of y that are so large as to fall beyond the scale in the figure. Reliable data above 0.5 torr could not be obtained because the Lorentzian component became too weak to measure accurately.

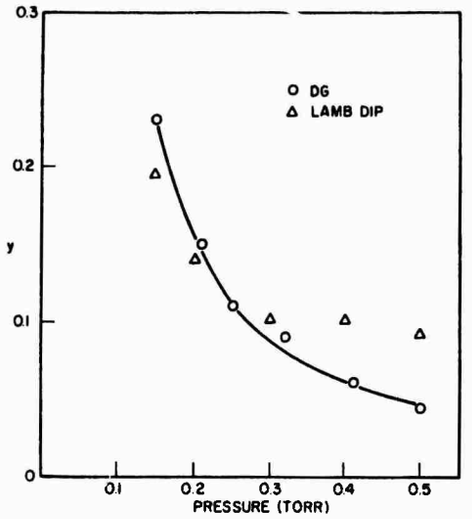

Fig. 9. Comparison of the parameter y as derived from the DG data and as measured from the Lamb dip.

It is difficult to obtain a precise fit of the data to all the relaxation parameters appearing in r for two reasons. First, the diffusion contribution to γ is complicated and depends on the exact beam geometry, which in the case of two overlapping beams is not well defined. Second, dissociation of the binary $CO_2 + N_2$ mixture used in the amplifier results in an average of the collision parameters for the various species present. We can, however, estimate a value for γ_{cr}. The mean L_t beam radius of 2 mm inside L_A gives a value for γ of 7×10^3 s^{-1} at 0.2-torr pressure. From rotational relaxation measurements [11], $S_r \simeq 10^7$ s^{-1} torr^{-1}. The rotational coupling factor $1 + \gamma/x_J S_r$ is therefore unity and A becomes $1/x_J \simeq 15.5$ for $J = 18$ at $T = 400$°K. Using $Ku = 23$ MHz, $\gamma' = 12$ MHz/torr and $r = 0.7$ at 0.2 torr, γ_{cr} is calculated from (17) to be $\gamma_{cr} \simeq 9 \times 10^5$. Since $\gamma_{cr} \simeq S_s + S_r > S_r \simeq 2 \times 10^6$ s^{-1} at 0.2 torr, the deduced value of γ_{cr} is at least a factor of 2 smaller than expected. This discrepancy is not surprising because we have not included collisional coupling between the various vibrational levels of CO_2. It is known that collisional coupling among the $(00°\nu_3)$ levels [16] and between (10°0) and the lower $(\nu_1\nu_2^l 0)$ levels [17], [18] are rapid. These levels should still be partially collisionally coupled to the (00°1) and (10°0) levels at our operating pressures. The factor A must therefore be multiplied by the effective number of vibrational levels coupled to the ones being stimulated by the laser field. Increasing A brings the value of γ_{cr} deduced from our measurements into closer agreement with the expected value.

The major limitation in the present study is the inability to extend the range of measurements in pressure due to laser instabilities. With more stable oscillators it may be possible to separate the contributions of the

[5] The authors are indebted to H. T. Powell who made these measurements.

elastic and rotational contributions to the cross-relaxation parameter γ_{cr} and study collisional decoupling effects through changes in A. The difficulty of these measurements, however, lie in the fact that these various effects are coupled and that r can no longer be measured accurately when it becomes appreciably greater than unity.

Appendix I

We first write the steady-state equations for levels $J' \neq J$. They are

$$0 = w_{J'}(v) - \gamma N_{J'}(v) - S_s\left[N_{J'}(v) - f(v)\int_{-\infty}^{\infty} dv'\, N_{J'}(v')\right] - S_r\left[(1 - x_{J'})N_{J'}(v) - x_{J'}f(v)\sum_{k\neq J'}\int_{-\infty}^{\infty} dv'\, N_k(v')\right].$$

By first integrating over v, rearranging the sum over k and then summing over $J' \neq J$ we obtain

$$\sum_{J'\neq J}\int_{-\infty}^{\infty} dv\, N_{J'}(v) = \frac{\sum_{J'\neq J} w_{J'} + (1 - x_J)S_r\int_{-\infty}^{\infty} dv\, N_J(v)}{\gamma + x_J S_r}.$$

The right side of the above expression can be expressed solely in terms of the parameters of the level pair J if we assume that a Boltzmann distribution among the rotational levels does exist in the absence of fields. In this case $\dot{N}_{J'}(v)|_s = \dot{N}_{J'}(v)|_r = 0$ and (3) of the text reduces to $w_{J'}f(v) = \gamma N^0_{J'}f(v) = \gamma(x_{J'}/x_J)N^0_J f(v)$. The sum $\sum_{J'\neq J} w_{J'}$ thus becomes $\gamma N^0_J(1 - x_J)/x_J$. Substituting $\sum_{J'\neq J}\int_{-\infty}^{\infty} dv\, N_{J'}(v)$ into (6) with $\dot{N}_J(v) = 0$ and rearranging terms gives (7).

Appendix II

Integration of (7) gives the following expression for the total inversion density

$$\int_{-\infty}^{\infty} dv'\, N_J(v') = \frac{A\left(\frac{\gamma}{\gamma_t}\right)N^0_J F(\omega)}{1 - \frac{\gamma_{cr}}{\gamma_t}F(\omega)}$$

in which $F(\omega) = \int_{-\infty}^{\infty} dv\, f(v)[1 + (2/\gamma_t)R(\omega, v)]^{-1}$. Using the strong Doppler broadening and weak saturation assumptions results in the approximation

$$F(\omega) \simeq 1 - \xi(\omega).$$

For a traveling wave field

$$\xi(\omega) \simeq (\sqrt{\pi}\, Ku)^{-1}\exp\left[-(\omega - \omega_0/Ku)^2\right](\pi/\gamma_t)(p/\hbar)^2E^2.$$

$\xi(\omega)$ for a standing wave is exactly twice the traveling wave value. Substituting the above value of $\int_{-\infty}^{\infty} dv'\, N_J(v')$ in (7) gives

$$N_J(v) = \frac{BN^0_J(v)}{1 + \left(\frac{2}{\gamma_t}\right)R(\omega, v)}$$

$$\delta N_J(v, \omega) \simeq N^0_J(v)\left[B\left(\frac{2}{\gamma_t}\right)R(\omega, v) + (1 - B)\right]$$

The quantity B equals

$$A(\gamma/\gamma_t)\{1 + \gamma_{cr}[1 - \xi(\omega)]/[\gamma_t - \gamma_{cr} + \gamma_{cr}\,\xi(\omega)]\}.$$

Use of the weak saturation condition in expanding $(1 - B)$ gives (15). Since weak saturation implies small changes in inversion, $\delta N_D(v, \omega)/N^0_J(v) = 1 - B \ll 1$ imply $B \simeq 1$. This result immediately gives (14).

Conclusion

We have measured the frequency profile of the saturated gain in rotation vibration lines of the CO_2 molecule at pressures where individual lasering transitions display the Lamb dip. Each transition saturates in a mixed inhomogeneous–homogeneous broadened manner due to spectral cross relaxation induced by collisions that change the molecule's velocity.

A rate equation treatment shows that in CO_2 this mixed saturation behavior, characterized by the mixed broadening parameter r, which is the ratio of the amplitude of the Lorentzian component to the amplitude of the Doppler component in the differential inversion, is a balance between the three collision processes of elastic scattering, rotational thermalization, and vibrational decay. The depth of the Lamb dip in the laser intensity, which reflects the influence of these various collision processes, is given by the expression $y = [1 + 4/r]^{-1}$.

References

[1] W. R. Bennett, Jr., "Hole burning effects in a He–Ne optical maser," *Phys. Rev.*, vol. 126, 1962, pp. 580–593.
[2] W. E. Lamb, Jr., "Theory of an optical maser," *Phys. Rev.*, vol. 134, 1964, pp. A1429–A1450.
[3] P. W. Smith, "Linewidth and saturation parameter for the 6328 Å transition in a He–Ne Laser," *J. Appl. Phys.*, vol. 37, 1966, pp. 2089–2093.
[4] A. Szöke and A. Javan, "Effects of collisions on saturation behavior of the 1.15 μ transition of Ne studied with He–Ne laser," *Phys. Rev.*, vol. 145, 1966, pp. 137–147.
[5] M. A. Pollack, T. J. Bridges, and A. R. Strand, "Central tuning dip in a submillimeter molecular laser," *Appl. Phys. Lett.*, vol. 10, 1967, pp. 182–183.
[6] C. Borde and L. Henry, "Study of the lamb dip and of rotational competition in a CO_2 laser," *IEEE J. Quantum Electron.*, vol. QE-4, Nov. 1968, pp. 874–880.
[7] T. W. Hansch and P. E. Toschek, "Observation of saturation peaks in a He–Ne laser by tuned laser differential spectrometry," *IEEE J. Quantum Electron.* (Corresp.), vol. QE-4, July 1968, pp. 467–468.
[8] T. Kan, H. T. Powell, and G. J. Wolga, "Observation of central tuning dips in N_2O and CO_2 molecular lasers," *IEEE J. Quantum Electron.* (Corresp.), vol. QE-5, June 1969, pp. 299–300.
[9] Yu. V. Brzhazovsky, V. P. Chebotayev, and L. S. Vasilenko, "Collision effect on the saturation character of vibration-rotation transitions for 00°1–10°0 band of CO_2," *IEEE J. Quantum Electron.*, vol. QE-5, Mar. 1969, pp. 146–151.
[10] C. P. Christensen, C. Freed, and H. A. Haus, "Gain saturation and diffusion in CO_2 lasers," *IEEE J. Quantum Electron.*, vol. QE-5, June 1969, pp. 276–283.
[11] P. K. Cheo and R. L. Abrams, "Rotational relaxation rate of CO_2 laser levels," *Appl. Phys. Lett.*, vol. 14, 1969, pp. 47–49.
[12] D. F. Hotz and J. N. Ferrer, "Intrinsic flux limits for continuous and Q-pulse gain for the 10.6 μ line of CO_2," *J. Appl. Phys.*, vol. 39, 1968, pp. 1797–1800.
[13] B. L. Gyorffy, M. Borenstein, and W. E. Lamb, Jr., "Pressure

broadening effects on the output of a gas laser," *Phys. Rev.*, vol. 169, 1968, pp. 340–359.
[14] A. B. Kolchenko and S. G. Rautian, "Interaction of atoms with radiation field in the strong collision model," *Sov. Phys.—JETP*, vol. 27, 1968, pp. 511–518.
[15] A. Dienes, "On the physical meaning of the 'two nondegenerate levels' atomic model in nonlinear calculations," *IEEE J. Quantum Electron.*, vol. QE-4, May 1968, pp. 260–263.
[16] L. O. Hocker, M. A. Kovacs, C. K. Rhodes, G. W. Flynn, and A. Javan, "Vibrational relaxation in CO_2 using an induced fluorescence technique," *Phys. Rev. Lett.*, vol. 17, 1966, pp. 233–235.
[17] C. Bradley Moore, R. E. Wood, B. L. Hu, and J. T. Yardley, "Vibrational energy transfers in CO_2 lasers," *J. Chem. Phys.*, vol. 46, 1967, pp. 4222–4231.
[18] C. K. Rhodes, M. J. Kelley, and A. Javan, "Collisional relaxation of the 10°0 state in pure CO_2," *J. Chem. Phys.*, vol. 48, 1968, pp. 5730–5731.

Reprinted by permission from
IEEE JOURNAL OF QUANTUM ELECTRONICS
Vol. QE-7, No. 4, April 1971